OXIDATION STABILITY AND ACTIVITY OF BULK, SUPPORTED AND PROMOTED MOLYBDENUM CARBIDE CATALYSTS FOR METHANE REFORMING

By

ANNA RINI SEKAR DARUJATI

A dissertation submitted in partial fulfillment of
the requirements for the degree of

DOCTOR OF PHILOSOPHY

WASHINGTON STATE UNIVERSITY
Department of Chemical Engineering

MAY 2005

To the Faculty of Washington State University:

The members of the Committee appointed to examine the dissertation of ANNA RINI SEKAR DARUJATI find it satisfactory and recommend that it be accepted.

_____
Chair

_____

_____

_____

ACKNOWLEDGMENT

Over the years, there are many people whose contribution and advice have made my graduate career one of the most valuable and enjoyable learning experiences in my life. My gratitude goes to Dr. William J. Thomson, my great advisor, for providing technical expertise, guidance, space and freedom to learn, and for sharing his diverse experience. His invaluable advice and good humor will always be remembered.

I would also like to thank to my committee members, Dr. Richard Zollars, Dr. Reid Miller, and Dr. Ursula Mazur for all the valuable inputs and contribution to my dissertation. The staff members of the Chemical Engineering department, JoAnn McCabe and Diana Thornton deserve thanks for their outstanding administrative support. I would also like to acknowledge all assistant made by Jon Windsor, a junior in the Department of Chemical Engineering who prepared some of the catalysts used in this study.

A special thanks to my good friend and colleague, Alex Platon, for the friendship, various help and all the dynamic discussions. Last but not least, to my best friend and beloved husband, David LaMont whose unwavering belief in my abilities has served to fuel my perseverance and determination to succeed in graduate school. I could not thank him enough for his tremendous support and encouragement.

OXIDATION STABILITY AND ACTIVITY OF BULK, SUPPORTED AND PROMOTED MOLYBDENUM CARBIDE CATALYSTS FOR METHANE REFORMING

Abstract

By Anna Rini Sekar Darujati, Ph.D.
Washington State University
May 2005

Chair: William J. Thomson

The objective of the research presented here is to understand and to improve the oxidation stability of molybdenum carbide (Mo_2C) as a catalyst for oxidative methane reforming. The first of three studies was aimed at identifying the behavior of low surface area, bulk Mo_2C in the presence of reforming gases. Reforming products, such as CO and H_2, were found to inhibit Mo_2C oxidation. However, the carburization of MoO_2 by CH_4 at these temperatures was found to be insignificant. A "stability ratio", was then formulated to correlate the partial pressure of reforming gases to the stability of Mo_2C. In the second study, the oxidation stability of supported and promoted Mo_2C was studied. A ceria-promoted $Mo_2C/\gamma\text{-}Al_2O_3$ was the most stable catalyst, though stability was heavily influenced on the synthesis procedure. The interaction between ceria and $\gamma\text{-}Al_2O_3$ is hypothesized to preserve the ceria particles from agglomeration allowing the ceria to actively undergo redox reaction on the surface of the catalyst during reforming. The effect of reforming products, specifically CO, on the stability of both the unpromoted and

ceria-promoted $Mo_2C/\gamma\text{-}Al_2O_3$ catalysts was also investigated. Whereas high CO partial pressure was beneficial for the stability of $Mo_2C/\gamma\text{-}Al_2O_3$, it significantly lowered the stability of the ceria-promoted $Mo_2C/\gamma\text{-}Al_2O_3$ by reducing most of the ceria to Ce_2O_3, which primarily diminished the redox ability of the ceria, and also increased the tendency for CO disproportionation to form inactive carbon. The third study was a successful determination of the kinetics of reforming over the ceria-promoted $Mo_2C/\gamma\text{-}Al_2O_3$ catalyst. The high activation energy of the ceria-promoted Mo_2C (45.5 kcal/mol) was similar to that previously measured for a bulk Mo_2C catalyst, although the activity of the ceria-promoted catalyst was higher. The ceria greatly enhanced the activation of CO_2, which supported our previous observation of the high stability of this catalyst during reforming. A reaction mechanism, taking into account the activation of CH_4 on the surface of Mo_2C and the activation of CO_2 on the surface of ceria and Mo_2C, was consistent with the kinetic model. The rate-determining step was hypothesized to be the extraction of carbidic carbon by oxygen adsorbed on the ceria.

TABLE OF CONTENTS

LIST OF TABLES

LIST OF FIGURES

CHAPTER TWO

This work is dedicated to my dear father and mother, Hardjono and Soephiana Hardjono, for the unconditional love, hard work, and patience

ATTRIBUTION

This dissertation comprises four chapters and three appendices. Chapter 1 contains the general background of the dissertation and describes the objectives and motivation for the research in each chapter. Chapters 2 – 4 consist of individual manuscripts detailing specific aspects of reforming over molybdenum carbide catalysts. Each manuscript is written based on the format of the peer-reviewed scientific journal in which it has been published or submitted for publication. Chapter 5 is the concluding chapter, which also presents recommendations for future work. In each manuscript, Anna R.S. Darujati designed and executed the experiments and performed data analysis. The appendices details the description of the equipment (Appendix A), the catalyst characterization (Appendix B) and the tabulated kinetics data (Appendix C).

Chapter 2, entitled "Oxidation stability of Mo_2C catalyst under fuel reforming conditions" has been published in *Applied Catalysis A.* 253 (2003) 397. This manuscript are co-authored with William J. Thomson who provided technical expertise and guidance on the organization of the content and also with David C. LaMont who contributed to the technical content.

Chapter 3, entitled "Stability of supported and promoted-supported Mo_2C in dry methane reforming" is currently under review for *Applied Catalysis A*. Dan Dugan of the Safety and Radiation Office at Washington State University provided technical assistance for the neutron activation analysis. Surface analysis of the catalysts with X-Ray

photoelectron spectroscopy was conducted by Louis Scudiero in the Department of Chemistry, Washington State University. William J. Thomson provided expertise and advice on the technical content.

Chapter 4, entitled "Kinetic study of a Ceria Promoted-Mo_2C/γ-Al_2O_3 for Dry-methane Reforming" was submitted to *Chemical Engineering Science*. This manuscript is co-authored with William J. Thomson who provided technical assistant and organization of the manuscript.

CHAPTER ONE

INTRODUCTION

1. Current Demands for Production of Hydrogen

Hydrogen is used extensively as a feedstock for many applications, such as petroleum refining, ammonia synthesis, methanol production, food processing, electronics and metal manufacturing. In an oil refinery, hydrogen is primarily used in hydro-processing units such as hydrodesulfurization and hydrotreating. With more stringent environmental regulations demanding cleaner fuel for automobiles (less aromatic and sulfur compounds), hydrogen consumption for hydro-processing plants has significantly increased. In non-refinery applications, ammonia production accounts for 40% of the world's H_2 consumption [1], followed respectively by its use in manufacturing electronic industries and in hydrogenation of edible fats and oils. Another prospective use of hydrogen, which has been under intensive study, is the application of hydrogen as an alternative clean fuel, since combustion of H_2 at its point of use produces only water and no CO_2. However, until hydrogen can be obtained economically from water, hydrogen will almost exclusively be produced from hydrocarbons, and this will be accompanied by the production of CO_2. Although the development of water electrolysis for H_2 production has been carried out for decades, the high cost of electricity and high purity of water required for this process has limited its application. Other means for H_2 production, which have been under investigation, include the decomposition of methane [2-4], solar energy for photoelectrolysis and photocatalysis of water [6], biomass conversion [5] and dehydrogenation in membrane reactors [7,8]. However, in order to meet the demand of

the consumer market, the H_2 pressure will have to be at least 20 atm, which means external compression of the product is required. Otherwise, these H_2 production technologies can only be used for specialty applications, where high H_2 pressure are not required. As long as natural gas and other fossil fuels are still relatively cheap, the most economical and viable method for producing H_2 is still via oxidation of fossil fuel with steam, CO_2, O_2 or a combination of these. This process is called oxidative reforming and is usually carried out at high pressures (20 – 40 atm) and temperatures (~ 850 ^oC). The common methane reforming reactions are steam reforming of methane (SMR), dry-methane reforming (DMR) and partial oxidation of methane (POM). The following reactions describe these processes along with their reaction enthalpies.

$$\text{SMR: } CH_4 + H_2O \rightarrow CO + 3H_2, \qquad \Delta H^{300K} = 49.4 \text{ kcal/mol} \quad (1)$$

$$\text{DMR: } CH_4 + CO_2 \rightarrow 2CO + 2H_2, \qquad \Delta H^{300K} = 59.1 \text{ kcal/mol} \quad (2)$$

$$\text{POM: } CH_4 + \tfrac{1}{2}\, O_2 \rightarrow CO + 2H_2, \qquad \Delta H^{300K} = -8.5 \text{ kcal/mol} \quad (3)$$

Both SMR and DMR are endothermic reactions; therefore the reactions are normally operated at high temperatures (< 850^oC). Another process, which is a combination of POM with either SMR or DMR is known as autothermal reforming. As indicated by its name, in autothermal reforming the heat generated due to the exothermicity of POM is used to supply the endothermic SMR or DMR reaction. In practice, the choice of reforming technology is determined by the type of the hydrocarbon feedstock, the scale of operation [10] and the desired CO-to-H_2 ratio in the product gases.

Most of the CO produced in the reformers is then used to produce additional hydrogen via the water-gas shift reaction (WGS):

$$CO + H_2O \leftrightarrows CO_2 + H_2 \qquad \Delta H^{300K} = -9.7 \text{ kcal/mol} \quad (4)$$

This reaction is exothermic and is favored at low temperatures, therefore, the temperature at the exit of the reformer must be reduced to about 550^{o}C for high temperature shift and to about 200^{o}C for low temperature shift. Since reforming reactions are usually accompanied by WGS, the presence of co-produced CO_2 in the exit gas is unavoidable.

2. Current Issues with Steam Reforming Catalysis

Steam methane reforming on a commercial scale is typically carried-out over Ni supported on α-Al_2O_3 (12-20% Ni). The major problem associated with Ni catalyst is the formation of carbon due to CH_4 cracking (5) and CO disproportionation (6) reactions, which are also catalyzed by Ni [11,12]:

$$CH_4 \rightarrow C + 2H_2 \quad (5)$$

$$2CO \rightarrow CO_2 + C \quad (6)$$

The rapid accumulation of carbon can eventually deactivate the Ni catalyst by forming whisker carbon and also plugs the reformer tubes. Therefore, industrial reformers are operated in the presence of excess steam (steam-to-carbon ratios of 2.5 - 3) to keep coking under control by promoting coke gasification:

$$C + H_2O \rightarrow CO + H_2 \quad (7)$$

However, this requires additional energy to generate the excess steam to balance the coking problem, and significantly increases the energy cost of the process. In addition, Ni catalyst is very sensitive to sulfur poisoning, and consequently, the feedstock must be thoroughly cleaned of sulfur. Many attempts have been made to improve the performance of Ni catalyst, and these include the addition of alkali promoters, such as potassium and/or calcium, to suppress the excessive formation of carbon, and sulfur treatment of Ni catalyst to improve the catalyst resistance to sulfur poisoning. Despite the maturity of catalyst technology for reforming, these problems provide ample opportunities for finding alternative catalysts.

3. Alternative Reforming Catalysts

Supported noble metal catalysts, such as supported Pt, Rh, Ru, Ir and Pd, are known to be active for reforming [13-16]. These catalysts are also more tolerant to sulfur poisoning and relatively more coking resistant than conventional Ni catalyst. The major drawback of these catalysts, however, is the high cost associated with the very low availability of these metals in nature. Therefore, the application of noble metal catalysts for reforming has been only to specialty applications, and is not used on an industrial scale. Transition metal carbides, especially molybdenum carbides constitute an important family of catalysts due to their electronic resemblance to noble metal catalysts, such as Pt and Pd [17]. In particular, molybdenum carbide (Mo_2C) catalysts have been studied for

many reactions, such as reforming [18-20], water-gas shift [21], methane hydrogenation [22], CO_2 hydrogenation [23], hydrocarbon isomerization [24], ammonia synthesis [25], alcohol synthesis [26] and hydrodesulfurization [27-29]. Since of the elements contained in this catalyst are abundant in nature; it is much cheaper than noble metal catalysts, which allows it, at least economically, to be a potential substitute for noble metals.

3.1. Current Issues with Mo_2C Catalysts for Reforming

3.1.1. Oxidation Stability of Bulk Mo_2C in Reforming

The application of Mo_2C for reforming is very attractive, because Mo_2C is less susceptible to coking than Ni catalyst, therefore, reforming can be carried out using a stoichiometric feed [18]. Moreover, this catalyst is stable at the high temperatures used in reforming, and the activity of Mo_2C in hydrodesulfurization implies that these catalysts are more sulfur resistant than Ni [27-29]. However, oxidation of Mo_2C to form MoO_2 was found to be a major cause of deactivation during reforming at atmospheric pressure [18-20]. It was reported that stability of Mo_2C in reforming was only observed when the reformer was operated at high pressure (8 bar) or at a slightly elevated pressure (1.2 bar) with recycle of product gases [30]. Although the stability of Mo_2C in reforming was proposed to relate with its redox chemistry, the oxidative stability of Mo_2C and the quantification of how to stabilize Mo_2C against oxidation has never been understood until completion of the study in Chapter Two. Some important performance characteristics related to the stability of Mo_2C were obtained, namely the thermal decomposition

temperature of Mo_2C and oxidation temperature of Mo_2C in the presence of various reforming gases, as well as the prediction of stable reforming conditions.

3.1.2. Stability of Supported and Promoted Mo_2C in Reforming

The investigation of the stability of Mo_2C catalysts was further broadened by catalyst modification, using supports and promoters. While there was some evidence in the literature that the oxidation stability of Mo_2C could be improved by means of a zirconia support [31,32], no study had been conducted to investigate the effect of adding promoters on the stability and activity of Mo_2C in reforming. Therefore, the stability of Mo_2C over oxide supports and in the presence of promoters in DMR was studied in Chapter Three. The results of this study show which factors most strongly affected the stability and activity of supported Mo_2C, such as the thermal stability of the support, the Mo loading and the addition of a ceria promoter.

3.1.3. Kinetics of Promoted-Mo_2C in Reforming

Based on the results described in Chapter Three, a kinetic study of DMR over a ceria-promoted Mo_2C was studied and is described in Chapter Four. While several groups have obtained kinetic parameters for DMR over Mo_2C [20,30,32,33], most were conducted under conditions where oxidation [20,32], or mass transfer resistance [30] was dominant. Therefore, the experiments reported here were carefully carried out with selected feed gas compositions, which prevented the oxidation of Mo_2C, and at molar velocities which

ensure that the kinetic measurements were obtained in the absence of mass transfer limited conditions. By comparing these results to those obtained on bulk Mo_2C under similar conditions [33], it was concluded that the ceria-promoted Mo_2C was more active than the bulk Mo_2C. The reaction mechanism, which also explained the high stability of this catalyst (Chapter Two) was also proposed.

References:

1. Scholz, W.H., Gas Sep. Purif. 7 (1993) 131.
2. Matsukata, M., Matsushita, T., Ueyama, K., Chem. Eng. Sci. 51 (1996) 2769.
3. Li, Y., Armor, J.N., Appl. Catal. B 1 (1992) L31.
4. Armor, J.N., Catalysis Today 26 (1995) 147.
5. Wang D., Czernik, S., Montane, D., Mann, M, Chornet, E., Ind. Eng. Chem. Res. 36 (1997) 1507.
6. Takata, T., Furumi, Y., Shinohara, K., Tanaka, A., Hara, M., Kondo, J., Domen, K., Chem. Mater. 9 (1997) 1063.
7. Maksuda, T., Koike, N., Kubo, E., Kikuchi, E., Appl. Catal. A 96 (1993) 3.
8. Laegsgaard Jorgensen, S., Mogensen, G., Lehmann, P., Hyldoft, P., Hojlund Nielsen, P., Catal. Today 25 (1995) 303.
9. Armor, J.N., Appl.Catal. A 176 (1999) 159.
10. Aasberg-Petersen, K., Hansen, J.-H.B., Christensen, T.S., Dybkjaer, I., Christensen, P.S., Nielsen, C.S., Madsen., S.E.L.W., Rostrup-Nielsen, J.R., Appl.Catal. A 221 (2001) 379.
11. Foster, N.R., Appl. Catal. 19 (1985) 1.
12. Gesser, H.D., Hunter, N.R., Prakash, C.P., Chem. Rev. 85 (1985) 235.
13. Qin, D., Lapszewicz, J., Catalysis Today 21 (1994) 551.
14. Qin, D., Lapszewicz, J. Jiang, X., J. Catal. 159 (1996) 140.
15. Zhang, Z., Tsipouriari, V.A., Efstathiou, A.M., Verykios, X.E., J. Catal. 158 (1996) 51.
16. Rostrup-Nielsen, J.R., Bak Hansen, J.H., J. Catal. 144 (1993) 38.
17. Levy, R.B., Boudart, M., Science 181 (1973) 547.
18. York, A.P.E., Claridge, J.B., Tsang, A.J., Green, M.L.H., Chem. Comm. (1997) 39.
19. York, A.P.E., Claridge, J.B., Brungs, A.J., Marquez-Alvarez, C., Tsang, S.C., Green, M.L.H., Stud. Surf. Sci. Catal. 110 (1997) 711.
20. Claridge, J.B., York, A.P.E., Marquez-Alvarez, C., Brungs, A.J., Sloan, J., Tsang, S.C., Green, M.L.H., J. Catal. 180 (1998) 85.
21. Patt, J., Moon, D.J., Phillips, C., Thompson, L., Catal. Letters 65 (2000) 193
22. Liu, W., Xu, Y., J. Catal. 185 (1999) 386.
23. Nagai, M., Kurakami, T., Omi, S., Catalysis Today, 45 (1998) 235.
24. Ledoux, M.J., Huu, C.P., Guille, J., Dunlop, H., J. Catal. 134 (1992) 383.
25. Kojima, R., Aika, K., Appl. Catal. A 219 (2001) 141.
26. Woo, H.C., Park, K. Y., Kim, Y.G., Nam, I.-S., Chung, J.S., Lee, J.S., Appl. Catal. 75 (1991) 267.
27. Aegerter, P.A., Quigley, W.W.C., Simpson, G.J., Ziegler, D.D., Logan, J.W., McCrea, K.R., Glazier, A., Bussell, M.E., J. Catal. 164 (1996) 109.
28. McCrea, K.R., Logan, J.W., Tarbuck, T.L., Heiser, J.L., Bussel, M.E., J. Catal. 171 (1997) 255.
29. Dhandapani, B.B., Ramanathan, S., Yu, C.C., Fruhberger, B., Chen, J.G., Oyama, S.T., J. Catal. 176 (1998) 61.
30. Sehested, J., Jacobsen, C.J.H., C.J.H., Rokini, S., Rostrup-Nielsen, J.R., J. Catal. 201 (2001) 206.
31. Nagai, M., Kurakami, T., Omi, S., Catalysis Today, 45 (1998) 235.

32. Nagai, M., Oshikawa, K., Kurakami, T., Miyao, T., Omi, S., J. Catal. 180 (1998) 14.
33. LaMont, D.C., Thomson, W.J., "*Dry Reforming Kinetics over a Bulk Molybdenum Carbide Catalyst*", Chem. Eng. Sci., 2004, in press.

CHAPTER TWO

OXIDATION STABILITY OF Mo_2C CATALYSTS UNDER FUEL REFORMING CONDITIONS

Anna R.S. Darujati, David C. LaMont, William J. Thomson*

Department of Chemical Engineering, Washington State University, P.O. Box 642710, Pullman, WA 99164-2710, USA

* Corresponding author. Tel.: +1 509 335 8580; FAX: +1 509 335 4806; e-mail: thomson@che.wsu.edu

Abstract

The oxidation stability of a low surface area Mo_2C catalyst has been studied in the presence of gases associated with the steam and dry (CO_2) reforming of methane, at temperatures up to 850°C and pressures to 8 bar. The oxidation onset temperatures were found to be about 600°C when the carbide was exposed to either steam or CO_2. There appears to be two distinct mechanisms for Mo_2C oxidation: direct oxidation at temperatures below 750°C and thermal decomposition followed by oxidation of the Mo metal at temperatures above 750°C. Although onset temperatures were similar, CO_2 was a stronger oxidant than steam at the higher temperatures. Both H_2 and CO were found to inhibit oxidation and the effect can be explained by their influence on the reactions governing carburization and oxidation. The water gas shift reaction readily occurred over the catalyst and it was found that a carburizing ratio, defined as the ratio of carburizing gases to oxidizing gases, was able to predict stability, with oxidation occurring at ratios of 0.8 or lower. The effect of pressure on the onset temperature of CO_2 oxidation of the carbide was found to be negligible, even when inhibited by CO.

Keywords: molybdenum carbide, steam-methane reforming, oxidation, stability, dynamic X-ray diffraction.

1. Introduction

The vast potential of fuel cells and their appealing benefits as an alternative energy source, such as high efficiency and near zero emissions, have increased interest in finding new catalysts for producing hydrogen from a variety of fuels. Two catalysts that have been used primarily for fuel reforming are Ni and noble metals. However, the low resistance of Ni catalysts to carbon formation and the high cost of the noble metal catalysts, provide incentives for alternative catalyst investigations.

High surface area metal carbides, particularly of the group VI transition metals, have been reported to possess catalytic properties comparable to those of noble metal catalysts for a variety of reactions [1-9]. Claridge *et. al.* [6], using temperature programmed reaction (TPR), synthesized high surface area carbide catalysts and reported that the carbides of molybdenum and tungsten were active catalysts for dry methane reforming (DMR), steam-methane reforming (SMR) and the partial oxidation of methane under stoichiometric feed conditions at 8 bar without any signs of catalyst deactivation. However, they reported that the molybdenum carbide catalyst deactivated at atmospheric pressure due to oxidation, forming MoO_2 after about 3 hours on stream. They suggested that the longer residence time at the higher pressure, which leads to the increased exposure of the catalyst to carburizing gases, contributed to the stability of the carbide catalysts at elevated pressure. Recently, Sehested *et. al.* [10] demonstrated that high surface area molybdenum carbides were stable for 22 hours with 85% conversion under DMR conditions at 8 bar with excess CO_2 (CO_2/CH_4=1.7) in a single pass, packed bed reactor. However, XRD scans of the post reacted catalysts indicated that the carbide was

partly oxidized, with oxidation more prevalent at the reactor inlet; presumably due to exposure to net oxidizing conditions in that region. The oxidation of Mo_2C by CO_2 to form MoO_2 was hypothesized to be faster than the carburization of MoO_2 with CH_4 to form Mo_2C. Therefore, they concluded that carbide stability was due to the reaction of CO with MoO_2 to form Mo_2C, and that these kinetics were faster at higher pressures. They evaluated this hypothesis by operating at low pressures, but with a recycle stream that produced "back-mix" behavior and achieved stability for about 60 hours at high conversion, with a 1.17 fresh feed ratio of CO_2/CH_4. However, deactivation then took place, and since the spent catalyst was found to be pure Mo_2C, it was attributed to the loss of catalyst surface area.

Since low surface area molybdenum carbides have been considered to be a prime obstacle for catalytic applications, most of the previous research in this area has focused on the synthesis of high surface area catalysts [11-15]. However, other work in our laboratory demonstrated that the activity of Mo_2C for SMR at 8 bar was independent of the surface area, showing that a low surface area molybdenum carbide catalyst was stable for over 96 hours [16]. Furthermore, high surface area molybdenum carbide catalysts prepared by TPR methods, were found to behave similarly to the low surface carbide catalyst under DMR conditions at 8 bar pressure. In fact the results were similar to those reported by Sehested ***et. al***. [10], in that slow deactivation was observed, with no signs of oxidation. This prior work suggests that the stability of carbide catalysts under fuel reforming conditions may be related to redox chemistry and this, in turn, has prompted the present study, which is directed at the determination of conditions under which

molybdenum carbide catalysts will oxidize when exposed to various combinations of reforming gases at temperatures up to 850°C.

2. Experimental

2.1. Catalyst Characterization

The molybdenum carbide catalyst used in this study was a commercial Alfa Aesar Mo_2C lot# K17J11 (99.5% metals purity, <325 mesh). This catalyst was chosen for study in order to insure control of the catalyst properties before exposure to the oxidative reforming gases. That is, the high surface area catalysts are typically synthesized "in-situ" [6,10], using TPR methods, so catalyst properties are not directly measured prior to their use. That and the fact that surface area does not seem to be important for high temperature fuel reforming, were the basis for this choice. The bulk "Aesar" Mo_2C catalyst was characterized by X-Ray powder diffraction and shown to be pure β-Mo_2C (hcp) with an average crystallite size of 40 nm as estimated by the Debye-Scherrer method. The BET surface area of the fresh Aesar catalyst (Coulter BET Analyzer) was found to be less than 1 m^2/g and the carbon content of the Aesar Mo_2C was calculated to be 5.92 ± 0.21 wt.%, close to the stoichiometric value of 5.9%.

2.2. Experimental Procedures

All of the experiments were conducted *in-situ* using a Phillips X'Pert XRD System (Co Kα source), operated dynamically (DXRD) and equipped with a RAYTECH Position Sensitive Detector. The hot stage was an Anton Parr XRK 900, capable of operating at temperatures up to 900°C, pressures to 10 bar and with flow-through gases, so that it could be used to dynamically monitor the crystalline changes of the catalyst during exposure to reforming gases. In all cases, two high-resolution XRD scans at 45 – 49 and 27.5 – 32.5 °2Θ, were used to monitor changes in the Mo_2C, MoO_2 and Mo phases. Typically, 0.4 grams of Mo_2C were loaded on the sample holder and then pretreated in 42 SCCM of UHP H_2 (99.999%) at 700°C for one hour to remove any oxygen impurities prior to performing oxidation experiments. The outlet gas compositions were monitored by a Shimadzu GC 14A equipped with a Hayesep D column operating at 60 to 175°C. A bubble flow meter was used to measure the flow rates of exit gases and the flow of the feed gases was controlled by Brooks model 5850E mass flow controllers.

Steam was generated by delivering water to a steam generator, using a syringe pump and was then premixed with other gases in a stainless-steel heated line before introducing the mixture to the chamber. A total gas flow rate of 38 SCCM was used for all experiments. After H_2 pretreatment, the carbide catalyst was cooled to 40°C and then exposed to pre-purified N_2 while heating to 500°C at 10°C/minute, at which point, the predetermined concentrations of reforming gases were introduced into the chamber and the temperature was raised to 600°C. In non-isothermal experiments, the temperature was

then increased to 850°C, in 25°C increments, with XRD scans taken every 25°C. Isothermal experiments were also carried out by rapidly raising the temperature to 775°C in flowing nitrogen and then switching to the desired gas composition. Experiments consisted of the introduction of either of the two oxidizing gases, CO_2 or steam, with and without reducing and carburizing gases. Most experiments were conducted at 1 bar total pressure, but the effect the effect of total pressure on CO_2 oxidation was also studied, using pressures as high as 8 bars.

3. Results

3.1. Oxidation of Mo_2C in Steam

Figure 1 shows the DXRD results for an oxidation experiment carried out in 25% steam at atmospheric pressure. As can be seen, at temperatures between 625°C and 650°C, a peak corresponding to MoO_2 appears and continues to grow while the carbide peak decreases in intensity. Neither the Mo metal phase nor the MoO_3 phase was observed in these experiments, indicating that Mo_2C was directly oxidized to MoO_2 via the following reaction:

$$Mo_2C + 5H_2O \leftrightarrows 2MoO_2 + CO + 5H_2 \quad (1)$$

Although it is possible for the MoO_3 phase to melt/vaporize at high temperatures, its pure-phase melting point is 795°C, well below the initial oxidation temperatures observed here.

These results, in terms of the integrated peak areas of Mo_2C and MoO_2, normalized to the Mo_2C peak at 600°C, are shown in Figure 2 for both 5% and 25% steam. In both cases, the last temperature at which Mo_2C was stable was 600°C, and thus it appears that the initial onset of oxidation of Mo_2C is not a function of steam partial pressure, at least at these low pressures. Note however, that there is an increase in the oxidation rate at about 750°C and it is higher for the higher steam pressure. This "second stage" of oxidation at 750°C was observed in all of the oxidation experiments conducted in this study.

3.1.1. Oxidation of Mo_2C in Steam/H_2

Since H_2 is the major product of reaction (1), the effect of H_2 on the oxidation of Mo_2C in steam was studied by exposing Mo_2C to H_2/H_2O ratios as high as 0.64, while maintaining a constant steam feed pressure of 0.25 bar, and these results are plotted in Figure 3 in terms of the formation of both MoO_2 and Mo. From Figure 3A, it can be seen that as the hydrogen pressure is raised, the oxidation onset temperature is delayed and the initiation of the second stage of oxidation is less apparent. At the highest hydrogen pressure, the oxide phase is not observed, even at 850°C. However, as shown in Figure 3B, the Mo metal peak begins to form at 750°C at H_2/H_2O ratios of 0.48 and greater. It should be noted that the Mo and MoO_2 peak areas have been corrected for their relative

diffraction intensities, so the Mo metal concentrations are actually higher than the oxide concentrations at a ratio of 0.48. At the higher ratio of 0.64, Mo is the only product, although its rate of formation is lower. Whereas the metal could appear as a result of reduction of the oxide by the reverse of reaction (2):

$$Mo + 2H_2O \leftrightarrows MoO_2 + 2H_2 \quad (2)$$

this reaction is not thermodynamically favored, even at the highest H_2/H_2O ratio. However, at temperatures of about 700°C, the thermal decomposition of Mo_2C:

$$Mo_2C \leftrightarrows 2Mo + C \quad (3)$$

is thermodynamically favored and has been observed in previous studies [5,16-18]. Consequently, a series of DXRD experiments was conducted where the carbide was exposed to inert gases (N_2 and Ar) and to H_2 as the temperature was ramped to 850°C. In inert atmospheres, thermal decomposition took place at about 750°C but the carbide was totally stable in H_2 pressures of 0.05 and 0.5 bar, at temperatures up to 850°C and for as long as 4 hours at that temperature. This is in disagreement with the results of Ledoux *et. al.* [5] and Nagai *et. al.* [17], who observed decomposition of high surface area Mo_2C catalysts in 1.0 bar of H_2, at 650 and 800°C, respectively. However, in both cases, XPS was used to detect the occurrence of Mo_2C decomposition in H_2, which would be far more sensitive than XRD, which can only detect bulk phase changes. Given that the following reaction can also occur in the presence of H_2:

$$Mo_2C + 2H_2 \leftrightarrows 2Mo + CH_4 \quad (4)$$

and that its equilibrium constant at 750°C is 1.35 x 10^{-4} bar^{-1} (Fig. 4), ppm levels of surface CH_4 could easily prevent bulk decomposition, even though some surface decomposition could occur. In fact, Hojo *et. al*. [19], in a separate XRD study of the sintering of low surface area Mo_2C, found that all samples were stable up to 1500°C in H_2. Interestingly, Leclercq *et. al.* [18] carried out experiments with a low surface area Mo_2C catalyst (9 m^2/g) and, using XRD, also found it to be stable in 1.0 bar of hydrogen at 700°C.

Since oxidation rates increase at about 750°C, coincident with Mo_2C decomposition in an inert environment, it is possible that decomposition to the metal is an intermediate step in oxidation at higher temperatures. In order to explore this possibility, a separate set of isothermal, high temperature oxidation experiments were conducted in order to isolate the high temperature oxidation from that occurring at the lower temperatures. In these experiments, the temperature was rapidly raised to 775°C in flowing nitrogen and the sample was then exposed to 25% steam, with and without hydrogen. In all these experiments, there was no evidence of bulk carbide decomposition at the point where steam was introduced. Figure 5 shows a comparison of the results of steam oxidation for the non-isothermal experiments ramped from both 600°C and 775°C, along with an isothermal experiment conducted at 775°C. Given that the rate of change of the MoO_2 peak during a ramp is essentially the same, independent of the starting temperature, it can be concluded that the presence of the oxide formed at low temperatures does not affect

the higher temperature oxidation rate. As can be seen, the isothermal rate data decrease with time, a possible indication of a diffusion limited oxidation rate. The effect of H_2 on the high temperature oxidation at 775°C was also examined, using the highest H_2/H_2O ratio (0.64) employed in the low temperature non-isothermal experiments. The results were identical in that there was no detectable oxide formed, but the Mo metal formed slowly up until 200 minutes reaction time, at which point it remained constant for an additional 160 minutes.

3.2. Oxidation of Mo_2C in CO_2

Carbon dioxide is also a potential oxidant of Mo_2C, whether supplied in dry-methane reforming or produced by the water gas shift reaction during SMR. Oxidation experiments in 5% and 25% CO_2 were carried out in the same manner, as with steam and the results for oxidation onset were essentially the same as with steam. That is, there was no dependence of the oxidation onset temperature on CO_2 concentration and the onset temperature was the same; i.e., 625°C. However, the rate of the second stage of oxidation was higher with CO_2, as can be seen from Figure 6, which shows a comparison of oxidation in 25% CO_2 with oxidation in 25% steam. Note that there is the same "plateau" in oxidation rate, between 700°C and 750°C; probably indicative of the fact that the first stage of oxidation becomes diffusion limited until the second stage is initiated. In the first stage, oxidation occurs via equation (5), which was also corroborated:

$$Mo_2C + 5CO_2 \leftrightarrows 2MoO_2 + 6CO \quad (5)$$

by the appearance of CO in the exit gas at about 625°C, and there was no indication of the formation of either Mo or MoO_3.

3.2.1. Oxidation of Mo_2C in CO_2/CO

Since that CO is a product of CO_2 oxidation in reaction (5), similar experiments were also conducted in CO/CO_2 mixtures. Specifically, the carbide was exposed to CO/CO_2 ratios between 0.4 and 0.8 at temperatures of 600 – 850°C, using a constant feed partial pressure of CO_2 equal to 0.25 bar, and the experimental results are shown in Figure 7. From these results, it can be seen that the addition of CO retards the CO_2 oxidation of Mo_2C in a manner similar to the effect of H_2 on the oxidation by steam, except that oxidation could not be totally prevented, even at the highest CO/CO_2 ratio. A comparison of CO_2 versus steam oxidation at isothermal high temperature conditions (775°C) is shown in Figure 8. Based on these results it can be concluded that CO_2 is a stronger oxidizing agent than steam and the high temperature oxidation cannot be totally prevented by CO at the highest concentration employed in this study ($CO/CO_2 = 0.8$).

The effect of higher pressures on Mo_2C oxidation was also evaluated by studying the effect of pressure on CO_2 oxidation, using a 25% CO_2 concentration at pressures from 1 to 8 bar at 700°C. These conditions were chosen on the basis of Claridge *et. al.*'s [6] conclusions that 8 bar pressure was necessary to avoid carbide oxidation and the fact that problems with CO cracking in the DXRD chamber restricted the maximum temperature to 700°C. In addition, the effect of CO on the carbide oxidation at high pressures was

also evaluated at these same pressures, using a CO/CO_2 ratio of 0.2, which was the highest ratio possible without experiencing CO cracking at 8 bar. It was found that over the temperature range tested in this study, there were no significant effects of pressure on either direct oxidation in CO_2 or with CO inhibition.

3.3. Oxidation of Mo_2C in Reforming Gas Mixtures

In the early applications of Mo_2C to reforming, it was mentioned that the reformer had to be run at equilibrium conversions in order to avoid oxidation [6]. This observation prompted Sehested *et. al*. [10] to run a dry reformer in a recycle mode, using an extremely high recycle ratio. While they reported improved stability, the catalyst underwent a slow deactivation, which was attributed to loss of surface area. They argued that the oxidation resistance was influenced by the activity of the catalyst for the Water Gas Shift reaction (WGS: $CO + H_2O \leftrightarrows CO_2 + H_2$), as originally reported by Patt *et. al*. [2]. However, no mention was made as to the whether the surface area loss was due to sintering or coking. Consequently, a series of experiments were conducted here, where the catalyst was exposed to various mixtures of CH_4, H_2, CO and CO_2, at concentrations based on equilibrium conversions of combined SMR/WGS reactions at 800°C. While CH_4 pressures were limited to a maximum of 0.05 bar, it was found that, in every case, the catalyst was totally oxidation resistant at 800°C, for 6 hours. Since CH_4 conversions were essentially 100%, subsequent experiments were then conducted to determine which of the other components were responsible for the stability, and to attempt to correlate the results with a "carburizing ratio", which was defined as the ratio of the pressure of

carburizing gases (H_2 + CO) to the pressure of oxidizing gases (H_2O + CO_2). Note that hydrogen is indirectly a carburizing gas since it can interact with the carbide to form methane. The results of these experiments for the high temperature oxidation are shown in Table 1 and it appears that the stability of the carbide does correlate with this carburizing ratio, with stability favored at ratios greater than 0.8.

4. Discussion and Conclusions

Based on these results, there appears to be two separate routes for the oxidation of Mo_2C catalysts in reforming atmospheres; one is prevalent at about 600^oC, and the other at temperatures above 750^oC. At the lower temperatures, oxidation in steam and CO_2 proceeds via reactions (1) and (5), respectively:

$$Mo_2C + 5H_2O \leftrightarrows 2MoO_2 + CO + 5H_2 \quad (1)$$

$$Mo_2C + 5CO_2 \leftrightarrows 2MoO_2 + 6CO \quad (5)$$

These reactions occurred at about 625 ^oC and were independent of steam and CO_2 pressures up to 0.25 bar. Reaction (1) was readily inhibited by hydrogen and reaction (5) was inhibited by CO, and both are consistent with thermodynamics at these temperatures (Fig. 5). The equilibrium constant for reaction (1) is such that moderate concentrations of H_2 favor the reverse reaction. In fact, it is doubtful that this reaction will occur at H_2/H_2O ratios above 0.4, consistent with the results in Figure 3. The effect of CO on reaction (1)

was not specifically evaluated in these experiments, due to the rapid occurrence of the water gas shift reaction over the carbide catalyst, as has been reported by others [2]. With respect to reaction (5), the ability of CO to inhibit reaction (5) is also consistent with thermodynamics, where even low CO/CO_2 ratios favor the reverse reaction.

At higher temperatures, however, the situation is quite different. It is hypothesized that at temperatures above 750^{o}C, the following mechanism is dominant:

$$Mo_2C + 2H_2 \leftrightarrows 2Mo + CH_4 \quad (4)$$

$$Mo + 2H_2O \leftrightarrows MoO_2 + 2H_2 \quad (6)$$

$$Mo + 2CO_2 \leftrightarrows MoO_2 + 2CO \quad (7)$$

That is, Mo_2C decomposes to the metal at about 750^{o}C, and the metal is then rapidly oxidized by either H_2O or CO_2. The rates of reactions (6) and (7) are sufficiently high, that the metal is not detected in the XRD scans. This was confirmed by separate DXRD experiments where Mo was exposed to 25% steam at 750^{o}C and the initial oxidation rate was found to be five times faster than the initial oxidation rate of Mo_2C. However, bulk decomposition is easily prevented by even low H_2 concentrations, as has been reported in the literature [18,19] and verified by our own DXRD experiments. It appears that this is due to the formation of surface concentrations of CH_4 by reaction (4), which then forces reaction (8):

$$2MoO_2 + 5CH_4 \leftrightarrows Mo_2C + 4CO + 10H_2 \quad (8)$$

to the right, as can be seen from the equilibrium constants in Figure 4. The presence of the Mo metal phase at high temperatures and H_2 pressures can be explained by the presence of steam, which results in the reforming of the CH_4 that is formed by reaction (4). This was verified by separate experiments where very low concentrations of methane readily reformed at temperatures between 600°C and 850°C. Further evidence to support this mechanism is the fact that the Mo phase appears prior to the oxide at $H_2/H_2O = 0.48$ (see Figure 3).

For this mechanism to be viable, it must also explain the difference in the rate of Mo formation when the H_2/H_2O ratio is raised from 0.48 to 0.64. As shown in Figure 3, the rate of formation of Mo is much slower at the higher ratio, and this result is repeatable. An explanation here lies in the effect of H_2 on the steam reforming of the surface CH_4 that forms from reaction (4). At higher hydrogen pressures, the reforming rate would be adversely affected, resulting in higher surface CH_4 concentrations and consequently in lower Mo formation rates. Thus, the relative occurrence of Mo versus MoO_2 is a complex function of the effect of hydrogen on both the kinetics of the steam reforming of methane and the steam oxidation of Mo metal.

The fact that CO is not able to completely prevent CO_2 oxidation of the carbide at the higher temperatures, can now be explained. Whereas the oxidation of Mo_2C by CO_2 follows a similar pattern as in steam oxidation, there is no H_2 present to prevent carbide decomposition at the higher temperatures. Thus, the fact that CO_2 appears to be a stronger oxidant at higher temperatures is probably due to the fact, that metal formation cannot be

prevented and oxidation of the metal by CO_2 is a relatively fast reaction. Thus, CO has a smaller influence on the kinetics of the CO_2 oxidation of Mo than does H_2 on the steam oxidation of Mo.

Based on the results reported here, a carburizing ratio is able to predict the stability of the carbide to oxidation, with stability predicted at ratios higher than 0.8. These result are also consistent with the recycle experiments of Sehested *et. al*. [10] who did not observe oxidation, since their carburizing ratios were on the order of 8-10. On the other hand, the stabilizing effect of higher pressures, as reported by Claridge *et. al*. [6], cannot be explained through the use of the carburizing ratio. However, their observations were made in the presence of reforming, at higher reactant/product concentrations and higher temperatures. The effect of high concentrations of CH_4 was not evaluated in this work, due to equipment limitations. This implies that a definitive prediction of the stability of Mo_2C to oxidation would require a knowledge of the interactive kinetics of oxidation and carburization, will be necessary, as first suggested by the same authors. Another factor to consider is the effect of space velocity on oxidation stability. The space velocities used by Claridge *et. al*. were lower than those employed here and by Sehested *et. al*. In fact, when Claridge *et. al*. attempted higher space velocities, the catalyst underwent rapid oxidation, indicating that the catalyst is not stable to oxidation in the stoichiometric feed. So it is possible that there is a separate effect of pressure, which is tied to the state of mixing at the catalyst surface.

Acknowledgement

This material is based on work supported by the National Science Foundation under Grant CTS-0209372. The authors also wish to acknowledge the support of BP for providing partial support to A.R.S. Darujati.

References

1. M. Nagai, K. Oshikawa, T. Kurakami, T. Miyao, S.Omi, J. Catal. 180 (1998) 14.
2. J. Patt, D.J. Moon, C. Philips, L. Thompson, Catal. Letter. 65 (2000) 193.
3. S. Ramanathan, S.T. Oyama, J. Phys. Chem. 99 (1995) 16365.
4. J. Choi, J.R. Brenner, L.T. Thompson, J. Catal. 154 (1995) 33.
5. M.J. Ledoux, C.P. Huu, J. Guille, H. Dunlop, J. Catal. 134 (1992) 383.
6. J. B. Claridge, A.P.E. York, A.J. Brungs, C. Marques-Alvarez, J. Sloan, S.C. Tsang, M.L.H. Green, J. Catal. 180 (1998) 85.
7. C.C. Yu, S. Ramanathan, B. Dhandhapani, J.G. Chen, S.T. Oyama, J. Phys. Chem. B 101 (1997) 512.
8. K.R. McCrea, J.W. Logan, T.L. Tarbuck, J.L. Heiser, M.E. Bussell, J. Catal. 171 (1997) 255.
9. B. Dhandhapani, S. Ramanathan, C.C. Yu, B. Fruberger, J.G. Chen, S.T. Oyama, J. Catal. 176 (1998) 61.
10. J. Sehested, C.J.H. Jacobsen, S. Rokini, J.R. Rostrup-Nielsen, J. Catal 201 (2001) 206.
11. Volpe, L., Boudart, M., J. Solid State Chem. 59 (1985) 332.
12. Lee, J.S., Oyama S.T., Boudart, M.J., J. Catal. 106 (1987) 125.
13. Ledoux, M.J., Pham-Huu, C., Catal. Today 15 (1992) 263.
14. Preiss, H., Meyer, B., Olchewski, C., J. Mater Sci. 33 (1998) 713.
15. Choi, J.G., Curl, R.L., Thompson, L.T., J. Catal. 146 (1994) 218.
16. David C. LaMont, Andrew J. Gilligan, Anna R.S. Darujati, Anand S. Chellappa, and William J. Thomson, "*The Role of Surface Area on the Activity and Stability of Mo_2C Catalysts for Oxidative Methane Reforming*", Appl. Catalysis A, in press.
17. Nagai, M., Kurakami, T., Omi, S., Catal. Today 45 (1998) 235.
18. Leclercq, G., Kamal, M., Lamonier, J. F., Feigenbaum, L., Malfoy, P., Leclercq, L., Applied Catal. 121 (1995) 169.
19. Hojo, J., Tajika, M., Kato, A., J. of the Less-Common Metals, 75 (1980) 11.

Table 1. Oxidation Results in Various Gas mixtures

No.	CO [bar]	H_2 [bar]	CO_2 [bar]	H_2O [bar]	N_2 [bar]	Carburizing Ratio[1]	T [°C]	Results
1	0.02	0.16	0.02	0.16	0.65	1.00	800	No oxidation
2	0	0.16	0.02	0.16	0.67	0.89	800	No oxidation
3	0.02	0	0.02	0.16	0.81	0.11	800	Oxidation
4	0	0	0.25	0	0.76	≈ 0	775	Oxidation
5	0.20	0	0.25	0	0.56	0.80	775	Oxidation
6	0.15	0.05	0.20	0.05	0.56	0.80	775	Oxidation
7	0	0	0	0.25	0.76	0.10	775	Oxidation
8	0	0.16	0	0.25	0.60	0.64	775	Mo metal formation
9	0.03	0.06	0.06	0.24	0.63	0.28	775	Oxidation
10	0.05	0.09	0.09	0.25	0.53	0.40	775	Oxidation
11	0.14	0.09	0.25	0.14	0.39	0.59	775	Oxidation
12	0.31	0.16	0.20	0.05	0.28	1.88	775	No oxidation
13	0.03	0.26	0.04	0.25	0.43	1.00	775	No oxidation
14	0.13	0.15	0.15	0.13	0.45	1.00	775	No oxidation

[1] $(H_2+CO)/(H_2O+CO_2)$

A.R.S. Darujati *et. al*. (Figure 1)

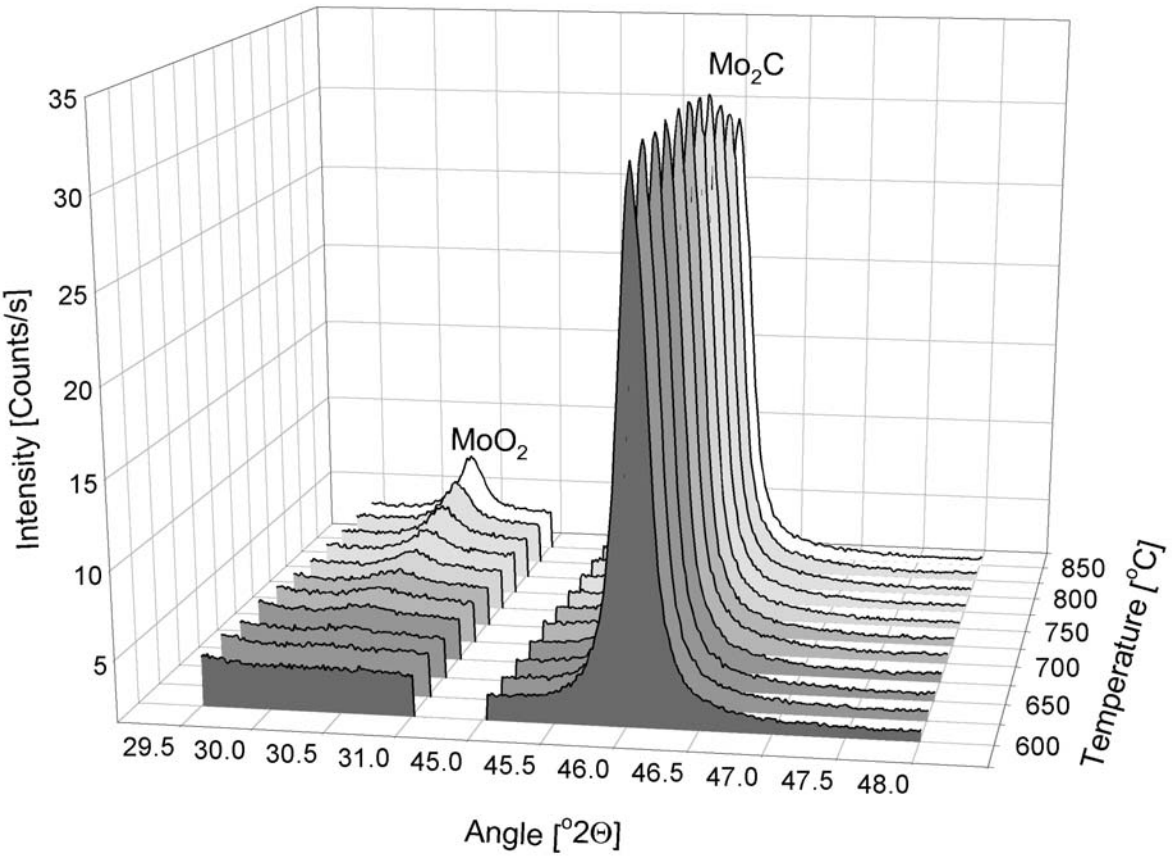

Figure 1. *In-situ* DXRD scans (Co Kα radiation) – oxidation of Aesar Mo_2C phase with P_{H2O} = 0.25 bar.

A.R.S. Darujati *et. al*. (Figure 2)

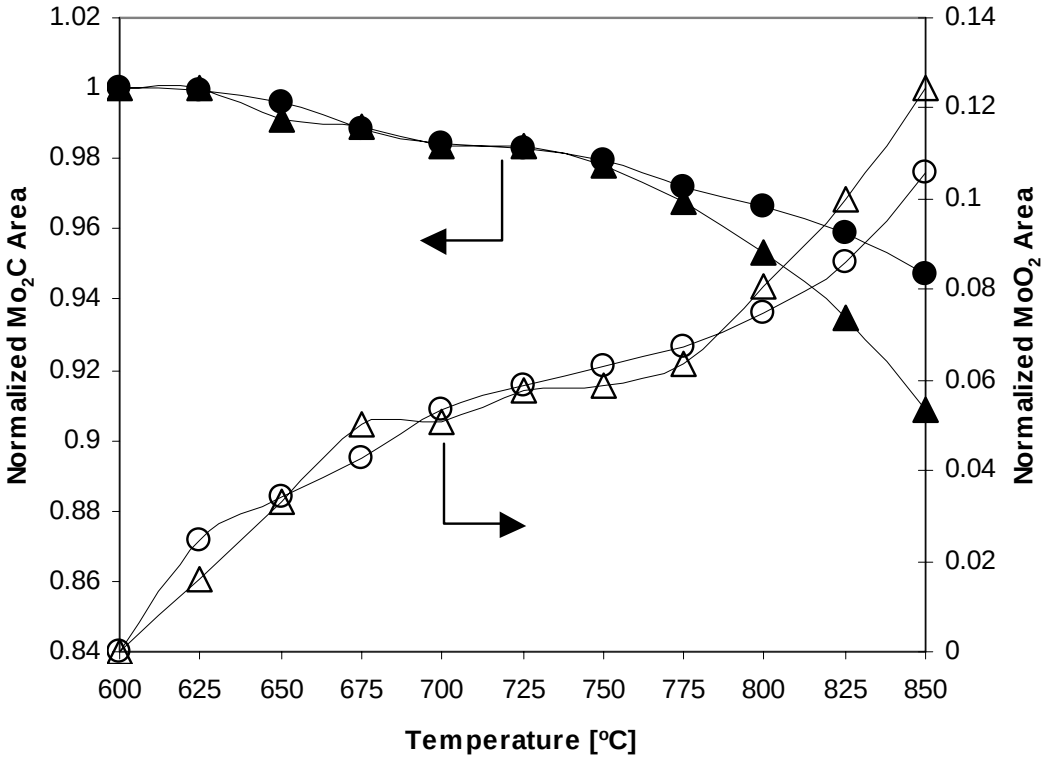

Figure 2. Normalized peak areas of Mo_2C and MoO_2 during oxidation of Mo_2C in steam. Mo_2C, P_{H2O} = 0.25 bar (▲); Mo_2C, P_{H2O} = 0.05 bar (●); MoO_2, P_{H2O} = 0.25 bar (△); MoO_2 , P_{H2O} = 0.05 bar (○). Connecting lines added for clarity.

A.R.S. Darujati *et. al*. (Figure 3A and 3B)

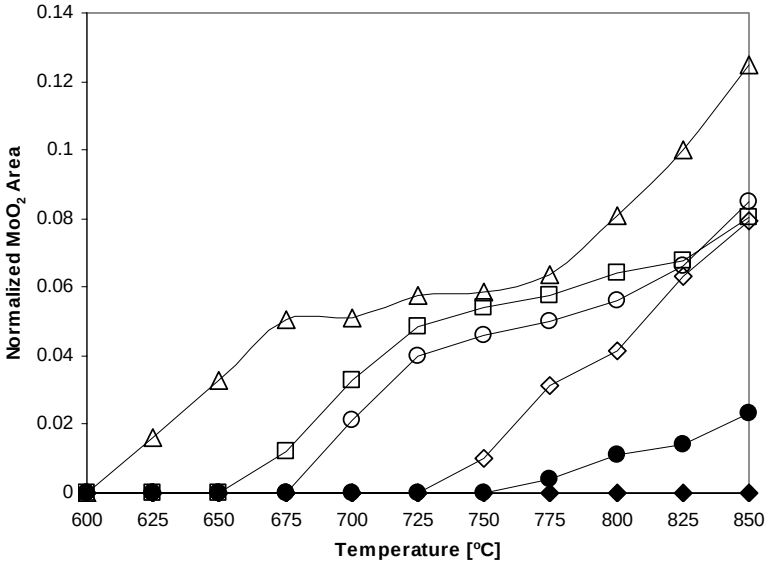

Figure 3A. Normalized peak areas of MoO_2 in steam/H_2 at P_{H2O} = 0.25 bar H_2/steam = 0 (△); H_2/steam = 0.2 (□); H_2/steam = 0.28 (○); H_2/steam = 0.4 (◇); H_2/steam = 0.48 (●); H_2/steam = 0.64 (◆). Connecting lines added for clarity

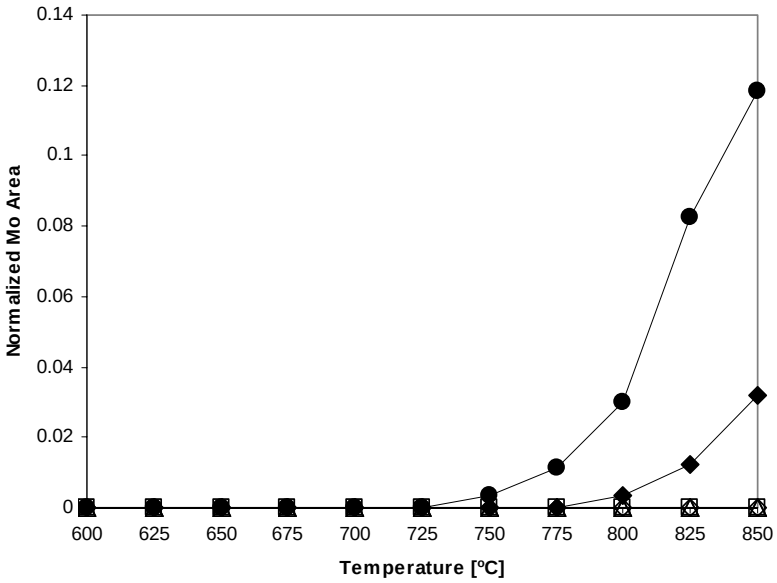

Figure 3B. Normalized peak areas of Mo during oxidation of Mo_2C in steam/H_2 at P_{H2O} = 0.25 bar H_2/steam = 0 (△); H_2/steam = 0.2 (□); H_2/steam = 0.28 (○); H_2/steam = 0.4 (◇); H_2/steam = 0.48 (●); H_2/steam = 0.64 (◆). Connecting lines added for clarity.

A.R.S. Darujati *et. al*. (Figure 4)

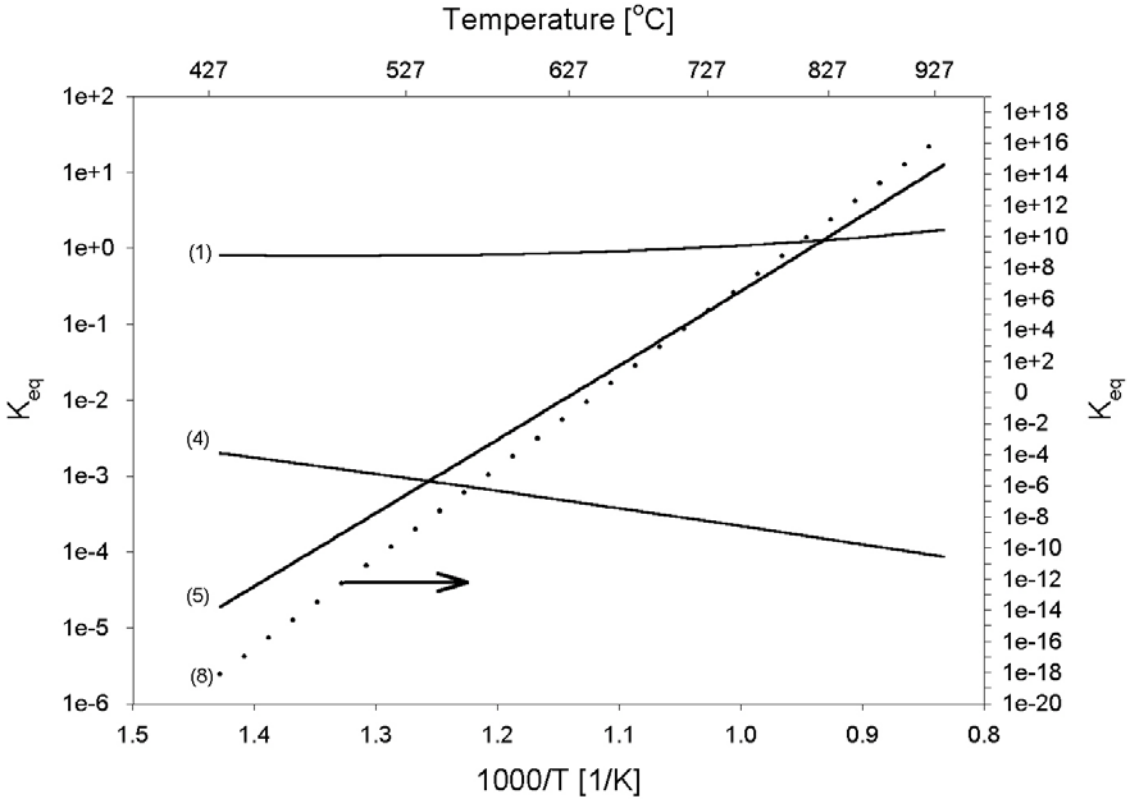

Figure 4. Equilibrium constants for reactions (1), (4), (5) and (8).

A.R.S. Darujati *et. al*. (Figure 5)

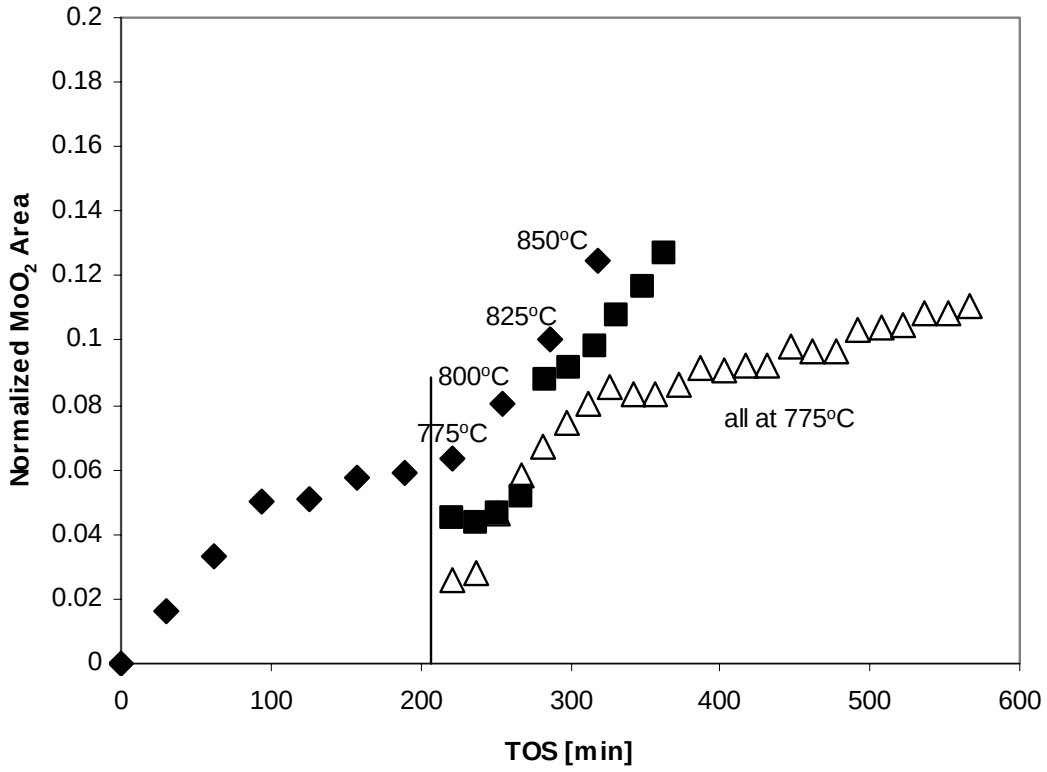

Figure 5. High temperature oxidation at P_{H2O} = 0.25 bar. Temperature ramp from 600°C (◆); Temperature ramp from 775°C (■); isothermal temperature at 775 °C (△).

A.R.S. Darujati *et. al*. (Figure 6)

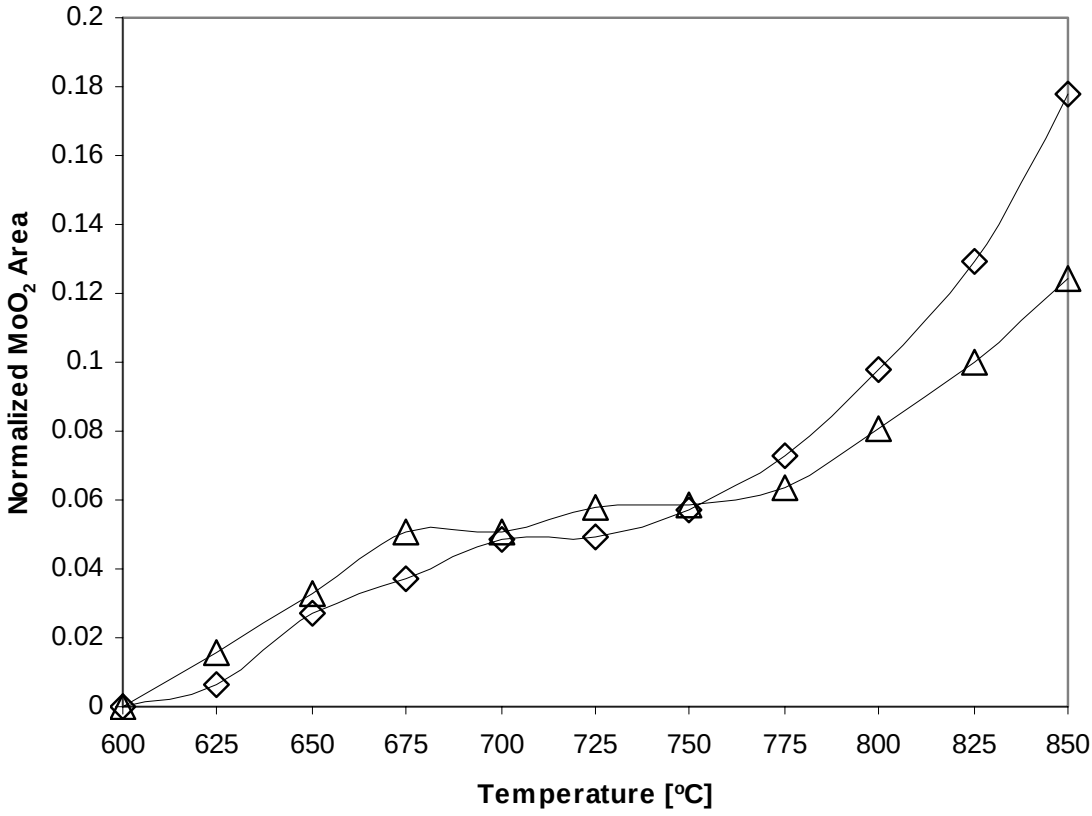

Figure 6. Comparison of H_2O and CO_2 oxidation as a function of temperature.

P_{H2O} = 0.25 bar (△); P_{CO2} = 0.25 bar (◇)

A.R.S. Darujati *et. al*. (Figure 7)

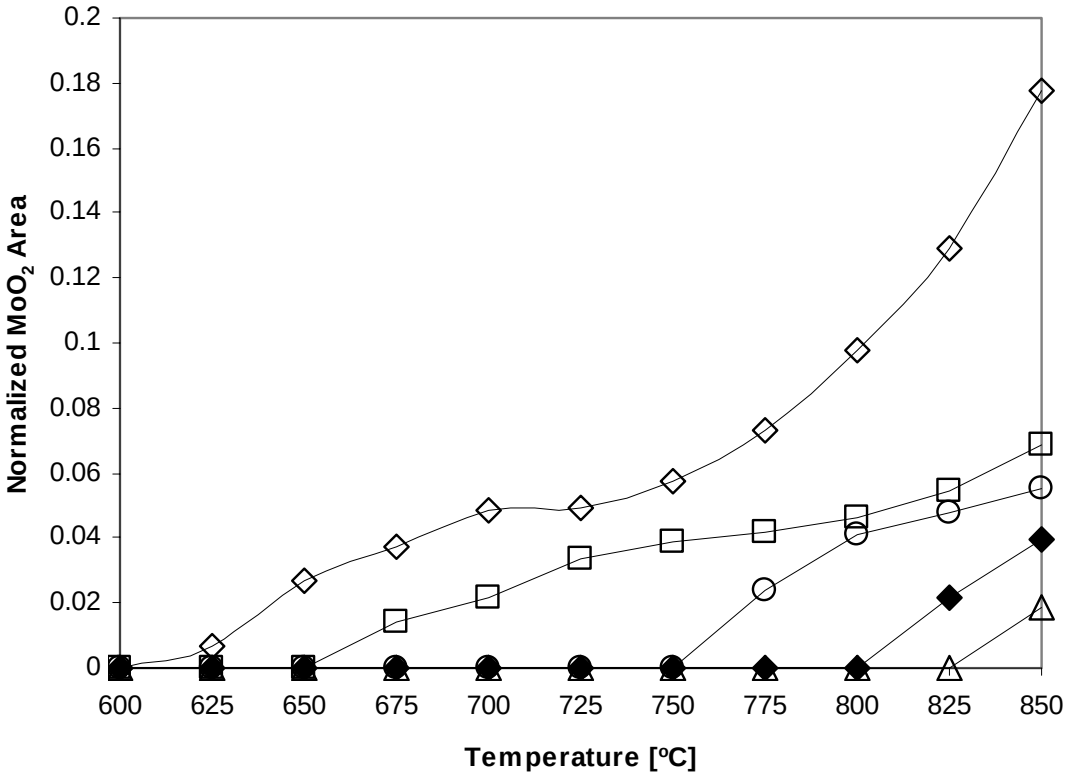

Figure 7. Effect of CO on CO_2 oxidation at P_{CO2} = 0.25 bar. CO/CO_2 = 0 (◇); CO/CO_2 = 0.2 (□); CO/CO_2 = 0.4 (○); CO/CO_2 = 0.6 (◆); CO/CO_2 = 0.8 (△). Connecting lines added for clarity.

A.R.S. Darujati *et. al*. (Figure 8)

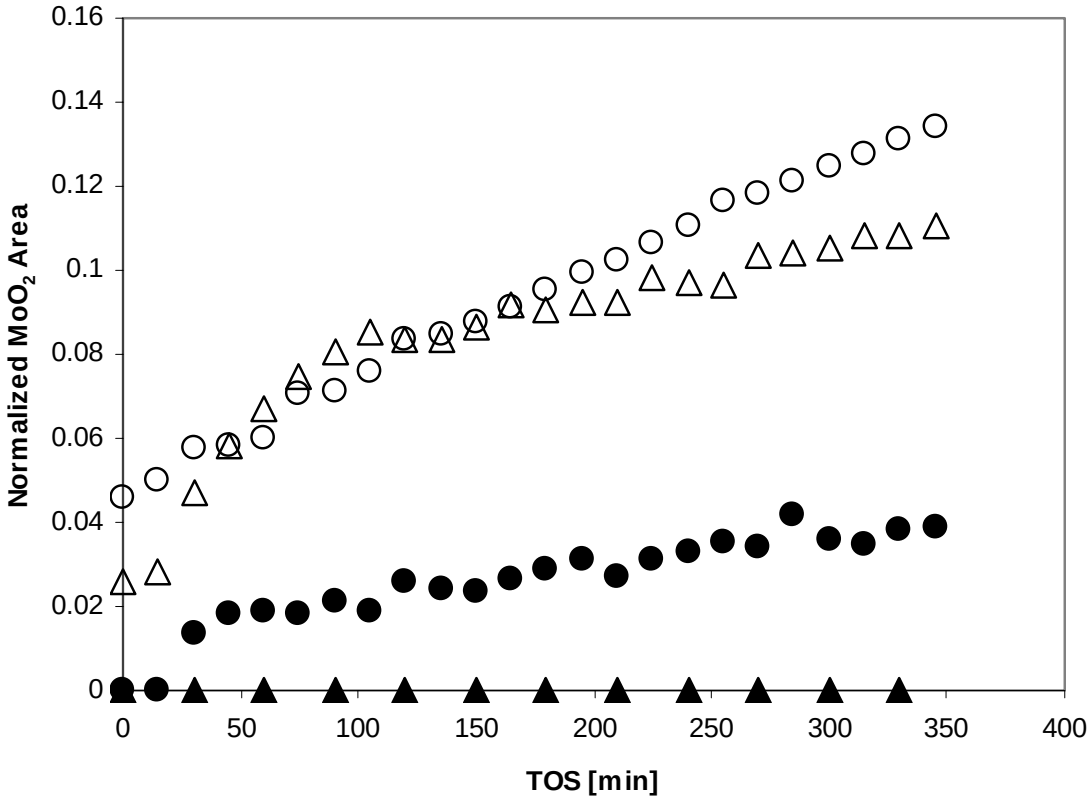

Figure 8. Comparison of H_2O and CO_2 oxidation at 775°C; $H_2/H_2O = 0$ (△); $CO/CO_2 = 0$ (○); $H_2/H_2O = 0.64$ (▲); $CO/CO_2 = 0.8$ (●).

CHAPTER THREE

STABILITY OF SUPPORTED AND PROMOTED-Mo_2C CATALYSTS IN DRY-METHANE REFORMING

Anna R.S. Darujati, William J. Thomson*

Department of Chemical Engineering, Washington State University, P.O. Box 642710, Pullman, WA 99164-2710, USA

* Corresponding author. Tel.: +1 509 335 8580; FAX: +1 509 335 4806; e-mail: thomson@che.wsu.edu

Abstract

The stability of Mo_2C in dry-methane reforming (DMR) was studied over Al_2O_3, ZrO_2 and MgO supports and in the presence of Ce, K and Zr promoters at 900 ^oC, 1 bar, a GHSV of 3,800 h^{-1} and a stoichiometric feed. All catalysts deactivated via moving front oxidation under these conditions. The γ-Alumina appeared to be superior compared to other supports due to its high surface area and high thermal stability, and $Mo_2C/\gamma\text{-}Al_2O_3$ had a much higher activity than a bulk Mo_2C catalyst. Over this support, a high Mo loading was found to be crucial for maintaining the stability of the catalyst due to the higher concentration of more reducible Mo oxides and the higher CH_4 conversion over the carbide. The impregnation order was found to be an important factor for Ce, and the 3 wt.% $Ce\text{-}Mo_2C/\gamma\text{-}Al_2O_3$ was found to be the most stable catalyst due to the redox properties of the Ce promoter. On the other hand, the addition of CO in the feed, while preventing oxidation of all catalysts, resulted in slow deactivation due to coking over the Ce-promoted catalyst.

Keywords: Molybdenum Carbide, Supports, Promoter, Oxidation, Stability, Dry-methane Reforming

1. Introduction

Molybdenum carbide (Mo_2C) has been studied as a catalyst for steam methane reforming (SMR) [1,20], dry methane reforming (DMR) [1-5] and partial oxidation of methane (POM) [6], with the majority of the studies having been carried out over unsupported Mo_2C. The first study conducted by York *et. al.* [1] found that these catalysts possessed reforming activity comparable to noble metals while being less susceptible to coking than nickel, but deactivated via oxidation of Mo_2C to inactive MoO_2. Analogous conclusions have been drawn by other researchers, and several studies have focused on the oxidative stability of Mo_2C under reforming conditions [1-4]. Oxidation of Mo_2C during reforming has been found to be preventable by operating the reformer at higher pressures [1,20] or at atmospheric pressure under either back-mix conditions [3] or temperatures in excess of 950 ^oC [4]. In line with these findings, we previously showed [7] that Mo_2C catalysts were stable in the presence of reforming gases at atmospheric pressure, provided that a "stability ratio", defined as the ratio of carburizing gases to oxidizing gases,

$$R_s = \frac{P_{H_2} + P_{CO}}{P_{CO_2} + P_{H_2O}}$$

was maintained at values greater than 0.8. Furthermore, LaMont and Thomson [4] found that the stability of Mo_2C during DMR was related to the mass transfer of reforming product gases ($CO+H_2$) from the surface of the catalyst. Under mass transfer limited conditions, such as high pressure, high temperature and low molar feed velocities,

oxidation of Mo_2C to form MoO_2 could be prevented [4]. These observations also explain the stability of Mo_2C at high pressure formerly proposed by York *et. al.* [1].

Dispersing the active metal on a high surface area support material and the use of promoters is known to improve catalyst stability and activity. However, only a few studies have been conducted to test the effect of supports and promoters on the stability of Mo_2C under reforming conditions. Brungs *et. al.* [8] reported that among several Mo_2C supported catalysts tested for DMR, a γ-Al_2O_3 support was superior to ZrO_2, SiO_2 and TiO_2. On the other hand, studies by Tsuji [9] and Naito [10] have shown that the stability of ZrO_2-supported Mo_2C with a low Mo metal loading (1 wt. %) was superior to that of both unsupported Mo_2C and Mo_2C supported on other materials. Zirconia was proposed to reduce coke formation and CO_2 activation was reported to take place at the metal – support interface, thereby reducing oxidation of Mo_2C.

In this paper, a systematic study of the effect of supports and promoters on the stability of Mo_2C during DMR is presented. The activity and stability of Mo_2C were tested using oxide supports, ranging from a high surface area γ-Al_2O_3, to a low surface area basic MgO; the latter being due to its ability to reduce coking over supported Ni [11] and noble metal catalysts in reforming [12]. Since a combination of promoters and supports can significantly improve catalyst stability, Ce, K and Zr promoters were tested due to their properties as textural and structural promoters. Ceria promotion was chosen on the basis of reports that it increased the stability of Ni reforming catalysts [13-15]. Several studies have demonstrated that ceria-promoted Ni can also undergo redox

reactions with CO_2 [16], can promote increased dispersion of active metals [14,15] and inhibit the phase transformation of γ-Al_2O_3 to α-Al_2O_3 [17]. Potassium was chosen due to its ability to control coking during reforming over Ni catalysts [18,19] and zirconia was chosen since earlier work suggested the presence of a redox mechanism similar to that with ceria [16,20].

2. Experimental

2.1. Catalyst Synthesis

Except for MgO, all supports were purchased from Alfa Aesar. The MgO support was synthesized by calcination of magnesium carbonate, $4MgCO_3.Mg(OH)_2.4H_2O$ (Alfa Aesar), at 800^{o}C for 4 hours in air, as described by Ruckenstein [12]. In general, catalysts were synthesized using the incipient wetness impregnation method. This preparation consisted of support impregnation with a solution of $(NH_4)_6Mo_7O_{24}.4H_2O$ precursor followed by drying, and calcination of the sample at 500 ^{o}C for 4 hours to form MoO_3. The carbide was synthesized by in-situ reduction of the supported MoO_3 in 50 μmol/s H_2 at 850 ^{o}C for 2 hours, followed by drying and carburization of the reduced sample in a 20% CH_4/H_2 mixture (126 μmol/s) at 675 ^{o}C for 2 hours to produce supported Mo_2C. Since the maximum loading per impregnation was limited by the solubility of the metal precursor in solution, multiple impregnations were carried out as required. Whenever multiple impregnations were done, samples were dried at 90^{o}C for 15 hours between impregnations. The Mo loading was varied between 5 and 30 wt.%.

All promoted-supported catalysts were prepared by impregnation of the supports with a solution of promoter precursors, such as K_2CO_3 (Alfa Aesar), $Ce(NO_3)_3.6H_2O$ (Alfa Aesar) and $ZrO(NO_3)_2.6H_2O$ (Aldrich). The loadings of the promoters were 0.1, 0.5 and 3 wt.% for K and Ce, and 3 and 15 wt.% for Zr. Although in most cases, the promoter precursor was impregnated and calcined prior to impregnation with the Mo precursor, in a limited number of experiments the influence of the promoter impregnation sequence on the stability of the catalysts was also evaluated. In these experiments, all catalysts were calcined prior to performing in-situ carburization, which was the last step during catalyst preparation. For simplicity, unpromoted catalysts are denoted as x-Mo/support with x being the weight percentage of Mo. For example, 30Mo/γ-Al is 30 wt.% Mo_2C supported on γ-Al_2O_3. For promoted-supported samples, the catalysts identification follows the order of deposition and calcination. For example, 30Mo-3Ce-*c* means 30 wt. % molybdenum is impregnated before 3 wt.% Ce and both Mo and Ce are impregnated before calcination. Tables 1 and 2 show all the catalyst samples that were employed in this study, along with their BET surface areas.

2.2. Catalyst Characterizations

Catalyst surface areas and pore volumes were measured with a Coulter SA 3100™ Analyzer. Repeated BET surface area measurement of synthesized catalysts indicated that the data were precise within 5%. Molybdenum loadings determined by calculation and measured by neutron activation analysis (NAA) showed that the calculated loadings

were within 8% of the measured values. A high temperature, in-situ X-ray diffractometer, XRD, (Phillips diffractometer, Co Kα radiation) was used to dynamically monitor the crystalline transformations of the supports in inert (N_2) or reducing (N_2/H_2) environments, and to monitor the crystal structure of the sample during each stage of synthesis. Surface concentrations of Mo and Ce in selected fresh samples were measured by X-ray photoelectron spectroscopy (XPS) with Mg Kα excitation energy of 1253.6 eV., and calculated on the basis of the Mo*3d,* Ce*3d* and Al*2p* energies. Based on three measurements of identical samples, the surface concentration values obtained from XPS varied within 10% of the averaged measured values.

2.3. Catalyst Testing

All dry-methane reforming (DMR) experiments were conducted by loading 1.3 g of the supported MoO_3 into an 8mm ID quartz tube microreactor for reduction in hydrogen and carburization. After carburization was completed, the reactor was cooled to room temperature, and then the gas composition was switched either to 100% CH_4 prior to starting reforming experiments, or to a 1% O_2/He mixture overnight, prior to removal from the reactor for characterization. The DMR experiments consisted in feeding a stoichiometric feed mixture ($CH_4 + CO_2$) at a rate of 70 SCCM (gas hourly space velocity (GHSV) of 3,800 h^{-1}) and a molar feed velocity (G) of 0.37 mol/cm^2/h. Experiments were initiated by ramping in pure CH_4 to 850^{o}C, at which time CO_2 was introduced to the reactor. The ramp was continued to 900^{o}C and held for 7 hours. An SRI gas chromatograph, equipped with molecular sieve 13X and Hayesep D columns, was used to

monitor the outlet gas compositions and a bubble flow meter was used to measure the exit gas flow rates. Experiments were terminated by stopping the flow of CO_2 and quenching the reactor in CH_4. A blank DMR experiment with only quartz wool at 900^oC showed a CH_4 conversion of less than 4%.

3. Results

3.1. Unpromoted Mo_2C Catalysts

As can be seen from Table 1, the surface area of freshly calcined, unpromoted-supported catalysts generally decreased as Mo loading increased, the exception being the low surface area MgO support. As expected, both carburization and reaction resulted in lowered surface area, probably as a result of the higher temperatures employed in those two processes. Nevertheless, the γ-Al_2O_3 support maintained relatively high surface areas on the order of 100 m^2/g, even after exposure to DMR conditions and was independent of Mo loading. Figure 1 shows the crystalline structure as measured by XRD, as the 30Mo/γ-Al catalyst was synthesized. In this sequence, the development of MoO_3, Mo and Mo_2C is readily evident as the catalyst is calcined, reduced in H_2 and finally carburized. Using the Debye-Scherrer equation, the average Mo_2C crystallite size of the 30Mo/γ-Al catalyst was found to be 186 Å.

Figures 2 and 3 show the stability testing results of the supported catalysts at 900^oC and 1 bar with stoichiometric feeds. Note that the conversions corresponding to the lower

surface area supports (Fig. 2) were all much lower than the equilibrium conversion of 97%. In addition to the low conversions, the MgO and α-Al_2O_3 supported catalysts suffered deactivation due to oxidation of the Mo_2C. In the case of α-Al_2O_3, this is attributed to the low CH_4 conversions, which do not generate sufficient H_2 and CO to keep the stability ratio above 0.8. While this is also true of the MgO supported catalyst, it also experienced sintering during the first hour of reaction, which was corroborated by XRD measurements that showed a 25% increase of MgO crystallite size as the temperature was increased from room temperature to 950 ^oC.

The Mo/Zr catalysts were more stable and the CH_4 conversions over these catalysts were higher, although still well below the equilibrium value. Between 5 and 30 wt.% Mo loadings, the conversions were all about the same and the catalysts slowly deactivated with a rate of about 1.5%/h. In a previous study, Tsuji *et. al.* [9] observed that the stability of ZrO_2-supported Mo_2C improved when the Mo loading was very low (<1 wt.%). As shown in Figure 2, reducing the Mo loading from 5 to 1 wt. % decreased the overall conversion to about 30%, however, the catalyst deactivated at about 1.3%/h, only slightly lower than that of the higher Mo loading catalysts. XRD scans of the 15 and 30 wt.% spent samples indicated that the catalysts had oxidized. In addition, separate sintering experiments of the ZrO_2 support resulted in a 70% increase of crystallite size as the temperature was increased from 600 to 950 ^oC, implying that sintering and oxidation were the cause of the slow but steady deactivation in these catalysts.

Figure 3 shows the CH_4 conversion with time on stream over the high surface area Mo/γ-Al catalysts. The initial CH_4 conversions for the two highest Mo loading catalysts were essentially at equilibrium, but both catalysts experienced significant deactivation over the course of the 7 hour run, with the 15Mo/γ-Al catalyst deactivating at a much higher rate. The initial conversion over the 5Mo/γ-Al catalyst was much lower (57%) and also deactivated, but at a lower rate. Analysis of the spent 15 and 30 wt.% Mo loading catalysts indicated that oxidation of the Mo_2C had occurred. It is likely that this was also true of the 5Mo/γ-Al catalyst but XRD was unable to detect MoO_2 in this low loading catalyst.

3.2. Promoted Mo_2C Catalysts

3.2.1. Effect of Promoter Loadings

The results over the unpromoted, supported catalysts showed that the high surface area γ-Al_2O_3 was the most active support. However deactivation of the catalyst over the γ-Al_2O_3 supports was due to oxidation and not to the sintering of the support. Consequently, the γ-alumina support was chosen to evaluate the effect of promoter addition on catalytic stability during DMR. The results described in the previous section also indicated that ZrO_2-supported Mo_2C, despite its relatively low CH_4 conversions, was the most stable support due to its low propensity for coking and oxidation. Because of this and since other researchers have reported improvement in the stability of Pt supported on ZrO_2-Al_2O_3 (10 wt. % Zr) for both DMR [21] and autothermal reforming

(ATR) [22], we also investigated the use of ZrO_2 as a promoter, with the goal of exploiting the thermal stability of γ-Al_2O_3 and the high coking resistance of ZrO_2. For Ce and K promoted catalysts, the loadings ranged from 0.1 to 3 wt.%, for both 15 and 30 wt. % Mo loadings. In the case of Ce and K, both the promoter and the Mo precursor were impregnated prior to calcinations. For Zr-promoted catalysts, the method previously employed by Souza *et. al.* [21] was used to synthesize catalysts with 3 and 15 wt.% Zr promoter loadings. This method was carried out by impregnating and calcining the Zr precursor on the γ-Al_2O_3 support prior to impregnation of the Mo precursor.

Table 2 shows a summary of the BET surface areas and the surface Mo concentrations of the promoted and unpromoted Mo/γ-Al catalysts. As can be seen, there was minimal influence of either Ce or K on the BET surface area of the calcined catalysts. However, a dramatic drop of surface area was observed in the spent K-promoted catalysts, particularly at the highest K content. Surface concentrations of Mo as measured by XPS are also listed in Table 2 for selected samples. As can be seen, Ce and Zr promotion appear to maintain the Mo concentration throughout the sample, somewhat more than the unpromoted catalysts. However, K promotion resulted in a significant decrease in the Mo surface concentration.

The DMR testing protocol for the promoted catalysts was identical to that of the unpromoted catalysts and the summary of the results are presented in Table 3. In general, increasing the promoter content did not significantly affect the initial CH_4 conversions or stability, as shown by the similar values of the final conversion between the unpromoted

and promoted catalysts. However, in the case of K-promoted catalysts, the addition of 3 wt.% K drastically lowers the initial CH_4 conversion. Zhu *et. al.* [23] also observed rapid deactivation of a K-doped Mo_2C/Al_2O_3 catalyst (K = 1.2 wt. %) during partial oxidation of methane at 850 ^oC, and reported the presence of MoO_2 and MoO_3 peaks from the XRD analysis of the spent sample.

3.2.1. Effect of Promoter Impregnation Sequence

For all of the promoted catalysts mentioned above, both the promoter and Mo precursors were added to the supports prior to calcination. Consequently, a limited number of experiments were also conducted to study the effect of the impregnation sequence on the stability of the 30Mo/γ-Al catalyst. In these experiments, 3 wt.% of promoters were added either after calcination of the MoO_3 precursor, or before impregnation of the Mo precursor.

Over both K- and Zr-promoted catalysts, there was no significant change on the stability with respect to the order of promoter deposition. However, over Ce-promoted catalysts, the stability of the catalysts correlates strongly with the impregnation order. Figure 4 shows the conversion profiles of the Ce-promoted catalysts synthesized with different promoter impregnation sequences. Impregnation and calcination of the Ce precursor followed by Mo impregnation (3Ce-*c*-30Mo) produced the catalyst with the highest stability. As can be seen, the initial methane conversion reached equilibrium but slowly deactivated to 80% conversion by the end of the run. In contrast, the catalyst

prepared by impregnating the Ce promoter after Mo impregnation and calcination (30Mo-*c*-3Ce), had the lowest stability of the 30 wt.% Mo loaded catalysts. This catalyst deactivated with a rate slightly higher than that of the unpromoted catalyst. The stability of Ce-promoted and unpromoted catalysts can be summarized in the following order: 3Ce-*c*-30Mo > 30Mo-3Ce-*c* ≈ 30Mo/γ-Al > 30Mo-*c*-3Ce. Since impregnation order was important over Ce-promoted catalyst with 30 wt.% Mo loading, we further investigated this effect over 15 wt.% Mo loading. However, the results (Figure 4) indicated that the impregnation order was not important at the lower Mo loading and the catalyst deactivated rapidly. Figure 5 shows the XRD analyses of the spent Ce-promoted catalysts. The 3Ce-*c*-15Mo scan clearly shows that oxidation had occurred, consistent with the fast deactivation of this catalyst. While slight oxidation was observed in the 30Mo-*c*-3Ce catalyst, MoO_2 is not detectible in the 3Ce-*c*-30Mo catalysts. This result is consistent with the observed stability of 3Ce-*c*-30Mo, which was best of all catalysts tested. We also observed that the X-Ray diffraction patterns of all of the freshly carburized Ce-promoted Mo/γ-Al catalysts (two are shown in Figure 6) did not exhibit peaks assigned to β-Mo_2C, but which are readily evident in the unpromoted Mo/γ-Al catalyst. This observation implies that the Ce-promoted catalysts had a higher Mo dispersion than that of the unpromoted catalyst.

As can be seen from Table 2, the surface areas of all promoted catalysts were independent of the impregnation order. Moreover, there was no significant change in the surface area of the spent promoted catalysts as compared to the fresh catalysts, with the exception of the K-promoted, high loading catalysts, which had a reduced surface area of

about 24%. Neither was there a dependence of the surface concentration of Mo on the impregnation sequence although, in the Ce- and Zr-promoted catalysts, it was somewhat higher than in the unpromoted catalyst. On the other hand, the surface Mo concentrations in the K-promoted samples were much lower than the Mo concentrations in the unpromoted samples.

3.3. Effect of CO addition

Previous work has shown that the addition of both CO and H_2 increases the feed stability ratio, R_s, thereby preventing oxidation of bulk Mo_2C catalysts [4,7]. Consequently, the effect of CO addition on the long-term stability of supported catalysts was also investigated for the most promising catalyst, 3Ce-*c*-30Mo. CO was chosen over H_2 in order to avoid interference by the reverse water-gas shift reaction, which would compete with the CO_2 reactant in the reforming reaction. In fact, even a separate experiment with equal concentrations of CO and H_2 in the feed, resulted in relatively high deactivation; presumably due to a preferred consumption of CO_2 via the water-gas shift reaction. Whereas prior tests in this study were terminated after 7 hours, these experiments were conducted for over 26 hours. The concentration of CO in the feed was set so as to give R_s values of 1.5 and 3, while the CH_4 : CO_2 ratio was kept at 1.0. Figure 7 displays the effect of CO addition on the CH_4 conversion for both the promoted and unpromoted catalysts, and as can be seen, stabilities were higher with the addition of CO. While it is true that increasing R_S increased the stability of both unpromoted and Ce-promoted catalysts, note that the Ce-promoted catalyst at $R_S = 3$ had lower conversions

and lower stabilities than the unpromoted catalyst at the same value of R_S. Visual observations of the spent catalysts from these experiments, clearly indicated that when R_S = 3, coke was being formed at the *bottom* of the bed, whereas oxidation at the top of the bed was apparent when R_S = 0. Note that the stability of the Ce promoted catalyst was higher at R_S = 1.5 than at R_S = 3.0 but just the reverse is true of the unpromoted catalyst.

4. Discussion

First of all, it should be pointed out that our experiments were conducted at atmospheric pressure using a stoichiometric feed, which was net-oxidizing according to the stability ratio criteria, R_s [4,7]. Under these conditions, the mass transfer rate of reforming product gases away from the surface of the catalyst was typically high enough to cause oxidation, as shown by LaMont and Thomson [4]. Therefore, the deactivation of all the supported Mo_2C catalysts via oxidation is to be expected and was confirmed by XRD scans of the spent 30Mo/γ–Al catalysts. These results are also consistent with those of Brungs and Claridge [20,8] who reported oxidation of these catalysts during DMR at 950^{o}C, at stoichiometric feed and atmospheric pressure.

The experimental results for the Mo_2C/MgO catalyst suggest that these catalysts were less stable than Mo_2C supported on either ZrO_2 or γ-Al_2O_3. Whereas Ruckenstein and Wang [12] observed high stability of a Rh/MgO catalyst during partial oxidation of methane at 750^{o}C, they attributed it to the strong interactions between Rh and MgO While a similar interaction was also found when MoO_3 was supported on MgO [24], the

temperatures employed in our study were higher than in either of those two studies. Therefore, the low thermal stability of MgO as confirmed by the in-situ XRD measurements and the low surface area of the spent sample, could explain the low activity of the Mo_2C/MgO catalysts in this study.

Contrary to Tsuji and Naito's findings [9,10], we did not observe a significant improvement on the stability of ZrO_2-supported Mo_2C at 1 wt.% Mo content. In comparing the two studies, they employed lower temperatures (850 ^oC vs. 900 ^oC) and thus, it is possible that the difference is due to the increased sintering with our Mo_2C/ZrO_2 catalysts, as evidenced by the low surface areas of the calcined and spent catalysts (Table 1). Nevertheless, the stability of the Mo_2C/ZrO_2 catalysts were higher than the Mo_2C/γ-Al_2O_3 catalysts, despite the relatively low conversions with the former. In addition to having a higher coking resistance, Mo_2C/ZrO_2 has been reported to have a higher oxidation resistance during reforming, attributed to CO_2 activation, which occurs at the junction between the Mo_2C and ZrO_2 interface [9,10].

Compared to ZrO_2 and MgO, γ-Al_2O_3 has the highest thermal stability and therefore, maintains its high surface area at high temperatures as verified by the in-situ XRD measurements that showed no sintering up to 950^oC. In addition to surface area, the higher activities of the Mo_2C/γ-Al_2O_3 catalysts could also be correlated to the known strong interactions between MoO_3 and Al_2O_3 to form molybdena monolayers, and the spontaneous spreading of MoO_3 on Al_2O_3 [25], both of which are favorable for keeping

the active metal in a higher dispersion state. While the latter phenomena are also true for Mo_2C/MgO [26], the thermal stability of MgO is much lower than that of γ-Al_2O_3.

The increased stability of Mo_2C/γ-Al_2O_3 at higher Mo loadings has also been observed by Claridge *et. al.* [20]. It is well known that higher Mo loadings result in increased octahedral coordinated $Mo_7O_{24}^{6-}$ species, which are more easily reduced [22]. This in turn results in higher activity and increased surface concentrations of carburizing gases which leads to improved oxidation resistance. Therefore, higher Mo loadings are necessary in order to keep supported Mo_2C catalysts stable under DMR conditions. The fact that initial conversions over 15Mo/γ-Al are similar to that of 30Mo/γAl, while its deactivation rate is about twice of that of the 30Mo/γ-Al (Fig. 3) may simply be related to the total quantity of Mo on these catalysts, since Mo_2C oxidation in fixed bed reactors is known to proceed by a "moving front" [2,3,5].

The results of the effect of promoter loadings when Mo and the promoter were impregnated prior to calcination, showed that increased Ce and Zr concentrations decreased the initial methane conversions but had no effect on the final conversions after 7 hours on stream. Although the addition of Ce increased the concentration of Mo exposed on the surface, there was no significant improvement on the stability of these catalysts. For K-promoted catalysts, increasing the K concentration dramatically reduced the CH_4 conversion, especially at the highest K concentration, and the overall conversion of this catalyst was lower than that of the Ce- and Zr-promoted catalysts. Other researchers have proposed an inverse correlation between potassium content and the

extent of NiO reduction [31,32], and a study by Zhu *et. al.* [23] reported a similar detrimental effect on the stability of K-promoted Mo_2C for the partial oxidation of methane. A TPR profile of their catalyst showed a decrease in catalyst reducibility upon the addition of K promoters, and they further suggested that K accelerated the sintering of the carbide. Similar results were also observed with K promotion of a MoO_3/Al_2O_3 catalyst [33]. Contrary to the findings of Zhu *et. al.*, we did not observe an increase in the crystallite size of the Mo_2C upon K promotion. In addition to inhibiting MoO_3 reduction, the negative effect of K on the stability of the carbide could also be related to the known high mobility of K. The tendency of K to migrate to the surface is consistent with the very low the values of Mo surface concentration in the K promoted catalysts (Table 2), even when the Mo loading was increased from 15 to 30 wt.%. Both of these effects lead to lower CH_4 conversion, decreasing the stability ratio with subsequent oxidation of carbide.

Whereas, in catalysts where both Ce and Mo were impregnated prior to calcinations, there was no effect on stability, there was a significant effect when Ce was impregnated and calcined prior to loading the Mo. As shown in Figure 4, the 3Ce-*c*-30Mo sample had greatly improved stability over the unpromoted catalysts, when the catalyst was calcined after Ce addition and prior to Mo impregnation. However, XRD and XPS analyses of the surface Mo concentration showed no significant differences. Molybdenum carbide is prone to oxidation under reforming conditions and Ce is known for its ability to influence redox chemistry [16]. It has also been reported that Ce loses its redox properties if its particles become too large [29,30]. Thus, one possible explanation here is that

calcinations after Ce impregnation serves to anchor Ce particles, preventing their agglomeration, and thereby retaining good redox capabilities.

With a stoichiometric feed ($R_S = 0$), Ce promotion dramatically improves the stability of the Mo_2C/γ-Al catalysts. Analyses of the spent catalysts indicated that Ce acted to increase the oxidation resistance of Mo_2C, particularly at the top of the bed where the concentration of carburizing gases is low. Ceria is known to influence redox reactions, and it is likely that it activates CO_2 via:

$$Ce_2O_3 + CO_2 \leftrightarrows 2CeO_2 + CO \qquad (1)$$

thereby helping to prevent oxidation of Mo_2C by CO_2. In fact, XPS analyses of freshly promoted Ce showed that about 60% of the ceria was in the form Ce_2O_3, while the remainder was CeO_2. However, when experiments were conducted at high values of the stability ratio by adding CO to the feed, the Ce-promoted catalysts were less stable than the unpromoted catalyts (Fig. 7). Since oxidation was not observed in these spent catalysts, but coking was observed at the bottom of the bed; i.e., where CO concentrations are highest, this could be attributed to CO disproportionation:

$$2CO \leftrightarrows C + CO_2 \qquad (2)$$

In fact, Putna *et. al.* [36] have shown that CO dissociation occurs over a Rh/ceria catalyst when the ceria is a reduced to Ce_2O_3. Based on these observations and the fact that the

Ce-promoted catalyst was more stable at $R_S = 1.5$ than at $R_S = 3$, it is reasonable to hypothesize that the presence of excess CO causes the reverse of Equation (1), which then leads to CO disproportionation with accompanying carbon formation. Thus, it would appear that, for Ce-promoted $Mo_2C/\gamma\text{-}Al_2O_3$ catalysts, there is an optimum value of R_S which would improve both oxidation and coking resistance via CO disproportionation.

Although bulk Mo_2C catalysts have remarkable coking resistance in reforming applications, they are susceptible to oxidation and have lower activities than Ni or noble metal based catalysts. As shown here and elsewhere [4,7], oxidation can be prevented through the use of Ce promotion or by operating at high values of R_S. However, supported Mo catalysts have a significantly higher activity than bulk Mo_2C catalysts as can be seen from Figure 8, which shows a comparison of supported and bulk catalysts, with and without CO in the feed. As can be seen, higher values of R_S increase stability and the activity of the supported catalysts are much higher than the bulk catalysts. Whereas the bulk catalyst at $R_S = 0$ appears to be stable over the 8 hour period, albeit at a lower CH_4 conversion, analysis of the spent catalyst indicated that oxidation of the Mo_2C was occurring at the top of the bed. Comparing this to the supported catalyst (30 $Mo/\gamma\text{-}Al_2O_3$), it would appear that the latter is less stable. However, there is over three times as much Mo in the bulk catalyst as in the supported catalyst. In other words, at $R_S = 0$, both catalysts are deactivating, it just takes over three times as long for the bulk catalyst to deactivate to the same degree. On the other hand, the activitiy of the supported catalyst is much higher, and with a combination of ceria and excess CO in the feed, the supported catalysts are certainly superior to the bulk catalysts.

5. Conclusions

The results presented here show that low surface area MgO and α-Al_2O_3 were ineffective supports for Mo_2C catalysts in dry reforming applications. While higher surface area ZrO_2 and γ-Al_2O_3 were more effective, the ZrO_2 support experienced serious sintering, which led to subsequent deactivation. Since Mo_2C oxidation was to be expected under these conditions, the γ-Al_2O_3 support was deemed to be superior in view of its thermal stability, even though deactivation via oxidation also occurred. It was also found that higher loadings of Mo_2C were needed in order to achieve higher activities and this is attributed to strong interactions between MoO_3 and Al_2O_3 at higher Mo loadings, forming molybdena monolayers, which result in a higher Mo_2C dispersion. The results of an evaluation of the effectiveness of K, Zr and Ce promotion show that K acted to lower the surface Mo concentration, causing low activities and rapid deactivation. Zr addition had little effect on either methane conversion or deactivation rates. The same was true for Ce addition when Ce and Mo were added prior to calcination. However, when Ce was impregnated and calcined before Mo impregnation there was a marked improvement in stability and only a small decrease in methane conversion. In this case, oxidation was not detected in the XRD scans of the spent catalysts. Based on previous literature it seems that this is due to the effectiveness of ceria acting to control redox chemistry and the dependency of this process on ceria particle size. Calcining ceria prior to Mo impregnation appears to anchor the ceria particles, preventing agglomeration and thus maintaining control of the redox chemistry.

Since previous work in our laboratory has demonstrated that the addition of CO in the feed can prevent Mo_2C oxidation, experiments with CO in the feed were also carried out over Ce promoted catalyst at stability ratios of 1.5 and 3.0. It was found that, in this case, the catalyst slowly deactivated due to coking at the bottom of the catalyst bed. It is hypothesized that the excess CO reduced the Ce completely to Ce_2O_3, at which point, CO disproportionated to carbon and CO_2. The magnitude of this effect was also seen to be dependent on the value of the stability ratio, implying that there is an optimum stability ratio with Ce-promoted Mo_2C catalysts, which would increase oxidation resistance and avoid coking. A comparison of supported catalysts with bulk catalysts shows the increased activity of the former, although deactivation will be more rapid, if oxidation occurs.

Acknowledgement

This material is based on work supported by the National Science Foundation under Grant CTS-0209372.

References:

1. York, A.P.E., Claridge, J.B., Tsang, A.J., Green, M.L.H., Chem. Comm. (1997) 39.
2. Claridge, J.B., York, A.P.E., Marquez-Alvarez, C., Brungs, A.J., Sloan, J., Tsang, S.C., Green, M.L.H., J. Catal. 180 (1998) 85.
3. Sehested, J., Jacobsen, C.J.H., C.J.H., Rokini, S., Rostrup-Nielsen, J.R., J. Catal. 201 (2001) 206.
4. LaMont, D.C., Thomson, W.J., Appl. Catal. A. 274 (2004) 173.
5. LaMont, D.C., Gilligan, A.J., Darujati, A.R.S., Chellappa, A.S., Thomson, W.J., Appl. Catal. 255 (2003) 239.
6. Pritchard, M., McCauley, R., Gallaher, B.N., Thomson, W.J., Appl. Catal. 275 (2004) 213.
7. Darujati, A.R.S., LaMont, D.C., Thomson, W.J., Appl. Catal. 253 (2003) 397.
8. Brungs, A.J., York, A.P.E., Claridge, J.B., Marquez-Alvarez, C., Green, M.L.H., Catal. Letters 70 (2000) 117.
9. Tsuji, M., Miyao, T., Naito, S. Catal. Letters 69 (2000) 195.
10. Naito, S., Tsuji, M., Miyao, T., Catal. Today 77 (2002) 161.
11. Ruckenstein, E., Hu, Y.H., Appl. Catal. A. 133 (1995) 149.
12. Ruckenstein, E., Wang, H.Y., Appl. Catal. A. 198 (2000) 33.
13. Cheng, Z.X., Wu, Q.L., Li, J.L., Zhu, Q.M., Catal. Today 30 (1996) 147.
14. Wang, S., Lu, G.Q., Appl. Catal. B. 19 (1998) 267.
15. Xu, G., Shi, K., Gao, Y., Xu, H., Wei, Y., J. Mol. Catal. A 147 (1999) 47.
16. Sharma, S., Hilaire, S., Vohs, J.M., Gorte, R.J., Jen, H.-W., J. Catal. 190 (2000) 199.
17. Ozawa, O., Kimura, M., J. Mater. Sci. Lett. 9 (1990) 291.
18. Horiuchi, T., Sakuma, K., Fukui, T., Kubo, Y., Osaki, T., Mori, T., Appl. Catal. A. 144 (1996) 111.
19. Osaki, T., Mori, T., J. Catal. 204 (2001) 89.
20. Stagg, S.M., Romeo, E., Padro, C., Resasco, D.E., J. Catal. 178 (1998) 137.
21. Souza, M.M.V.M., Aranda, D.A.G., Schmal, M., J. Catal. 204 (2001) 498.
22. Souza, M.V.M., Schmal, M., Appl. Catal. A 255 (2003) 83.
23. Zhu, Q., Zhang, B., Zhao, J., Ji, S., Yang, J., Wang, J., Wang, H., J. Mol. Catal. A. 213 (2004) 199.
24. Kumar, M., Aberuagba, F., Gupta, J.K., Rawat, Sharma, L.D., Dhar, G.M., J. Mol. Catal. A. 213 (2004) 217.
25. Stampl, S.R., Chen, Y., Dumesic, J.A., Niu, C., Gill Jr., C.G., J. Catal. 105 (1987) 445.
26. Kim, D., Wachs, I.E., Segawa, K., J.Catal. 146 (1994) 268.
27. Arnoldy, P., Franken, M.C., Scheffer, B., Moulijn, J.A., J. Catal. 96 (1985) 381.
28. Montoya, J.A., Romero-Pascual, E., Gimon, C., Del Angel, P., Monzon, A., Catal. Today 63 (2000) 71.
29. Cordatos, H., Bunluesin, T., Stubenrauch, J., Vohs, J.M., Gorte, R.J., J. Phys. Chem. 100 (1996) 785.
30. Bunluesin, T., Gorte, R.J., Graham, G.W., Appl. Catal. B. 14 (1997) 105.

31. DeCanio, S.J., Cataloo, M.C., DeCanio E.C., Storm, D.A., J. Catal. 119 (1989) 256.
32. Osaki, T., Mori, T., J. Catal. 204 (2001) 89.
33. Jiang, M., Bian, G-Z., Fu, Y-L., J. Catal. 146 (1994) 144.
34. Shyu, J.Z., Webor, W.H., Oandhi, H.S., J. Phys. Chem. 92 (17) (1998) 4964.
35. Momteiro, R. de Souza, Noronha, F.B., App. Catal. A 131 (1995) 89.
36. Putna, E.S, Gorte, R.J., Vohs, J.M. and G.W. Graham, J. Catal. 178 (1998) 598.

Table 1. BET Surface Area of Supported Catalysts

Catalyst	BET Surface Area [m^2/g]			
	Fresh	**Calcined**	**Post Carburization**	**Post Reaction**
α-Al_2O_3 supported Mo_2C				
α-Al_2O_3	3			
15 Mo/α-Al		-	-	-
ZrO_2 supported Mo_2C				
ZrO_2	104			
1 Mo/Zr		77	-	23
5 Mo/Zr		101	-	21
15 Mo/Zr		63	29	24
30 Mo/Zr		51	-	20
MgO supported Mo_2C				
MgO	37			
5 Mo/MgO		36	-	-
15 Mo/MgO		42	25	12
30 Mo/MgO		34	-	-
γ-Al_2O_3 supported Mo_2C				
γ-Al_2O_3	200			
5 Mo/γ-Al		197	162	99
15 Mo/γ–Al		156	145	113
30 Mo/γ–Al		108	117	93

Table 2. Properties of Promoted-Mo_2C/γ-Al_2O_3 Catalysts

Catalyst	BET Surface Area [m^2/g]			Surface concentration of Mo, [%][a]
	Calcined	Post Carburization	Post Reaction	
Unpromoted Mo_2C				
15Mo/γ-Al	156	145	113	11.9
30Mo/γ-Al	108	117	93	24.3
Ce-promoted Mo_2C				
15Mo–0.1Ce-*c*	160	-	131	-
15Mo–0.5Ce-*c*	150	-	109	-
15Mo–3Ce-*c*	151	136	103	18
3Ce–*c*–30Mo-*c*	83	93	86	32.6
30Mo–*c*–Ce-*c*	99	103	97	29.0
30Mo-3Ce-*c*	103	-	92	-
K-promoted Mo_2C				
15Mo–0.1K-*c*	159	-	110	-
15Mo–0.5K-*c*	168	-	104	-
15Mo–3K-*c*	137	128	98	7
3K–*c*-30Mo-*c*	85	95	72	12.8
30Mo–*c*–3K-*c*	93	96	77	12.3
30Mo-3K-*c*	96	-	74	-
Zr-promoted Mo_2C				
3Zr–*c*–15Mo-*c*	143	133	104	13.9
15Zr–*c*-15Mo-*c*	126	-	96	-
3Zr–*c*–30Mo-*c*	94	111	98	27.1
30Mo–*c*–3Zr-*c*	97	112	94	28.2

[a] Obtained from XPS analyses

Table 3. Summary of the Initial and Final Conversion of γ-Al_2O_3-Supported Mo_2C Catalyst in the Presence of Ce, K and Zr Promoters in DMR. (T = 900°C, GHSV = 3,800 h^{-1}, P = 1 bar, G = 0.37 mol/cm^2/h).

Catalyst	Initial Conversion [%]	Conversion at 7 h [%]
15Mo/γ-Al	97.0	38.4
30Mo/γ-Al	97.5	57.5
15Mo-0.1Ce-*c*	97.4	39.9
15Mo-0.5Ce-*c*	97.5	37.2
15Mo-3Ce-*c*	87.0	34.2
30Mo-3Ce-*c*	94.5	55.3
15Mo–0.1K-*c*	96.0	47.4
15Mo-0.5K-*c*	85.1	34.9
15Mo-3K-*c*	27.0	19.1
30Mo-3K-*c*	28.1	17.4
3Zr-*c*-15Mo	96.0	38.1
15Zr-*c*-15Mo	78.2	37.8
3Zr-*c*-30Mo	97.0	61.0

Darujati and Thomson, Figure 1

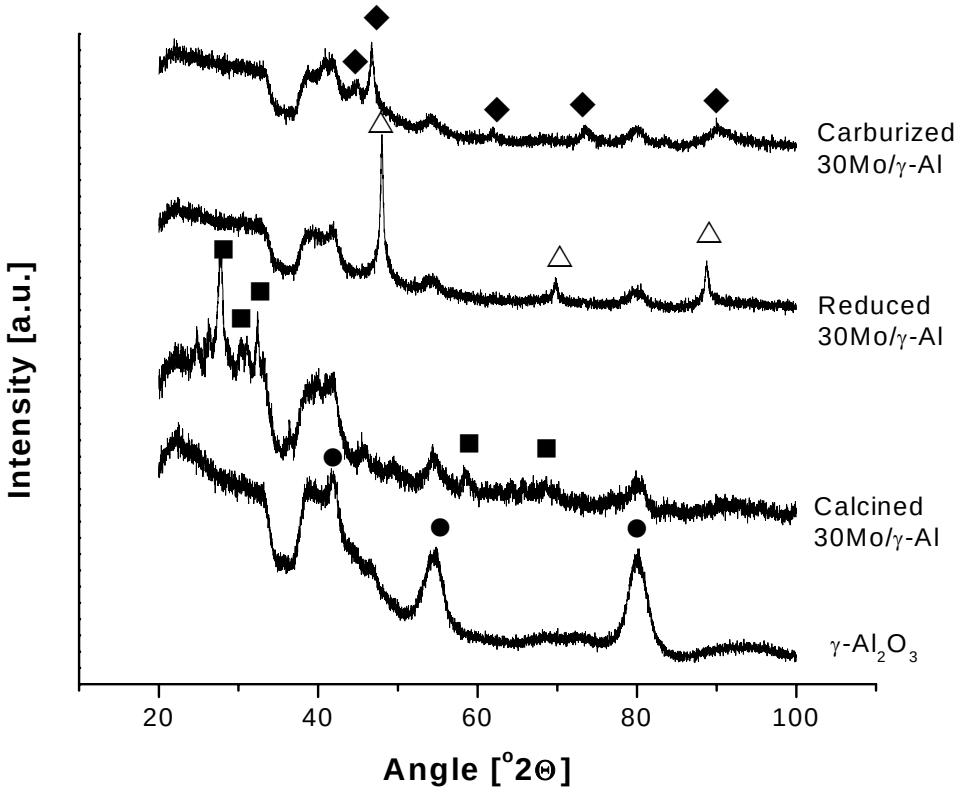

Figure 1. XRD scan of γ-Al_2O_3 support, calcined, reduced and carburized 30 Mo/γ-Al; γ-Al_2O_3 (●); MoO_3 (■); Mo (△); β-Mo_2C (◆).

Darujati and Thomson, Figure 2

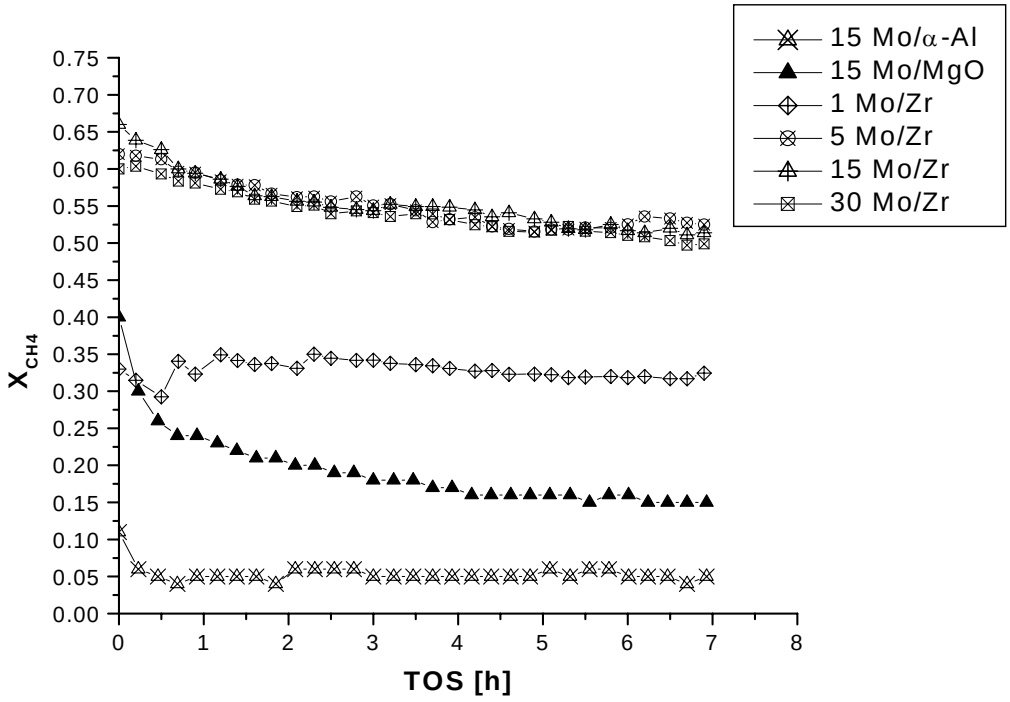

Figure 2. Methane conversion with respect of time on stream during dry reforming of Mo_2C catalysts over lower surface area supports (T=900^oC, P=1 bar, GHSV=3,800h^{-1}, *G* = 0.37 mol/cm^2/h, CH_4 : CO_2=1). Connecting lines are added for clarity.

Darujati and Thomson, Figure 3

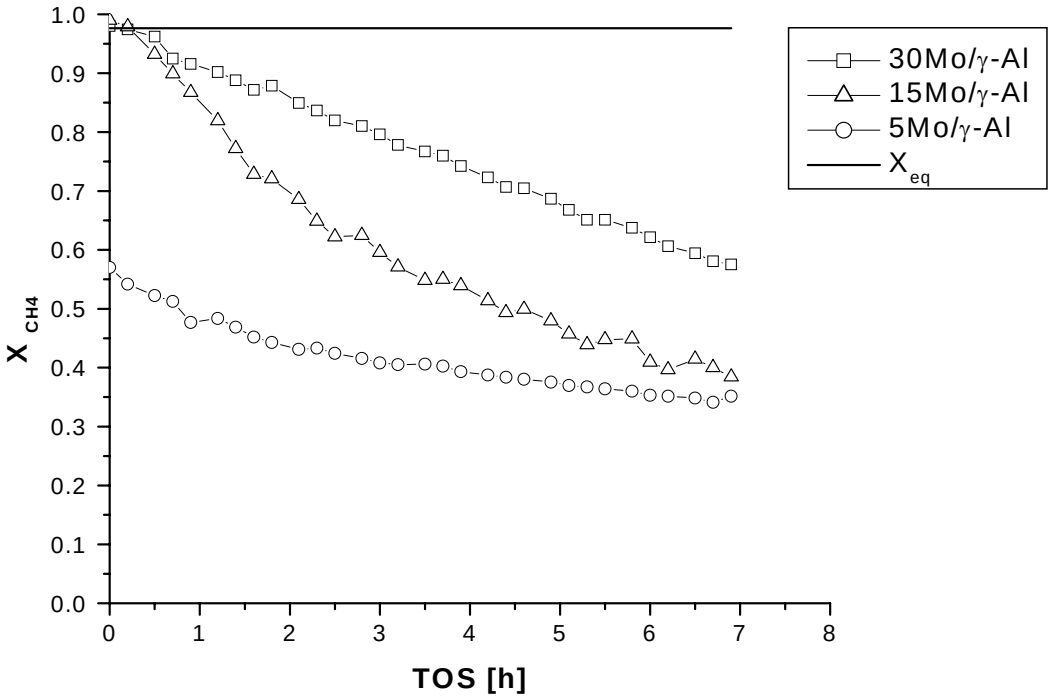

Figure 3. Methane conversion with respect of time on stream during dry reforming of Mo_2C catalysts over Mo/Al (T=900^{o}C, P=1 bar, GHSV=3,800h^{-1}, G = 0.37 mol/cm^2/h, CH_4 : CO_2=1). Connecting lines are added for clarity.

Darujati and Thomson, Figure 4

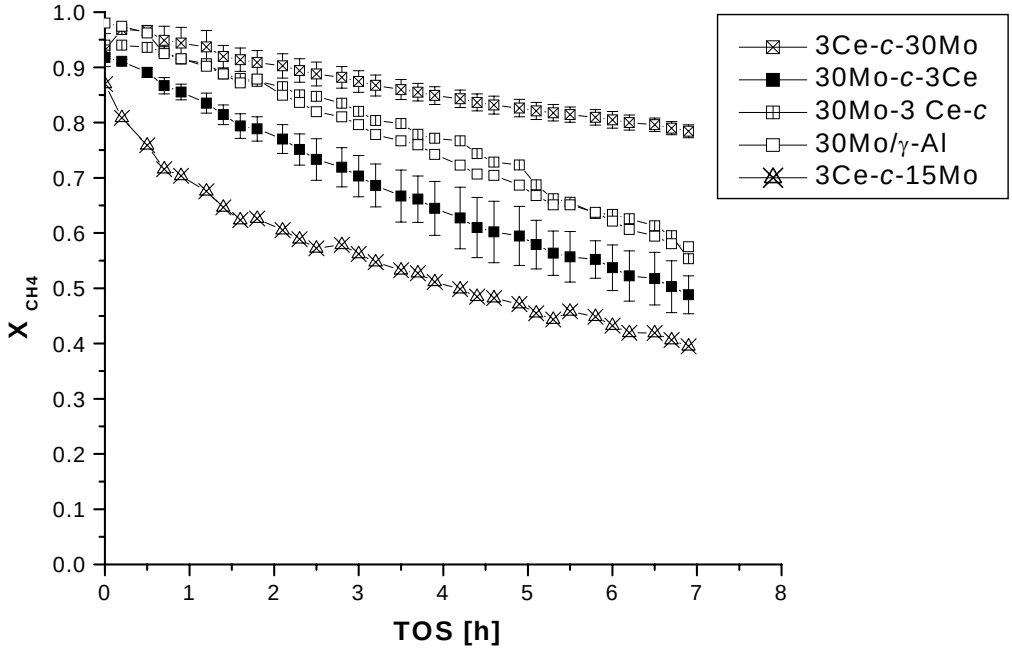

Figure 4. The effect of impregnation sequence of Ce promoter on the stability of supported Mo_2C in DMR (T = 900°C, GHSV = 3,800 h^{-1}, P = 1 bar, G = 0.37 mol/cm^2/h). Connecting lines are added for clarity.

Darujati and Thomson, Figure 5

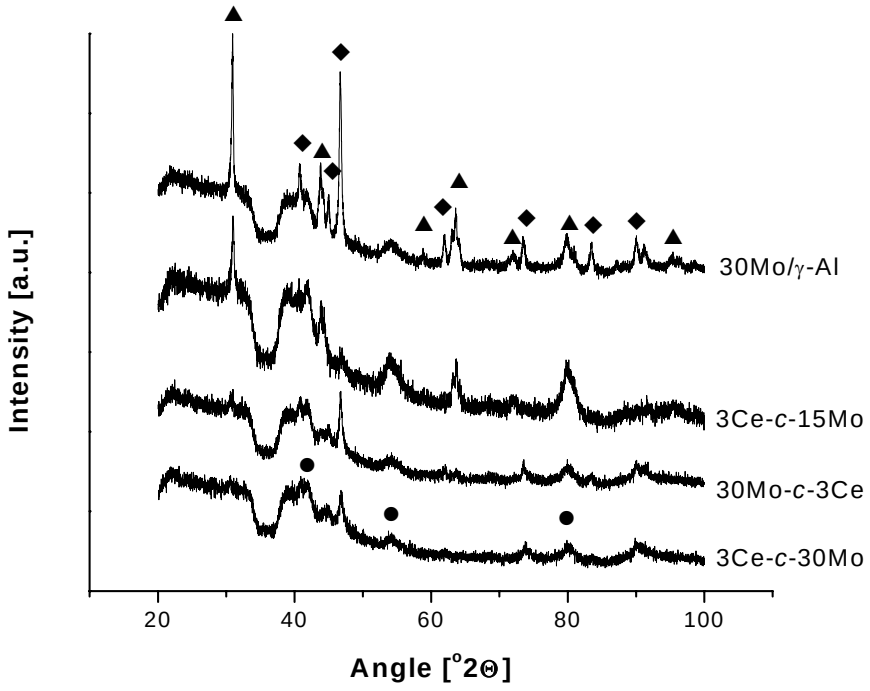

Figure 5. XRD scans of spent samples. γ-Al_2O_3 (●); β-Mo_2C (◆); MoO_2 (▲).

Darujati and Thomson, Figure 6

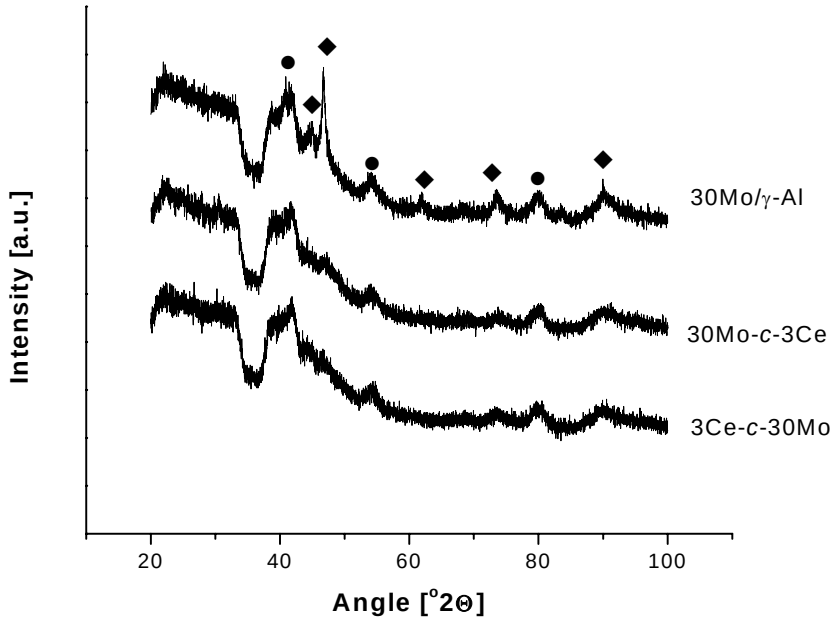

Figure 6. XRD scan of carburized unpromoted and ceria-promoted Mo_2C; γ-Al_2O_3 (●); β-Mo_2C (◆).

Darujati and Thomson, Figure 7

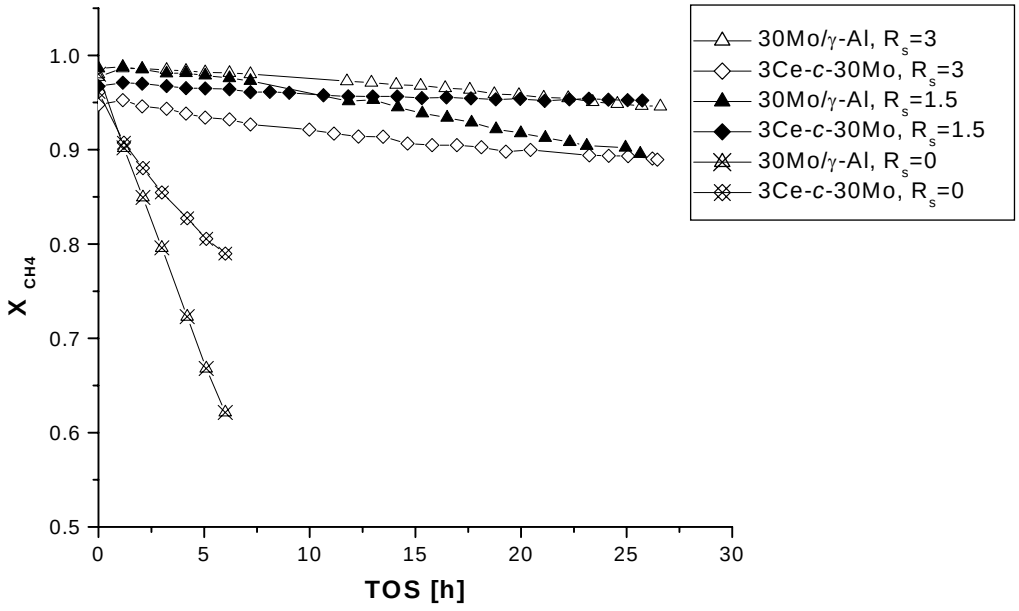

Figure 7. The effect of CO addition on the long term stability of 30Mo/γ-Al and 3Ce-*c*-30Mo catalysts. G = 0. 52 mol/cm^2/h, GHSV = 6,600 h^{-1} for R_s = 1.5 and G = 0.75 mol/cm^2/h, GHSV = 9,500 h^{-1} for R_s = 3; T = 900^{o}C, P = 1 bar. Connecting lines are added for clarity.

Darujati and Thomson, Figure 8

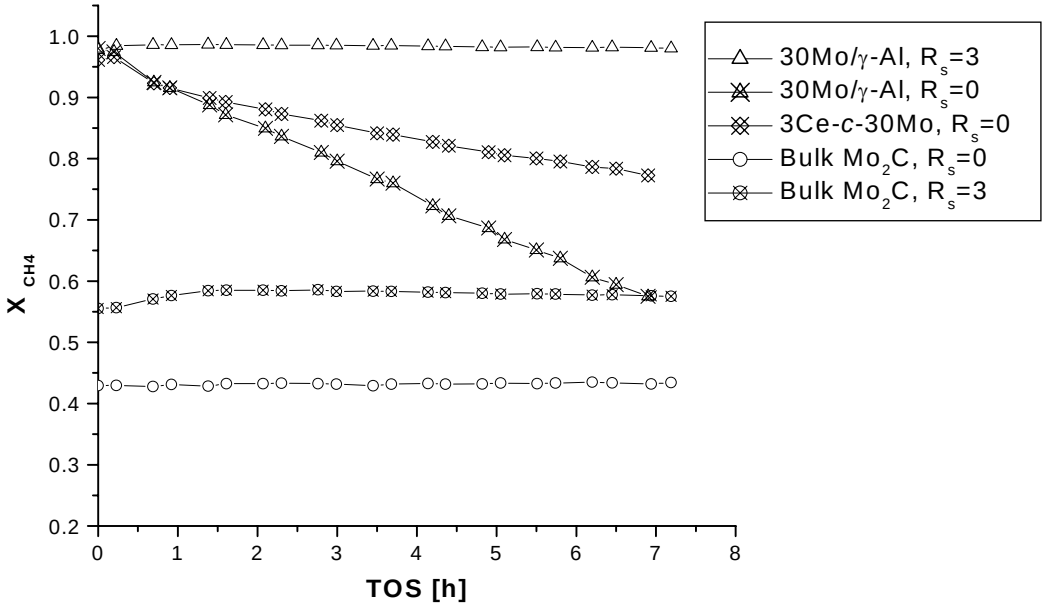

Figure 8. Stability of Ce-promoted Mo_2C, unpromoted Mo_2C and bulk Mo_2C in DMR with and without adding CO. $CH_4 : CO_2 = 1$; $G = 0.37$ for $R_s = 0$, and $G = 0.75$ for $R_s = 3$; T = 900 ^oC, P = 1 bar. Connecting lines are added for clarity.

CHAPTER FOUR

KINETIC STUDY OF A CERIA-PROMOTED $Mo_2C/\gamma\text{-}Al_2O_3$ CATALYST IN DRY-METHANE REFORMING

Anna R.S. Darujati and William J. Thomson*

Department of Chemical Engineering, Washington State University, P.O. Box 642710, Pullman, WA 99164-2710, USA

* Corresponding author. Tel.: +1 509 335 8580; FAX: +1 509 335 4806; e-mail: thomson@che.wsu.edu

Abstract

The kinetics of dry-methane reforming has been studied over a ceria-promoted Mo_2C/γ-Al_2O_3 (3 wt.% Ce, 30 wt.% Mo) catalyst at temperatures between 800 – 900 ^oC, and at CH_4 and CO_2 partial pressures up to 0.31 bar. Oxidation of the Mo_2C catalyst, which has plagued earlier kinetic studies, was avoided by co-feeding CO to produce a CO : CO_2 ratio of 3. The activation energy obtained from the data fit to a power law rate expression of 45.5 kcal/mol was found to be similar to that of bulk Mo_2C. However, the activity of the ceria-promoted catalyst, on a per unit mass of Mo_2C, was significantly higher than that of the bulk and is attributed to the higher metal dispersion of the former. A reaction mechanism, involving CH_4 activation on Mo_2C particles and CO_2 activation on both ceria and Mo_2C particles, with carbidic carbon extraction by oxygen on ceria as the rate-determining step, is consistent with the derived kinetic model and the high activation energy.

Keywords: molybdenum carbide, dry-methane reforming, kinetics, ceria promoter

1. Introduction

A number of studies have investigated molybdenum carbide (Mo_2C) as an alternative catalyst for steam-methane reforming (SMR) (Claridge et al., 1998; York et al., 1997) and dry-methane reforming (DMR) (Claridge et al., 1998; York et al., 1997; Sehested et al., 2001; LaMont and Thomson, 2004; LaMont et al., 2003) reactions due to its high coking resistance. Both SMR and DMR reactions are favorable at high temperatures, and are normally accompanied by the water-gas shift (WGS) or reverse water-gas shift (RWGS) reactions:

$$\text{SMR: } CH_4 + H_2O \rightarrow CO + 3H_2 \quad \Delta H^{300K} = 49.4 \text{ kcal/mol} \qquad (1)$$

$$\text{DMR: } CH_4 + CO_2 \rightarrow 2CO + 2H_2 \quad \Delta H^{300K} = 59.1 \text{ kcal/mol} \qquad (2)$$

$$\text{WGS: } CO + H_2O \leftrightarrows CO_2 + H_2 \quad \Delta H^{300K} = -9.7 \text{ kcal/mol} \qquad (3)$$

Typically, supported Ni is the catalyst used in industrial steam-methane reformers. However, due to the low coking resistance of Ni, the reformer has to be operated with excess steam to promote carbon gasification and prevent catalyst deactivation. Clearly, the high coking resistance of Mo_2C, which allows the reformer to be operated without excess oxidant, could be a major advantage for a large-scale application, since lower partial pressure of oxidant and lower steam generation requirements would translate to large energy savings. Moreover, its high thermal stability, low cost, and relative stability in the presence of sulfur (McCrea et al., 1997; Dhandapani et al., 1998; Aegerter et al., 1996; Pritchard et al., 2004) have made the application of Mo_2C catalysts for reforming

of sulfur-containing hydrocarbons particularly attractive. However, it is well known (Claridge et al., 1998; York et al., 1997) that Mo_2C catalysts are susceptible the oxidation of Mo_2C by CO_2 and H_2O to form inactive MoO_2:

$$Mo_2C + 5H_2O \leftrightarrows 2MoO_2 + CO + 5H_2 \quad (4)$$

$$Mo_2C + 5CO_2 \leftrightarrows 2MoO_2 + 6CO \quad (5)$$

The oxidative stability of Mo_2C in both SMR and DMR, was found to be strongly influenced by the concentration of both CO and H_2 (Darujati et al., 2003) and it was achieved at 775 ^oC as long as the ratio of these gases to CO_2 and H_2O (stability ratio, R_s) was higher than 0.8:

$$R_s = \frac{P_{H_2} + P_{CO}}{P_{CO_2} + P_{H_2O}} > 0.8 \quad (6)$$

Although carburization of MoO_2 by CH_4 is possible thermodynamically, both Sehested et al. (2001) and our prior study (Darujati et al., 2003) observed very little effect of CH_4 on the oxidative stability of Mo_2C during reforming. Therefore, a stoichiometric feed is a net oxidizing feed since at this condition R_s is equal to 0, which explains the observations of rapid oxidation of Mo_2C (Claridge et al., 1998; York et al., 1997; Sehested et al., 2001, LaMont et al., 2003). However, oxidation of Mo_2C at $R_s = 0$ was found by LaMont and Thomson (2004) to be preventable at high pressures as long as gas-solid mass transfer rates of the product gases (CO and H_2) from the surface are sufficiently low.

Because of oxidation, only a few studies have been conducted to determine the reaction kinetics of Mo_2C for reforming (Claridge et al., 1998; Sehested et al., 2001; LaMont and Thomson, 2004; Naito et al., 2002). However, two of these studies obtained kinetic data under conditions where oxidation of Mo_2C was dominant (Claridge et al., 1998; Naito et al., 2002). In one case, Claridge et al. (1998) obtained an activation energy of 22.8 kcal/mol for a bulk Mo_2C catalyst, while Naito et al. (2002), using a Mo_2C/ZrO_2 catalyst, obtained a reaction order for CH_4 and CO_2 of 1.7 and 0.8, respectively, but did not measure an activation energy. On the other hand, Sehested et al. (2001) conducted their study of a bulk Mo_2C catalyst in the presence of recycled product in an attempt to stabilize the Mo_2C catalyst, and obtained an activation energy of 19 kcal/mol for DMR between 700 – 800 ^oC. The authors stated that their experimental conditions were mass transfer limited, and information on the reaction orders was not reported. Recently, a DMR kinetic study by LaMont and Thomson (2004) was achieved by stabilizing the bulk Mo_2C catalyst by co-feeding CO with the reactant gases. In this case, mass transfer conditions were not limiting, and they obtained a much higher activation energy of 42.1 kcal/mol, which was attributed to the presence of a solid-state reaction in the rate-determining step. Their reported reaction orders for CH_4 and CO_2 were 1 and 0.7, respectively.

In the work reported here, the kinetics of DMR over ceria-promoted $Mo_2C/\gamma\text{-}Al_2O_3$ were studied. The ceria-promoted $Mo_2C/\gamma\text{-}Al_2O_3$ catalyst was chosen due to our previous study, which showed that this catalyst had superior stability and activity for DMR

(Darujati and Thomson, 2005). Both reaction orders and activation energy were determined under non-mass transfer limited conditions, and compared with those obtained by others for bulk Mo_2C (Claridge et al., 1998; Sehested et al., 2001; LaMont and Thomson, 2004). The effect of ceria promotion on the reaction mechanism was then proposed, based on the elucidated kinetic parameters.

2. Experimental

2.1. Catalyst Synthesis and Testing

All experiments were conducted with ceria-promoted $Mo_2C/\gamma\text{-}Al_2O_3$ (Ce = 3 wt.%, Mo = 30 wt.%). The catalyst was prepared by incipient wetness impregnation with cerium nitrate (Alfa Aesar) of the $\gamma\text{-}Al_2O_3$ support (CATALOX, -325 mesh) followed by drying at 100 ^oC for 12 hours and calcination at 500 ^oC for 4 hours in air. The calcined powder was then impregnated with the Mo precursor (ammonium heptamolybdate, Aldrich), re-dried, and re-calcined to form Ce promoted $MoO_3/\gamma\text{-}Al_2O_3$. Owing to the low solubility of the Mo precursor, multiple impregnations were required to reach the desired Mo loading. Transformation to the final form of the supported-Mo_2C catalyst was accomplished by H_2 reduction of the supported MoO_3 at 850 ^oC for 2 hours to form metallic Mo, followed by carburization in 20% CH_4/H_2 at 675 ^oC for 2 hours. Passivation of the carburized catalyst in 1% O_2/He overnight was conducted prior to removal from the reactor, due to the pyrophorric nature of the catalyst. The passivated catalyst was then mixed with fused $\alpha\text{-}Al_2O_3$ (Atlantic Equipment Engineers, particle size –100/+240 mesh,

99.8%) to yield a 7 wt.% dilution in order to minimize the pressure drop across the bed and minimize temperature gradients within the bed. Characterization measurements of this catalyst have been reported previously (Darujati and Thomson, 2005).

The experiments were conducted by loading 1.5 – 3 gram of the catalyst into a 88 mm ID quartz tube. A 50 mm ID tube furnace was used to heat the catalyst bed, with the temperature controlled by a quartz-sheathed K type thermocouple contacting the bottom of the catalyst bed. The inlet gas flow rates were controlled by Brooks mass flow controllers, while the exit gas flow rates were measured manually using a bubble flow meter. A condenser was installed at the exit line of the reactor to condense out any water in the product stream. Product analysis was performed with an on-line SRI gas chromatograph equipped with molecular sieve and Hayesep D columns, and a thermal conductivity detector (TCD). Each experiment was initiated by ramping in a mixture of UHP CH_4 and He to 850 ^oC, at which time both CO and CO_2 were introduced to the reactor. The ramping was continued to 900 ^oC and held at this temperature for 40 minutes. This treatment protocol was found to allow the passivated catalyst to be fully re-carburized (LaMont and Thomson, 2004). It was determined experimentally that CO introduction had to be carried out at high temperatures to avoid severe reduction of the ceria, which significantly decreased the stability of the catalyst during DMR. After holding at 900 ^oC for 40 minutes, the temperature was then reduced to the desired set point and held at this setting for the remainder of the experiment. In this study, the packed bed reactor was operated in an integral way, that is, at relatively large conversions, but still well below equilibrium. This was achieved by varying the inverse

CH_4 space velocity or which was defined as the ratio of the catalyst weight to the CH_4 molar flow rate (ISV_{CH4}, $g_{cat}.h/mol_{CH4}$). For each data point, three GC scans with a total time of 40 minutes were taken before adjusting the ISV_{CH4} to a new value. Conversions were based on CH_4 measurements, and multiple short experiments with 4 – 5 different ISV_{CH4} values were conducted to avoid catalyst deactivation due to coke accumulation. At the end of each experiment, the ISV_{CH4} was returned to its initial value to confirm that no deactivation had occurred. If the conversions between initial and final values differed by more than 7%, the data were rejected. In a limited number of experiments, this procedure was repeated by either increasing or reducing the ISV_{CH4} values over the same range, and no hysteresis effects were observed. Once an experiment was completed, the reactor was quenched in a mixture of CH_4 and He. The kinetic data were collected between 800 ^oC and 900 ^oC and over a CH_4 partial pressure range of 0.12 – 0.22 and a CO_2 partial pressure range of 0.19 – 0.33. This resulted in CO_2 : CH_4 ratios between 0.76 and 1.83. In all cases the CO : CO_2 ratio was maintained constant at 3.0.

2.2. Data Analysis

Differential analysis of the integral data was used to obtain kinetic parameters. In this analysis, a plot of CH_4 conversions versus ISV_{CH4} at each feed condition and each temperature was fit to a hyperbolic curve with 3 parameters ($X_{CH4,0}$, a and b) described by the following expression:

$$X_{CH4} = X_{CH4,0} + \frac{a(ISV_{CH4})}{b + (ISV_{CH4})} \quad (7)$$

This equation was then differentiated to give the rate of CH_4 consumption:

$$rate = \frac{dX_{CH4}}{d\left(ISV_{CH4}\right)} = \frac{ab}{\left\{b + \left(ISV_{CH4}\right)\right\}^2} \tag{8}$$

Separately, the partial pressures of CH_4 and CO_2 at each feed condition and each temperature were calculated from the CH_4 conversions, and assuming that the reverse water-gas shift (RWGS) was always at equilibrium. A table of CH_4 and CO_2 partial pressures, with the corresponding rate obtained from equation (8), could then be made for each experiment, and the combined data were fit to a power law rate expression (Eq. 9) to obtain the pre-exponential factor (A_o), the activation energy (E_a) and the reaction orders (α, β).

$$rate = A_o e^{\frac{-Ea}{RT}} P_{CH4}^{\alpha} P_{CO2}^{\beta} \tag{9}$$

3. Results

In order to stabilize the catalyst, CO was chosen instead of H_2 to achieve the desired R_s value, because its presence shifts the RWGS equilibrium toward H_2. Moreover, our previous study determined that CO was superior to H_2 in maintaining the stability of the ceria-promoted Mo_2C (Darujati and Thomson, 2005). Although the same study found that bulk oxidation of the Ce-promoted Mo_2C catalyst could be prevented by adding

excess CO at an R_s of 1.5, a higher value of Rs was found to be necessary to completely prevent oxidation of Mo_2C as shown in Figure 1. In this figure, the conversion values were all obtained after 1 hour on-stream, and until a value of R_S equal to 3.0 was reached, the conversions were decreasing with time. As can be seen, the one-hour methane conversion increased with increasing R_s up to 3. Beyond this value no significant increase of methane conversion was observed, indicating constant surface properties had been reached. It has been previously reported (LaMont and Thomson, 2004) that increased catalyst dilution lowered the stability of the Mo_2C during DMR at a stoichiometric feed, which was attributed to the higher accessibility of the oxidizing gases to the catalyst particles. Consequently, a higher R_s value was required to offset the lower oxidation stability of the diluted catalysts, and therefore, all experiments were conducted at an R_s value of 3.0.

All reaction rates were obtained at temperatures between 800 – 900 ^oC, and since transport phenomena tend to become rate determining with increasing temperature, a series of control experiments was first carried out at 900 ^oC, to determine the molar velocity at which the measured kinetic rate was due solely to the chemical reaction. Experimentally, this condition was determined by simultaneously increasing both the catalyst loading and the molar velocity of the feed until a value was reached at which conversion became independent on molar velocity. As can be seen in Figure 2, mass transfer resistance at 900 ^oC is observed at molar velocities lower than 0.28 mol/cm^2.h, and therefore, all experiments were conducted at molar velocities higher than this value.

The presence of internal mass transport resistance due to pore diffusion can be excluded here due to the small particle size of the catalyst (less than 40 μm).

Figure 3 shows a typical plot of methane conversion as a function of ISV_{CH4} along with the 95% confidence interval, which was obtained based on three identical experiments at 850 ^{o}C. The results show that most of the collected data fall within the prediction intervals. Separate repeatability experiments conducted at 825 ^{o}C also showed similar results, indicating that the data were reproducible even at low temperatures where the sensitivity of the GC was lower.

The values of a and b were obtained by fitting the methane conversion data versus ISV_{CH4} to equation (7), which was differentiated to give the reaction rate versus ISV_{CH4} (Eq. 8) for each feed condition. It has been observed (Bradford and Vannice, 1999) that DMR is strongly influenced by the simultaneous occurrence of the RWGS, which was typically close to equilibrium at the range of temperatures used in this study. Therefore, while the partial pressure of CH_4 could be directly calculated from the measured methane conversion, the partial pressure of CO_2 was calculated by taking into an account the presence of RWGS reaction, which was assumed to be at equilibrium. The partial pressure of water formed by RWGS in all experiments was found to be less than 0.02 bar, therefore, the occurrence of steam-methane reforming, if any, would not significantly affect the partial pressures of the gases. The rate expression for the Ce-promoted Mo_2C catalyst at 800 – 900 ^{o}C with partial pressures of CH_4 and CO_2 ranging from 0.02 – 0.24

bar and 0.02 – 0.31 bar, was then obtained by fitting equation (9) to the experimental data. The resulting rate expression is given in equation (10).

$$rate = 2.21x10^{8} e^{\frac{-45,500}{1.987T}} P_{CH4}^{0.95} P_{CO2}^{-0.18}, \quad (R^2=0.962) \tag{10}$$

A sensitivity analysis was conducted to determine the effect of each parameter to the fit. Forcing the CH_4 order to 1.0 slightly lower the fit (R^2=0.96), decreased the CO_2 order to –0.21, and decreased the activation energy to 44,800 cal/mol. Setting the reaction order of CO_2 to 0 also gave a slightly lower fit (R^2=0.955), with an activation energy of 45,800 cal/mol and a CH_4 reaction order of 0.80. The parity plot of the predicted rate from equation (10) versus the experimental rate is shown in Figure 4. As can be seen, the predicted rate fits well with the experimentally derived values over the range of measured rates. The small deviations from the parity line are due to inaccuracies (± 5-12%) in the measurements of the low conversions, which were particularly present at the lower temperatures.

In a separate evaluation of the validity of the reaction rate expression, equation (10) was used to predict the CH_4 conversions at previously untested reactant pressures and also at an extrapolated temperature of 925 ^{o}C. That is, the predicted CH_4 conversion was calculated by solving the differential equation containing the reaction rate expression, and then the experiment was conducted to measure the actual conversion. Figure 5 shows the predicted versus the measured conversions and, as can be seen, there is excellent agreement.

4. Discussion

Table 1 shows a comparison of kinetic parameters from the literature with those obtained here. As can be seen, the activation energy of the ceria-promoted Mo_2C is significantly higher than that of all the bulk Mo_2C catalysts, except for the value obtained by LaMont and Thomson (2004). However there are a number of limitations associated with most of the previous kinetic studies. For example, Claridge et al. (1998) used only one set of reactant pressures and operated at very low temperatures. Even then, they operated under oxidizing conditions and had to back-extrapolate their data to the point preceding oxidation. Sehested et al. (2001) also used only one set of reactant pressures, and admitted they were operating under mass transfer limited conditions. Unfortunately, only limited information was reported by Naito et al. (2002), and consequently, even though they reported reaction orders, they failed to mention the range of the reactant pressures. In addition, they only used one temperature and thus, were not able to report an activation energy. Thus, the only kinetic studies of DMR reaction kinetics under non-oxidizing conditions and negligible mass transport phenomena limitations, is this work and that conducted by LaMont and Thomson (2004) over a bulk Mo_2C catalyst. Therefore, the activity of bulk Mo_2C from their study and the activity of the ceria-promoted catalyst from this study can be directly compared.

The fact that the activation energies for the ceria-promoted and bulk catalysts were comparable, suggests that the nature of the active metal sites on these two catalysts are

similar. Since a separate DMR experiment over Ce/γ-Al_2O_3 indicated that the activity of the Ce/γ-Al_2O_3 was negligible, this implies that the DMR activity was essentially due to the Mo_2C itself. However, it would be expected that the number of the active sites on bulk and ceria-promoted Mo_2C would be different due to higher Mo_2C dispersion on the supported catalyst. Unfortunately, CO adsorption measurements over the ceria-promoted catalyst were unreliable, due to the known phenomena of strong CO adsorption on the ceria. Thus, comparison of catalyst activity on a per active sites basis (turn over frequency) could not be made. Consequently, the comparison of the activity between the bulk and the Ce-promoted Mo_2C catalyst in this study was made on a Mo weight basis. Using equal partial pressures of CH_4 and CO_2, such as 0.15 bar at 850 ^oC, the activity of the ceria-promoted Mo_2C catalyst was about 0.42 $mol_{CH4}/g_{.Mo}/h$. This activity is about 26 times higher than that of bulk Mo_2C obtained by LaMont and Thomson (2004), which was approximately 0.016 $mol_{CH4}/g_{.Mo}/h$, calculated from their rate expression under the same conditions.

A study by Claridge et al. (1998) proposed a mechanism, which involved a solid state reaction, to explain the competition of reforming and deactivation of Mo_2C. It was proposed that after CO_2 dissociation and CO desorption, the oxygen reacted with a carbon from the carbide leaving a carbon vacancy, which would be replenished by either a carbon from CH_4 dissociation or by an oxygen species to initiate the oxidation of Mo_2C to MoO_2. They also proposed a dual site noble metal mechanism where adsorbed oxygen species could react with adsorbed carbon from CH_4 dissociation. However, LaMont and Thomson (2004) argued that the carbon from CH_4 dissociation was unlikely to undergo

direct reaction with the oxygen species during DMR due to its short residence time on the Mo_2C surface. The high reactivity of carbon on the surface was corroborated by isotopic evidence, showing a rapid exchange between carbon from CH_4 and surface carbidic carbon (LaMont et al., 2003), and hydrogen exchange between CH_4 and CD_4 (Naito et al., 2002). In addition, previous observations of moving front oxidation (Claridge et al., 1998; Sehested et al., 2001; LaMont et al., 2003) are consistent with the low reactivity of CH_4 with the oxygen species in the presence of more reactive reforming gases, such as CO and H_2 (Darujati et al., 2003). Consequently, they proposed a mechanism to explain the fractional reaction order of CO_2 and the high activation energy, as well as taking into account the rapid carbon exchange between CH_4 and the Mo_2C surface. Surface reactions (11) and (12) describe their proposed mechanism:

$$CH_4 \leftrightarrows C(\blacklozenge) + 2H_2 \quad (11)$$

$$CO_2 \leftrightarrows O(\blacklozenge) + CO \quad (12)$$

where ($\blacklozenge$) represents a vacancy near the surface of the Mo_2C. Under oxidizing conditions, such as with a stoichiometric feed at high mass transfer rates, reaction (12) is more dominant. They also suggested that once reaction (12) is inhibited by the addition of excess CO, rapid carbon exchange between CH_4 and Mo_2C could occur. Meanwhile the CO_2 would adsorb on the carbon filled-site from reaction (11), extract the carbon to produce CO, and replenish a vacancy according to reaction (13):

$$CO_2 + C(\blacklozenge) \leftrightarrows 2CO + (\blacklozenge) \quad (13)$$

Taking this reaction as the rate-determining step of the overall process, it would account for the high activation energy.

Whereas the reaction order with respect to CH_4 in our study is almost unity and similar to that obtained by LaMont and Thomson (2004), our CO_2 reaction order was much lower. The near zero reaction order with respect to CO_2 indicates the presence of a different DMR mechanism over the ceria-promoted catalyst. It has been previously reported that the DMR mechanism over ceria supported Pd involved the reduction and re-oxidation of ceria (Sharma et al., 2000). Surface analysis by XPS of our fresh catalyst indicated that about 60% of the ceria was in the form Ce_2O_3, while the remainder was CeO_2. Therefore, if CH_4 undergoes decomposition and rapid carbon exchange with Mo_2C as proposed by LaMont and Thomson (2004), ceria could simultaneously undergo a redox reaction in the presence CO_2:

$$Ce_2O_3 + CO_2 \leftrightarrows 2CeO_2 + CO \qquad (14)$$

The adsorption of CO_2 on Ce_2O_3 in this manner is also consistent with our previous observation of the high oxidation stability of the Ce-promoted Mo_2C in DMR (Darujati and Thomson, 2005). With this mechanism, a rate expression of the form of equation (15) might be expected:

$$rate = \frac{k P_{CH4} P_{CO2}}{\left(1 + K P_{CO2}\right)} \qquad (15)$$

where k is the rate constant and K is the CO_2 adsorption equilibrium constant for reaction (14). The optimized kinetic parameters for each temperature are shown in Table 2, and the parity plot for this expression is given in Figure 6. As can be seen, the high K values effectively give a zero reaction order with respect to CO_2.

It is important to note that although the presence of excess CO in the feed was to prevent oxidation of Mo_2C by forcing reaction (12) to the left, the CO could also reduce the ceria by reversing reaction (14), and further undergo CO disproportionation to produce carbon and CO_2:

$$2CO \leftrightarrows C + CO_2 \qquad (16)$$

In fact, the phenomena of CO dissociation has been observed by Putna et al. (1998) over Rh/ceria catalyst, and it was reported to occur readily on the more reduced Ce_2O_3. Therefore, the low reaction order of CO_2 could also be explained by a simultaneous occurrence of the rapid activation of CO_2 onto the ceria and the carbon gasification reaction via the reverse of reaction (16). Analogous observations were made by Craciun et al. (1998) for CO oxidation over Pd/ceria. In their study, the strong adsorption of CO on the ceria support resulted in a zero reaction order with respect to CO.

Craciun et al. (1998) proposed a mechanism which involved surface reaction of the adsorbed oxygen on the ceria with the dissociated methane on the metal for SMR over

noble metals supported on ceria catalysts, and obtained an activation energy of 18 kcal/mol. Their observation of identical rates for Rh, Pt and Pd/ceria catalysts in SMR led to the conclusion that oxygen transfer from the ceria to the metals was the rate determining step. However, the much higher activation energy obtained from our study suggests the presence of an alternative rate-determining step. While the surface reaction of the adsorbed oxygen on the ceria with the adsorbed carbon on the Mo_2C (Eq. 18) is likely to occur, the adsorbed carbon on Mo_2C is hypothesized to be a carbidic carbon, originating from the carbon exchange between CH_4 and Mo_2C, and which has to be extracted by oxygen via a solid-state reaction similar to reaction (13) for bulk Mo_2C catalysts. Therefore, the overall DMR mechanism on the Ce-promoted Mo_2C is described by the following reactions:

$$CH_4 \leftrightarrows C(\blacklozenge) + 2H_2 \quad (11)$$

$$CO_2 \leftrightarrows O(\blacksquare) + CO \quad (17)$$

$$C(\blacklozenge) + O(\blacksquare) \rightarrow CO + (\blacklozenge) + (\blacksquare) \quad (18)$$

where (■) represents an adsorption site on the ceria. Thus, reaction (18) would not be a simple dual site reaction involving adsorbed carbon and adsorbed oxygen, but involves a solid-state reaction. This mechanism would be consistent with the high activation energy of the supported catalyst.

4. Conclusions

A kinetic study of DMR in the absence of mass-transfer limitations has been carried out over a stabilized ceria-promoted $Mo_2C/\gamma\text{-}Al_2O_3$ catalyst. The results described in this paper have shown that the addition of a ceria promoter appears to alter the DMR mechanism proposed earlier for bulk Mo_2C catalysts. While the activation energy of the promoted Mo_2C catalyst is similar to that reported for the bulk Mo_2C catalyst, the activity of the ceria-promoted catalyst is much higher, which is likely due to the higher dispersion of the promoted catalyst. Ceria promotion appears to affect the DMR reaction by enhancing relatively strong CO_2 adsorption, thereby lowering the reaction order of CO_2 to zero. The role of ceria to influence redox chemistry on the surface of the catalyst is consistent with our previous observation of the high stability of ceria-promoted Mo_2C catalysts in DMR. A mechanism, which accounts for both the CO_2 and CO redox reaction on the ceria particles, and CH_4 and CO_2 activation on the Mo_2C particles is proposed and is consistent with the kinetic model.

Acknowledgement

This material is based on work supported by the National Science Foundation under Grant CTS-0209372.

References:

Aegerter, P.A., Quigley, W.W.C., Simpson, G.J., Ziegler, D.D., Logan, J.W., McCrea, K.R., Glazier, A., Bussell, M.E., 1996. Thiophene Hydrodesulfurization over Alumina-Supported Molybdenum Carbide and Nitride Catalysts: Adsorption Sites, Catalytic Activites, and Nature of the Active Surface. Journal of Catalysis 164, 109-121.

Bradford, M.C.J., Vannice, M.A., 1998. CO_2 Reforming of CH_4 over Supported Pt Catalysts. Journal of Catalysis 173, 157-171.

Claridge, J.B., York, A.P.E., Brungs, A.J., Marquez-Alvarez, C., Sloan, J., Tsang, S.C., Green, M.L.H., 1998. New Catalysts for the Conversion of Methane to Synthesis Gas: Molybdenum and Tungsten Carbide. Journal of Catalysis 180, 85-100.

Craciun, R., Shereck, B., Gorte, R.J., 1998. Kinetic Studies of Methane Steam Reforming on Ceria-supported Pd. Catalysis Letters 51, 149-153.

Darujati, A.R.S., LaMont, D.C., Thomson, W.J., 2003. Oxidation Stability of Mo_2C Catalysts under Fuel Reforming Conditions. Applied Catalysis A 253, 397-407.

Darujati, A.R.S., Thomson, W.J., 2005. Stability of Supported and Promoted Molydenum Carbide Catalysts for Dry-methane Reforming. In review for Applied Catalysis.

Dhandapani, B.B., Ramanathan, S., Yu, C.C., Fruhberger, B., Chen, J.G., Oyama, S.T., 1998. Synthesis, Characterization, and Reactivity Studies of Supported Mo_2C with Phosphorus Additive. Journal of Catalysis 176, 61-67.

LaMont, D.C., Gilligan, A.J., Darujati, A.R.S., Chellappa, A.S., Thomson, W.J., 2003. The Effect of Mo_2C Synthesis and Pretreatment on Catalytic Stability in Oxidative Reforming Environments. Applied Catalysis A 255, 239-253.

LaMont, D.C., Thomson, W.J., 2004. The Influence of Mass Transfer Conditions on the Stability of Molybdenum Carbide for Dry Methane Reforming. Applied Catalysis A 274, 173-178.

LaMont, D.C., Thomson, W.J., 2004. Dry Reforming Kinetics over a Bulk Molybdenum Carbide Catalyst. Chemical Engineering Science, in press.

McCrea, K.R., Logan, J.W., Tarbuck, T.L., Heiser, J.L., Bussel, M.E., 1997. Thiophene Hydrodesulfurization over Alumina-supported Molybdenum Carbide and Nitride Catalysts: Effect of Mo Loading and Phase. Journal of Catalysis 171, 255-267.

Naito, S., Tsuji, M., Miyao, T., 2002. Mechanistic Difference of the CO_2 Reforming of CH_4 over Unsupported and Zirconia Supported Molybdenum Carbide Catalysts. Catalysis Today 77, 161-165.

Pritchard, M., McCauley, R., Gallaher, B.N., Thomson, W.J., 2004. The Effects of Sulfur and Oxygen on the Catalytic Activity of Molybdenum Carbide during Dry Methane Reforming. Applied Catalysis A 275, 213-220.

Putna, E.S., Gorte, R.J., Vohs, J.M., Graham, G.W., 1998. Evidence for Enhanced Dissociation of CO on Rh/Ceria. Journal of Catalysis 178, 598-603.

Sehested, J., Jacobsen, C.J.H., Rokni, S., Rostrup-Nielsen, J.R., 2001. Activity and Stability of Molybdenum Carbide as a Catalyst for CO_2 Reforming. Journal of Catalysis 201, 206-212.

Sharma, S., Hilaire, S., Vohs, J.M., Gorte, R.J., Jen, H.-W., 2000. Evidence for Oxidation of Ceria by CO_2. Journal of Catalysis 190, 199-204.
York, A.P.E., Claridge, J.B., Tsang, A.J., Green, M.L.H., 1997. Molybdenum and Tungsten Carbides as Catalysts for the Conversion of Methane to Synthesis Gas Using Stiochiometric Feedstocks. Chemical Communications (1), 39-40.

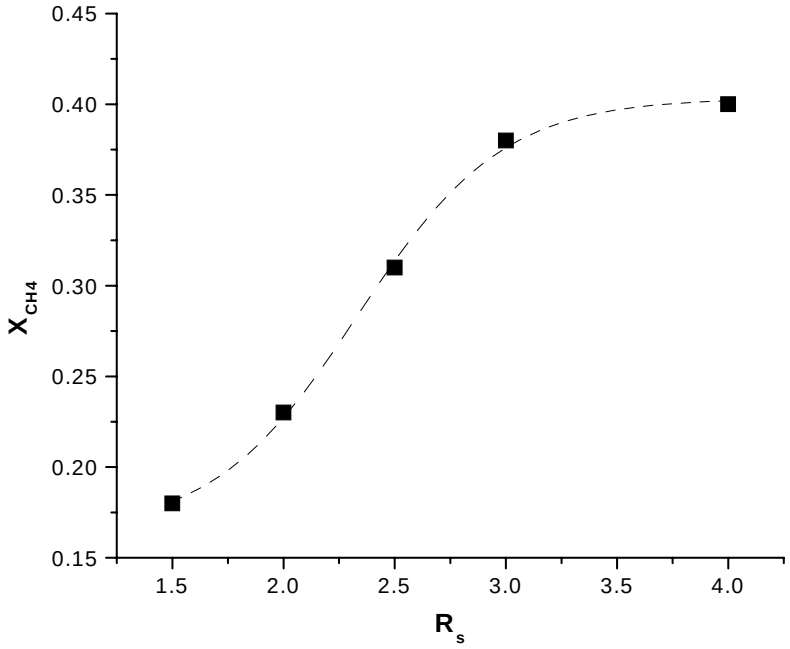

Figure 1. Methane Conversion at 1 hr on stream versus R_s (T = 900 ^oC, CO_2 : CH_4 = 1, GHSV = 26,000 h^{-1})

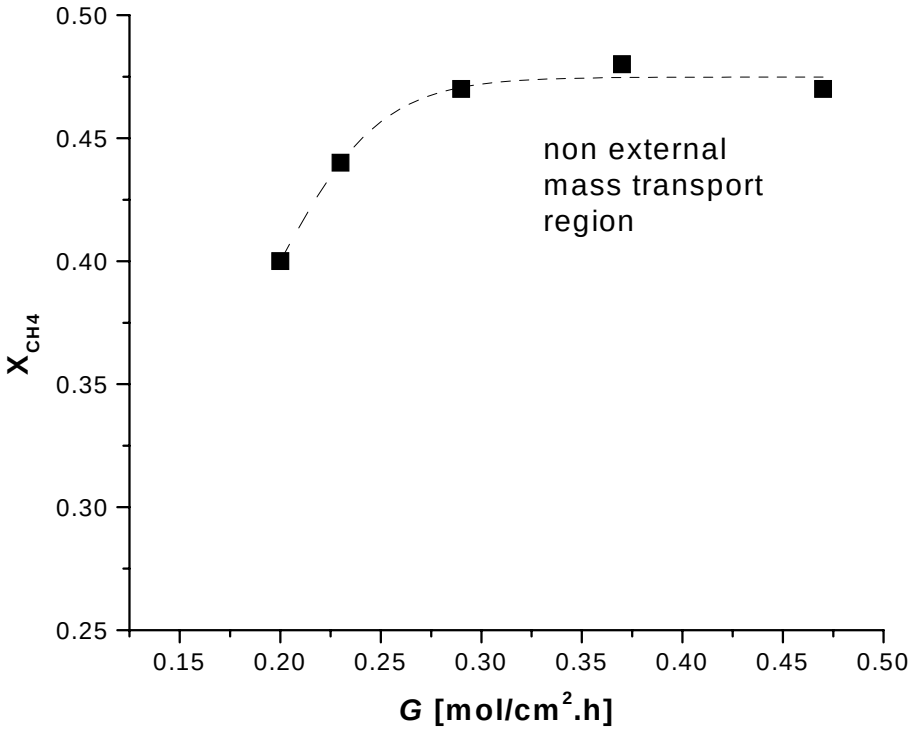

Figure 2. Mass transport determination at 900 ^{o}C, $CO_2 : CH_4 = 1$, GHSV = 26,000 h^{-1}.

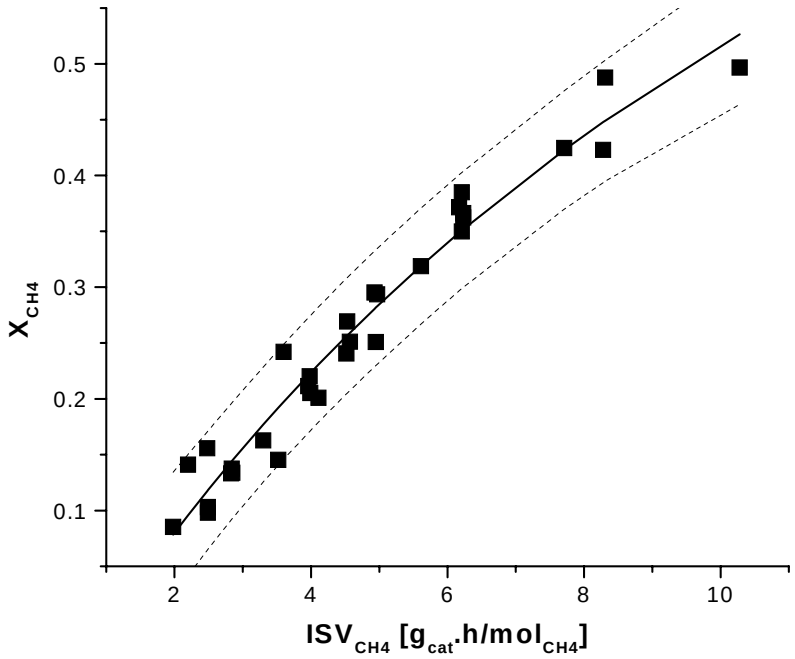

Figure 3. A typical plot of methane conversion versus ISV_{CH4}. Data were obtained at 850 ^{o}C, CO_2 : CH_4 = 1. The curves shown are curve fit with R^2 of 0.95 (—) and the prediction band curves for 95% confidence intervals on the population (- -).

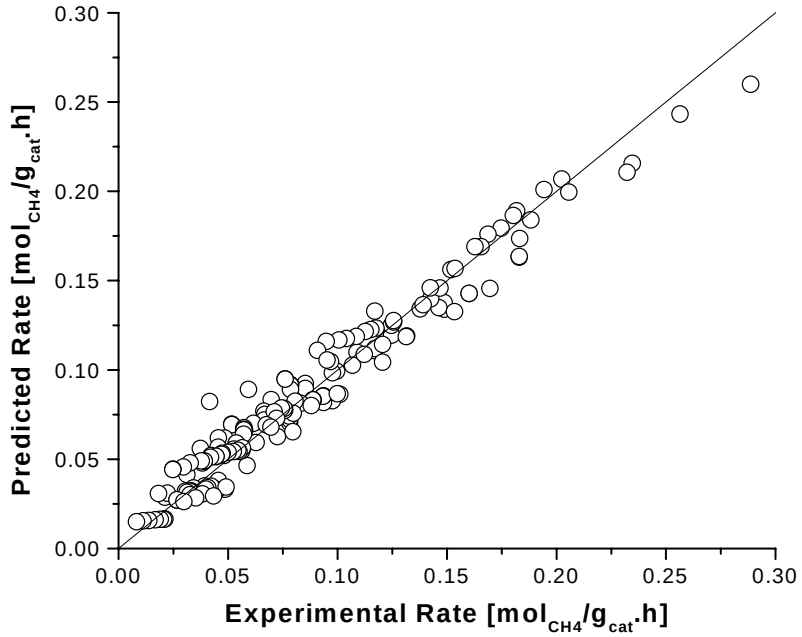

Figure 4. Parity plot of predicted rate obtained from equation (10) versus experimental rate

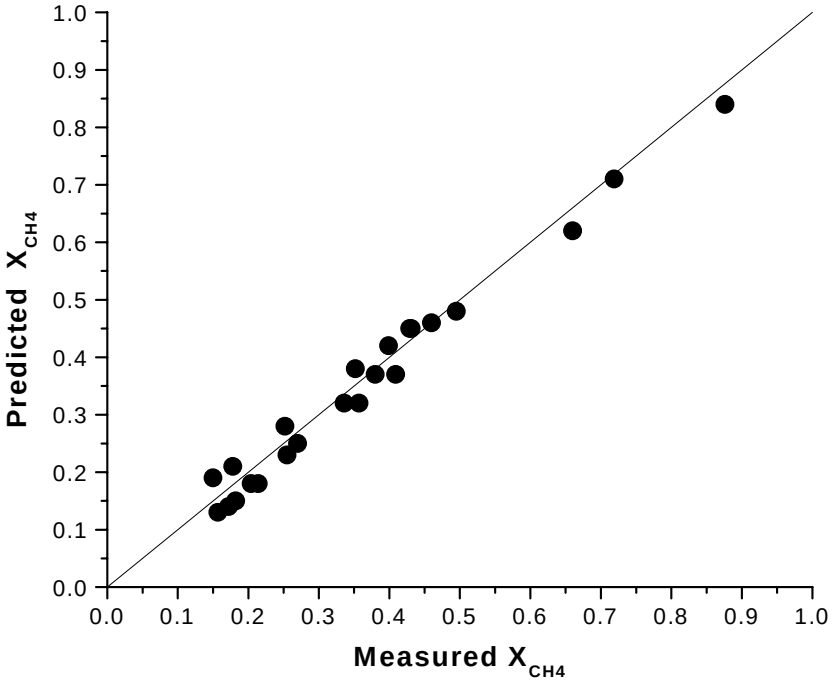

Figure 5. Parity plot of predicted X_{CH4} versus measured X_{CH4}

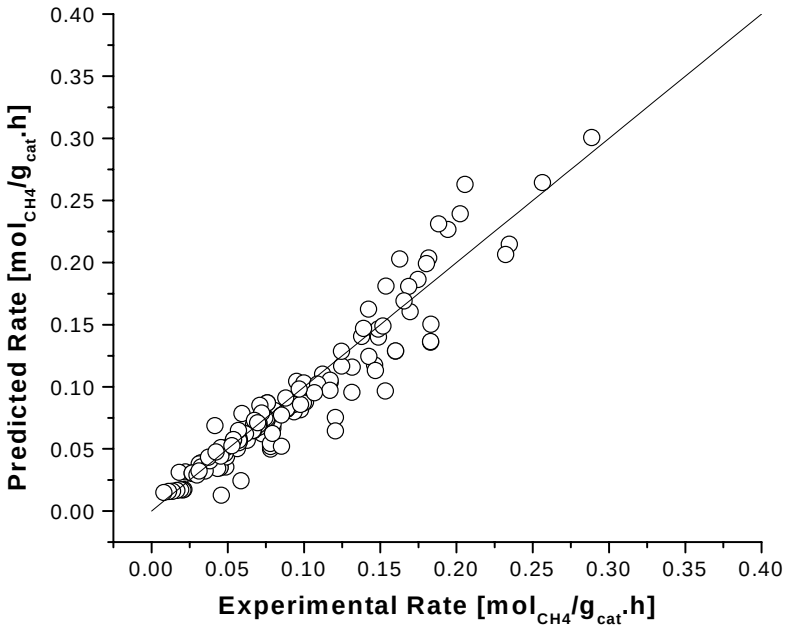

Figure 6. Parity plot of predicted rate obtained from equation (15) versus experimental rate

Table 1. Comparison of Literature DMR Kinetic Parameters for Mo_2C Catalysts

Catalyst	T [^oC]	P_{CH4} [bar]	P_{CO2} [bar]	α	β	E_a [kcal/mole]
Bulk Mo_2C[a]	800 – 900	0.15-0.32	0.11-0.23	1.2	0.7	41.2
Bulk Mo_2C[b]	700 – 800	0.74	0.86	-	-	19.1
Bulk Mo_2C[c]	627 – 697	2	2	-	-	23.8
1 wt.% Mo_2C/ZrO_2[d]	850	N/A	N/A	1.6	0.1	-
30 wt.% Mo_2C/Al_2O_3 (3 wt.% Ce) [e]	800 – 900	0.02-0.24	0.02-0.31	0.9	-0.19	44.4

[a] LaMont and Thomson (2004)
[b] Sehested et al. (2001)
[c] Claridge et al. (1998)
[d] Naito et al. (2002)
[e] This work

Table 2. Optimized Kinetic Parameters

T [^{o}C]	k [$mol_{CH4}/g_{cat}.h.bar^{2}$]	K [bar^{-1}]	R^2	P_{CH4} [bar]	P_{CO2} [bar]
900	60.6	42.7	0.69	0.02-0.24	0.02-0.29
850	23.6	43.6	0.82	0.07-0.23	0.09-0.30
800	10.8	47.8	0.74	0.08-0.21	0.14-0.31

CHAPTER FIVE

SUMMARY AND CONCLUSIONS

The preceding chapters describe the oxidative stability of Mo_2C and efforts to understand and improve the stability of Mo_2C as a reforming catalyst. Basic studies of bulk Mo_2C oxidative stability was presented in Chapter Two. It was concluded that, while the oxidation of Mo_2C in both CO_2 and steam occurred at a relatively low temperature (~ 600 ^oC), oxidation could be delayed in the presence of reforming gases such as CO and H_2. The reaction mechanisms which describe oxidation suppression by CO and H_2 via redox reactions were presented for the first time. On the other hand, there was very little effect of CH_4 in protecting the Mo_2C from oxidation. These results allowed a quantitative description of the conditions at which oxidation of Mo_2C can be prevented, succinctly summarized by the stability ratio, R_S; i.e., the partial pressure ratio of $CO + H_2$ to $CO_2 + H_2O$. At 775 ^oC, oxidation was prevented at all conditions at which the stability ratio was greater than 0.8.

As a part of our study to improve the stability of Mo_2C, modifications of the catalyst was accomplished through the utilization of various supports and promoters, as described in Chapter Three. It was concluded that the ability of γ-Al_2O_3 to maintain its high surface area at high temperatures, combined with its interaction with Mo at high Mo loading, were important factors for producing a high activity for the Mo_2C catalyst. Furthermore, the oxidation stability of this catalyst was greatly improved with the addition of ceria promoter. The ability of ceria to take-up and release oxygen during reforming provided

capacity to buffer surface oxygen, and was likely the cause of the improved stability of the catalyst. Over the ceria-promoted Mo_2C, the point during catalyst synthesis at which the ceria promoter was added was found to be critical to activity and stability. It was hypothesized that the interaction between ceria and γ-Al_2O_3 was necessary to prevent ceria agglomeration. Furthermore, a study on the effect of CO and H_2 on the stability of the ceria-promoted Mo_2C was also conducted, and it was successfully demonstrated that the long-term stability of the supported and ceria-promoted Mo_2C could be achieved by co-feeding CO. In fact, the activity of the ceria-promoted catalyst was much higher than that of the bulk Mo_2C. However, there appeared to be an optimum value of CO partial pressure for the ceria-promoted catalyst, created by the trade-off between oxidation prevention at high CO partial pressures and optimum oxygen buffering at low CO partial pressures.

A more in-depth study was conducted, which focused on the investigation of the DMR kinetics over the ceria-promoted Mo_2C described in Chapter Four. Benefiting from the knowledge that the Mo_2C could be stabilized in the presence of CO, the rate expression of ceria-promoted Mo_2C at temperatures between 800 – 900 ^oC was obtained. Careful evaluation was taken to ensure the measured reaction rate truly represented the chemical reaction. From the results of this study, the effect of ceria promoter on the reaction mechanism was identified, by comparing the rate expression of the ceria-promoted catalyst with the expression previously determined for the unpromoted bulk catalyst. While the presence of ceria did not affect the activation energy, it had a much higher activity, enhanced CO_2 adsorption, and altered the reaction order of CO_2. This

evidence supported the previous observation of the high stability of ceria-promoted Mo_2C described in Chapter Three. The high activation energy was consistent with a prior study in the literature, which attributed this phenomenon to the presence of a solid-state reaction. However, an alternative route for the promoted catalyst was proposed. This route accounted for the strong adsorption of CO_2 on the ceria and Mo_2C particles while taking into consideration the rapid carbon exchange between CH_4 and Mo_2C.

While significant improvement of the stability and activity of Mo_2C have been achieved over ceria-promoted Mo_2C, there should be subsequent work to further optimize the performance of Mo_2C catalysts. The most important would be to lower the activation energy, to allow for operation at lower temperatures and/or higher space velocities. On the other hand, the high activation energy of DMR over Mo_2C was associated with solid-state reactions. Therefore, it remains a question whether further modifications to this catalyst by addition of other metals, promoters, or supports could change the rate-limiting step to one not involving solid-state reaction of high activation energy, thus producing a catalyst capable of operation at lower temperatures. Still another subject for further work would be to utilize these catalysts in a "back-mix" environment, such as a fluidized bed reactor. This would keep the catalyst in the presence of product gases and eliminate the need for adding CO or H_2 to the feed to prevent oxidation.

APPENDIX A

EQUIPMENT DIAGRAM AND PROCEDURE

A.1. D-XRD System

The D-XRD system used in this study is shown in Figure A1. The flow rates of the feed gases were controlled by two Brooks Mass Flow controllers model 5850E, and two Brooks Mass Flow Sensors model 5860E, equipped with two needle valves, and were monitored by Brooks Read Out and Control Electronic 0154. Steam was generated by pumping water via a Cole-Parmer 74900 series syringe pump to a vaporizer. Once the steam generation was steady, a three-way valve was used to introduce the steam to a pre-mixer where it was mixed with the feed gases. The mixture was then delivered to the Anton Parr XRK 900 hot stage in a heated line. The hot stage was uniquely designed so that solid state-gas reactions can be studied under various gaseous atmospheres and under pressures as high as 10 bar. The maximum allowable temperature for this hot stage was 900°C. In the case of experiments at elevated pressures, a back-pressure regulator was installed at the outlet of the hot stage to control the pressure in the hot stage. A blank run in a mixture of He and Ar was used to determine the gas composition and that would result in thermal conductivity necessary to allow the temperature to be heated up to 850°C in the hot stage. The thermal conductivity of the gas required to heat the XRK 900 hot stage to 850C was found to be 0.29 W/m-K. The temperature in the hot stage was controlled by a Paar Physica TCU 750 Temperature Control Unit. An ice bath was used to condense water out of the exit gas prior to introducing it to the GC. The exit gas composition was analyzed by a Shimadzu GC 14-A equipped with a thermal conductivity

detector and a Hayesep D 20’ x 1/8‘’ nickel column and coupled to a Shimadzu Chromatopac GC Integrator. A mixture of 10% H_2 in He was used as a carrier gas. This carrier gas was chosen, because with this mixture, the H_2 peaks were completely inverted, allowing for accurate integration.

A.2. Reactor System

Figure A2 shows the microreactor system used in this study. The flow rates of the feed gases were controlled by Brooks Mass Flow Controllers Model 5850E. The gas mixtures were fed to a reactor system consisting of an 8 mm ID quartz tube reactor, which is placed inside a WATLOW furnace capable of heating to 1000^{o}C, and controlled by a WATLOW F4 temperature controller. Temperature of the bed was measured by a type K thermocouple sheathed in a quartz tube, which was placed on the bottom of the catalyst bed. The pressure of the reactor was controlled by a back-pressure regulator installed at the exit of the reactor. A condenser at the exit of the reactor was used to condense out any water generated during the experiment prior to introducing the gas to the gas chromatograph (GC). A SRI GC equipped with a thermal conductivity detector (TCD) and two columns, molecular sieve 13X and a hayesep D, was used to analyze the exit gas composition during the experiments.

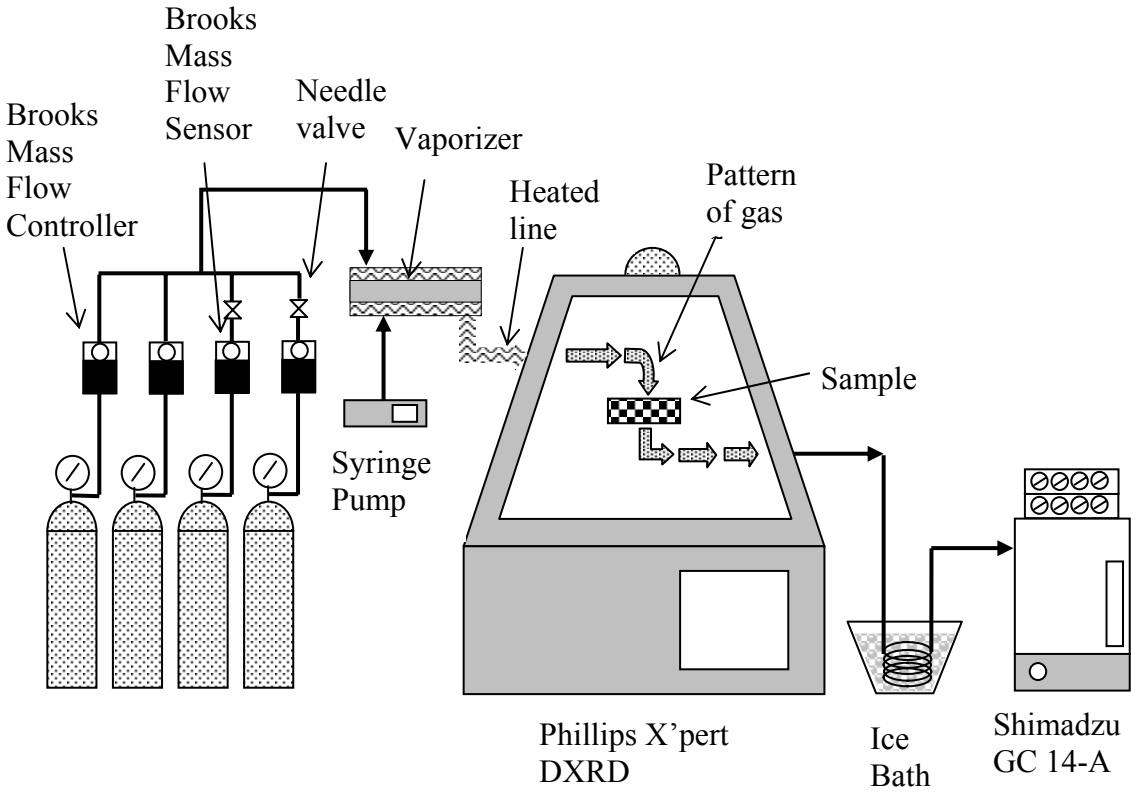

Figure A1. Schematic diagram of D-XRD system

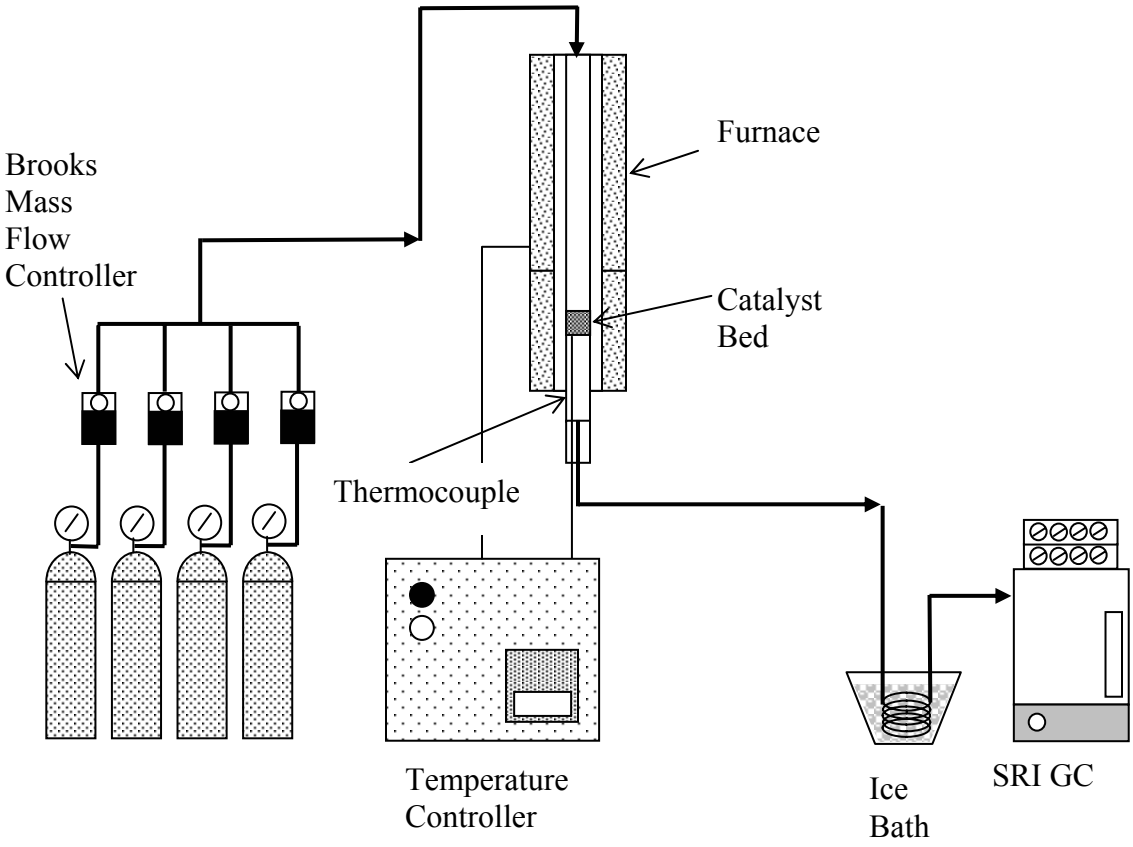

Figure A2. Schematic diagram of microreactor system

APPENDIX B

CATALYST CHARACTERIZATION

B.1. Neutron Activation Analysis (NAA)

Neutron activation analysis (NAA) was used to confirm the theoretical Mo loading used in Chapter 3. Characterization was done using samples with three different Mo loadings ranging from 5 to 30 wt.%. In addition, two samples with identical loading (30 wt.%) synthesized from different batches were characterized, to determine the reproducibility of the synthesis technique. Independent characterization using NAA was important, because, in general, when the Mo loading was below 15 wt.%, XRD did not yield any peaks corresponding to molybdenum oxide or molybdenum carbide. In all cases, NAA was performed over γ-alumina-supported (Mo/γ-Al) catalysts. NAA results for weight percentage of Mo in samples with theoretical Mo loadings of 5, 15 and 30 wt.% are 4.95, 13.89 and 27.57 ± 0.35 wt.%, respectively. Variation of Mo loading from sample to sample was found to be low, with calculated error of less than 2% of the average value. The discrepancy between theoretical Mo wt.% and NAA values increase with higher Mo loading. The much shorter half-life of Al^{28} (2.3 minutes) compared to that of Mo^{99} (2.7 days) was likely the source of this trend, since the relative content of Al decreases with increasing Mo loading.

B.2. X-Ray Photoelectron Spectroscopy (XPS)

Both surface concentration of Mo and ceria oxidation state of the Mo/γ-Al and Ce-promoted $Mo_2C/\gamma\text{-}Al_2O_3$ catalysts in Chapter 3 were measured by XPS. The surface concentration of Mo was defined as the ratio of the atomic concentration of Mo to the atomic concentration of (Mo+Al) and was calculated based on the Mo*3d* and Al*2p* energies. Figure B.1. shows an example of the Mo*3d* spectra of the 30Mo/γ-Al catalyst. The location of the Mo and the value of the full-width of height maximum (FWHM) were compared with the published values. Table B.1. shows the binding energy of various Mo species used as a reference in this study.

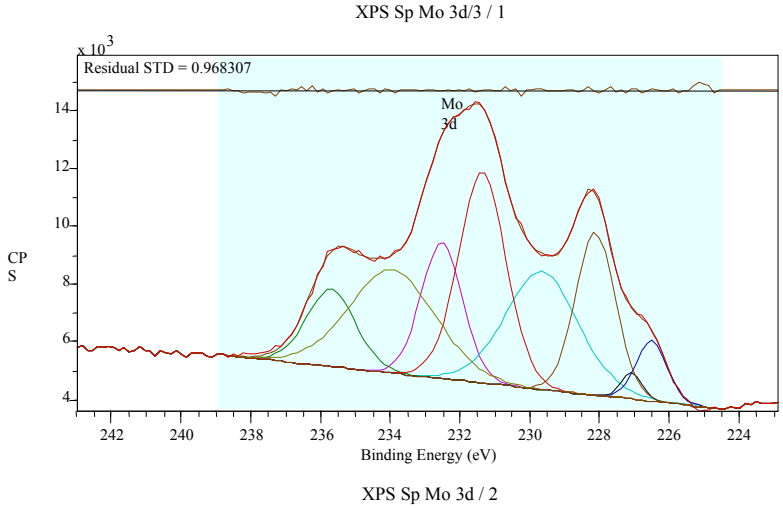

Figure B.1. The Mo*3d* spectra of the 30Mo/γ-Al catalyst (Binding energy [eV], NIST database: Mo = 228, Mo_2C = 228.8, MoO_2 = 231.1, MoO_3 = 232.7, 235.8.)

It is known that 10 peaks appear for the ceria in the Ce*3d* XPS spectrum. The oxidation state of ceria on the Ce-promoted $Mo_2C/\gamma\text{-}Al_2O_3$ was determined based on the following equations [1]:

$$Ce_2O_3 = v_o + v' + u_o + u' \quad (1)$$

$$CeO_2 = v + v'' + v''' + u + u'' + u''' \quad (2)$$

$$[Ce_2O_3] = \frac{Ce_2O_3}{Ce_2O_3 + CeO_2} \quad (3)$$

where v_o, v',u_o, u' and v, v'',v''', u, u'',u''' represents the peak related to Ce_2O_3 and CeO_2 species, respectively. The Ce_2O_3 and CeO_2 (Eq. 1 and 2) represents the corresponding sums of the peak areas related to the Ce^{3+} and Ce^{4+} XPS signals respectively. The example of XPS spectra of the Ce-promoted sample is shown in Figure B.2. In all our samples, only 9 peaks were detected since the peak assigned to v'' (B.E. = 889.5 eV) originated from Ce^{4+} was not identified. The spectra obtained by Zhang *et. al.* [2] were used as reference.

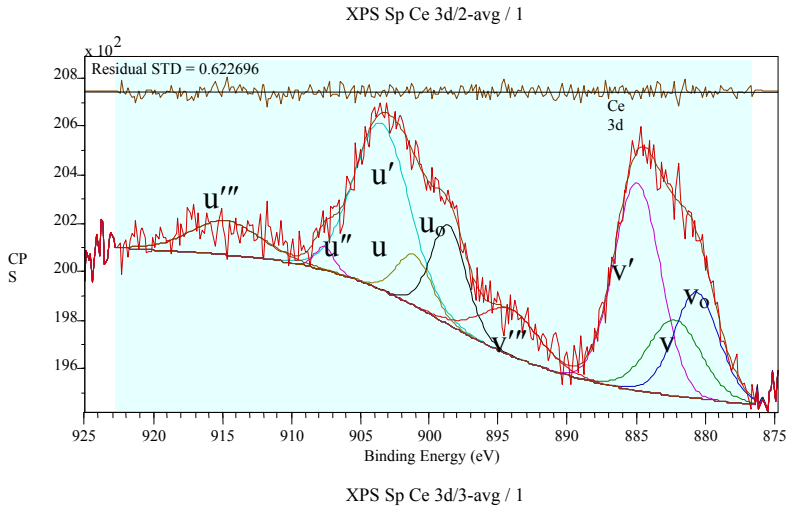

Figure B.2. An XPS spectra of ceria on Ce-promoted $Mo_2C/\gamma\text{-}Al_2O_3$ (Binding energy [eV], Zhang et. al. : $v_o = 881$, $v' = 886$, $u_o = 900$, $u' = 905$, $v = 882.5$, $v'' = 889$, $v''' = 896$, $u = 901$, $u'' = 908$, $u''' = 916$)

B.3. Crystalline Phase Analysis by X-Ray Diffractometer (XRD)

An X-Ray Diffractometer was used to both dynamically monitor the sintering of the support and to analyze the crystalline phase of the catalysts. Nitrogen was used as an inert gas during the sintering study, and the procedure of the dynamic measurement was similar with that described in Appendix A.1 Sintering of the support was determined by monitoring the crystallite size with respect to temperature, which was calculated using the Debye Scherrer equation:

$$Crystallite\ Size_{avg} = \frac{K\lambda}{B\cos\Theta} \qquad (4)$$

λ = wavelength of X-Ray source = 0.179026, nm for Co anode
K-factor = 0.9
B = full width at half maximum (FWHM), radian
2Θ = peak position

B.4. Temperature Program Reaction with Mass Spectrometer (MS)

Apart from other catalyst characterization techniques used in Chapter 3, temperature-programed reaction using an MS was conducted to qualitatively determine the effect of the various supports and promoters on the reducibility of MoO_3 in H_2/Ar. It is known that the reduction characteristics of supported catalysts are strongly related to the degree of the metal-support interaction and the character of the surface species formed during catalyst synthesis. Since a reduction step is important during synthesis of supported-Mo_2C, any aspect that is favorable to the reduction of Mo oxides is, therefore, an advantage for carburization.

Typically, 57 mg of samples were used for these experiments. Diffusion limitations were found experimentally to be absent, since experiments showed the H_2O spectra to be independent of sample mass and gas flow rate. The samples were treated in Ar at 200 ^oC for 1 hour and then exposed to a 25% H_2/Ar mixture while heating to 1000^oC at 3^oC/min. The evolution of H_2O was measured by monitoring the signal for m_{12} = 18. Vaporization of bulk MoO_3 at 795^oC was well above the reduction temperature of free MoO_3 in our sample, which was generally completed below 600 ^oC. Reduction of bulk MoO_3 (Alfa Aesar, 99.998 %) was used as a reference, and the result was compared with other study.

B.4.1. Mo/γ-Al and Bulk MoO_3 Samples

We conducted reduction experiments of Mo/γ-Al in H_2/Ar, and the results would serve as a basis for comparison to the results of promoted Mo_2C. Reduction of bulk

MoO_3 at identical conditions of flow, sample mass and heating rate provided a reference for analysis of supported MoO_3. Two stepwise reductions of MoO_3 can be seen in Figure B1, which correspond to the transformation of Mo^{6+} to Mo^{4+} (680 ^oC), and from Mo^{4+} to Mo^0 (850 ^oC). This results compared well with reduction profile and temperature obtained by Feng, *et. al*. [1]. Figure B.3. also shows H_2O evolution during temperature programed reduction over of Mo/γ-Al catalysts. Compared to the reduction of bulk MoO_3, the reduction over Mo/γ-Al is shifted to lower temperatures, suggesting a support effect. Over 30Mo/γ-Al, two major reductions occur over two temperature regions. At low temperatures, reduction peaks (T_{max}) at about 410, 455 and 530 ^oC correspond to the reduction of octahedral Mo^{6+} to Mo^{4+} and amorphous multilayered Mo oxides. At high temperatures (> 650 ^oC), the second broad-reduction peak with several shoulders can be assigned to the deep reduction of all Mo species including amorphous multilayered Mo oxides and Mo^{4+} to Mo^0. Our reduction observations are similar those obtained by Barath *et. al*. over alumina supported MoO_3 [4]. The reduction profile over 15Mo/γ-Al shows a similar trend with only two reduction peaks detected in the low temperature region and a weaker H_2O signal throughout the entire temperature range, as a result of the lower Mo content.

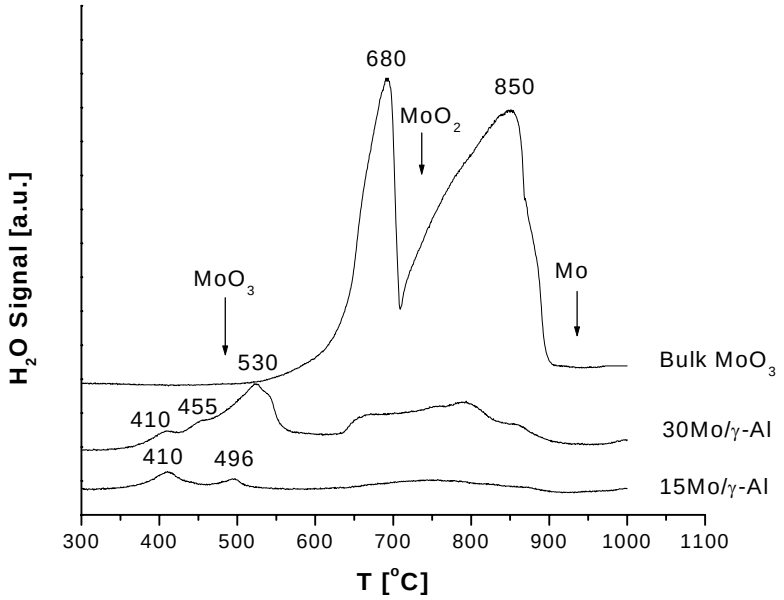

Figure B.3. Water evolution during reduction of Mo/γ-Al in H_2 (H_2 : Ar = 1 : 3, total flow rate = 40 SCCM, heating rate = 3°/min).

B.3.2. Ce-promoted Samples

Figure B.4. shows the reduction behavior of Ce-promoted catalysts in H_2/Ar. A similar pattern of two reduction peaks, observed with unpromoted Mo/γ-Al, was also observed over Ce-promoted catalysts. However, the shift in T_{max} of the first reduction and the change of the reduction spectra with respect to the impregnation sequence is an indication of the change in the type of surface species due to promoter addition. Compared to other catalysts, T_{max} of the first reduction peak for 3Ce-*c*-30 Mo is the lowest (506 °C), which could indicate the presence of more reducible Mo oxide species on the surface of this catalyst. The highest T_{max} of the first reduction region was observed

with the 30Mo-*c*-3Ce catalyst at 563 ^{o}C, which is a sign of the presence of less reducible Mo oxide species on the surface. There is an additional peak at high temperature (933 ^{o}C) indicated by 30Mo-3Ce-*c* catalyst. Since neither bulk CeO_2 or 3 wt% Ce/γ-Al_2O_3 reduction (not shown) indicated the presence of this peak, the presence of this peak in 30 Mo-3Ce-*c* sample might be due to reduction of a new species that resulted from an interaction between Mo and Ce formed during impregnation.

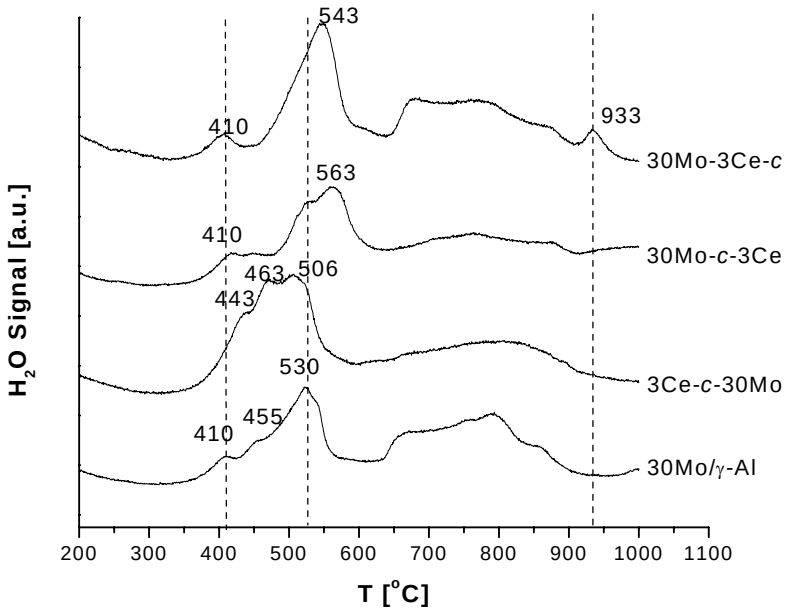

Figure B.4. Water evolution during reduction of Ce promoted catalysts in H_2 (H_2 : Ar = 1 : 3, total flow rate = 40 SCCM, heating rate = 3^{o}/min).

5.B.3. K-promoted Samples

Figure B.5. presents reduction profiles of K-promoted catalysts for the different impregnation sequences. The unpromoted catalyst 30Mo/γ-Al is also included for comparison. As has been observed by other researchers [5], for K-promoted catalysts, the reduction peak at 410 ^{o}C that was initially observed over the unpromoted catalyst disappears, and the first T_{max} is observed at a higher temperature (455 ^{o}C), suggesting the presence of less reducible Mo^{6+} species. There is no significant reduction observed over 3 wt.% K/γ-Al_2O_3 (not shown), which implies that K is not reducible in H_2 at these conditions. All K-promoted catalysts show a higher intensity H_2O signal compared with the unpromoted catalysts, which was previously observed by Feng *et. al.* [1]. Over K-promoted catalysts, peaks at about 455, 480, and a sharp peak at about 530 ^{o}C are observed in the temperature reduction region. In the high temperature region, one sharp peak at 800 ^{o}C and a small peak at 893 ^{o}C are observed. Neither the reduction profile nor the T_{max} of the K promoted samples changed as a result of the order of K promoter impregnation.

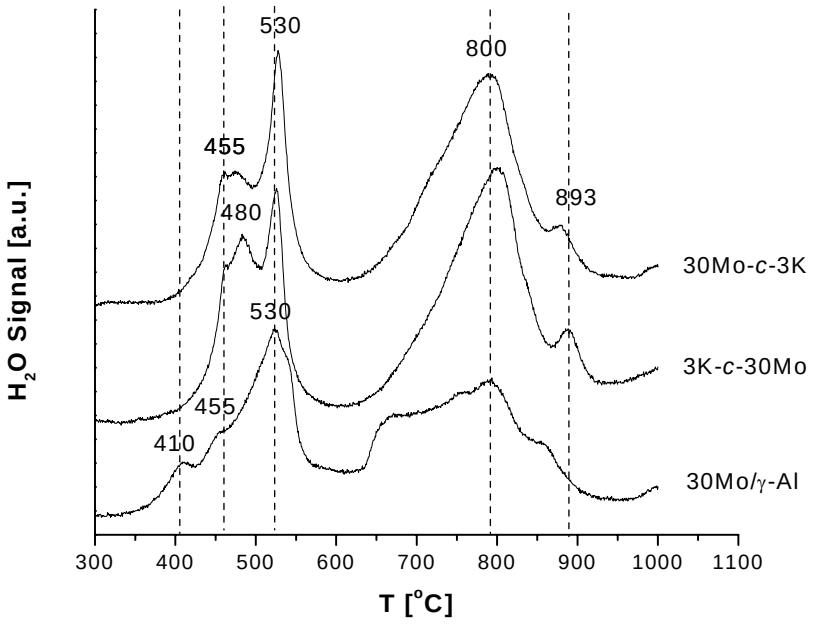

Figure B.5. Water evolution during reduction of K-promoted catalysts in H_2 (H_2 : Ar = 1 : 3, total flow rate = 40 SCCM, heating rate = 3^o/min).

5.B.4. Zr-promoted Samples

Figure B.6. presents the reduction spectra of the Zr-promoted catalysts in H_2/Ar from 250 – 1000 ^{o}C. For both 3Zr-*c*-30Mo and 30Mo-*c*-3Zr catalysts, the T_{max} at 410^{o}C, previously observed over the unpromoted catalyst, disappears, but the peak at 455^{o}C becomes more intense. In all cases, the reduction profile at temperatures above 410 ^{o}C show similarity with those of the unpromoted catalysts, except for 30Mo-*c*-3Zr catalyst, which indicates the formation of a high temperature reduction peak at 933 ^{o}C, previously observed over the 30Mo-3Ce-*c* catalyst. Since 3% Zr/γ-Al_2O_3 does not indicate any

reduction peak at this temperature, the peak at 933 ^{o}C could be associated with the reduction of a new peak formed due to Mo-Zr interaction.

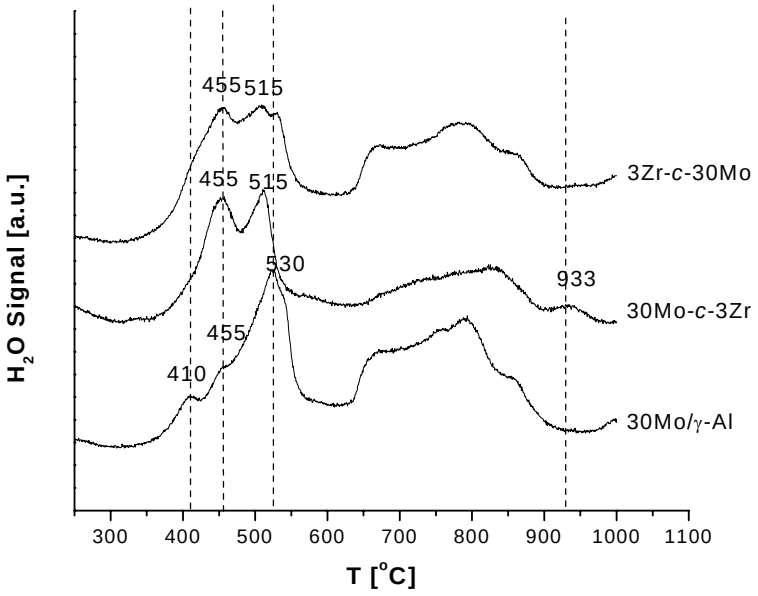

Figure B.6. Water evolution during reduction of Zr-promoted Mo_2C catalysts (H_2 : Ar = 1 : 3, total flow rate = 40 SCCM, heating rate = 3^{o}/min).

APPENDIX C

KINETICS RAW DATA

Case(*)	T[°C]	P_{CH4} [bar]	P_{CO2} [bar]	Rate [$mol_{CH4}/g_{cat}/h$]
1	900	0.129	0.168	0.16960
1	900	0.114	0.146	0.14880
1	900	0.119	0.152	0.14870
1	900	0.115	0.146	0.13780
1	900	0.097	0.121	0.13160
1	900	0.098	0.122	0.12470
1	900	0.088	0.110	0.11710
1	900	0.090	0.111	0.11710
1	900	0.087	0.108	0.10890
1	900	0.076	0.094	0.09960
1	900	0.076	0.093	0.09770
1	900	0.049	0.061	0.07810
1	900	0.050	0.063	0.07810
1	900	0.052	0.065	0.07800
1	900	0.028	0.036	0.05870
1	900	0.018	0.024	0.04580
2	900	0.190	0.182	0.20240
2	900	0.182	0.170	0.19430
2	900	0.166	0.149	0.18180
2	900	0.163	0.146	0.18030
2	900	0.154	0.136	0.17470
2	900	0.150	0.132	0.16870
2	900	0.142	0.123	0.16560
2	900	0.113	0.096	0.16010
2	900	0.113	0.096	0.16010
2	900	0.127	0.109	0.15180
2	900	0.105	0.089	0.14630
2	900	0.110	0.093	0.14260
2	900	0.088	0.075	0.13140
2	900	0.054	0.047	0.12480
2	900	0.054	0.047	0.12480
2	900	0.046	0.041	0.10900
3	900	0.240	0.175	0.30870
3	900	0.216	0.146	0.25640
3	900	0.182	0.117	0.23460
3	900	0.176	0.112	0.23220
3	900	0.135	0.084	0.18320
3	900	0.125	0.078	0.18300

3	900	0.125	0.078	0.18300
3	900	0.095	0.060	0.15340
3	900	0.107	0.067	0.14680
3	900	0.078	0.050	0.12060
3	900	0.069	0.044	0.12060
3	900	0.095	0.060	0.11700
3	900	0.059	0.038	0.08530
5	900	0.200	0.287	0.1856
5	900	0.178	0.247	0.1683
5	900	0.158	0.215	0.1428
5	900	0.143	0.192	0.1337
5	900	0.130	0.173	0.1224
5	900	0.119	0.158	0.1191
5	900	0.106	0.141	0.1046
5	900	0.081	0.109	0.0968
5	900	0.084	0.112	0.0968
5	900	0.068	0.092	0.0753
5	900	0.057	0.078	0.06930
2	875	0.170	0.155	0.12560
2	875	0.172	0.157	0.12560
2	875	0.163	0.147	0.11760
2	875	0.162	0.146	0.11520
2	875	0.160	0.143	0.11270
2	875	0.155	0.138	0.10860
2	875	0.153	0.136	0.10400
2	875	0.151	0.134	0.10060
2	875	0.150	0.132	0.09490
2	875	0.141	0.123	0.09080
2	875	0.109	0.094	0.07850
2	875	0.108	0.093	0.07850
2	875	0.105	0.090	0.07850
2	875	0.096	0.083	0.06970
2	875	0.086	0.074	0.06640
2	875	0.076	0.065	0.05170
2	875	0.075	0.065	0.05170
1	850	0.138	0.186	0.07960
1	850	0.130	0.172	0.07260
1	850	0.120	0.156	0.06280
1	850	0.108	0.138	0.05630
1	850	0.102	0.130	0.04830
1	850	0.101	0.128	0.04830
1	850	0.090	0.113	0.03830
1	850	0.074	0.093	0.03120
2	850	0.183	0.173	0.10100
2	850	0.172	0.159	0.09770
2	850	0.169	0.155	0.09360
2	850	0.180	0.170	0.09360
2	850	0.179	0.168	0.09340

2	850	0.173	0.161	0.08890
2	850	0.172	0.159	0.08880
2	850	0.173	0.160	0.08870
2	850	0.167	0.153	0.08320
2	850	0.171	0.158	0.08060
2	850	0.152	0.136	0.07980
2	850	0.158	0.142	0.07590
2	850	0.156	0.140	0.07580
2	850	0.159	0.144	0.07560
2	850	0.160	0.144	0.07440
2	850	0.152	0.136	0.07060
2	850	0.146	0.130	0.07040
2	850	0.150	0.134	0.07010
2	850	0.141	0.125	0.06690
2	850	0.150	0.134	0.06680
2	850	0.141	0.125	0.06660
2	850	0.136	0.120	0.06160
2	850	0.126	0.110	0.05760
2	850	0.130	0.114	0.05730
2	850	0.123	0.107	0.05730
2	850	0.128	0.112	0.05720
2	850	0.127	0.111	0.05720
2	850	0.115	0.100	0.04850
2	850	0.115	0.100	0.04560
2	850	0.102	0.089	0.04550
2	850	0.101	0.087	0.03740
3	850	0.231	0.165	0.11220
3	850	0.221	0.154	0.09520
3	850	0.190	0.126	0.07610
3	850	0.189	0.125	0.07610
3	850	0.174	0.113	0.05930
3	850	0.156	0.100	0.04160
5	850	0.205	0.297	0.09990
5	850	0.183	0.257	0.08800
5	850	0.172	0.238	0.07110
5	850	0.160	0.221	0.07220
5	850	0.150	0.204	0.06750
5	850	0.146	0.199	0.06960
5	850	0.134	0.183	0.05710
5	850	0.120	0.162	0.05380
5	850	0.121	0.163	0.05380
5	850	0.112	0.151	0.05270
5	850	0.102	0.138	0.04230
1	825	0.080	0.167	0.05620
1	825	0.076	0.160	0.04560
1	825	0.072	0.150	0.03930
1	825	0.072	0.149	0.03420
1	825	0.070	0.145	0.03420

1	825	0.063	0.129	0.02120
2	825	0.191	0.185	0.05650
2	825	0.181	0.171	0.05500
2	825	0.184	0.175	0.05450
2	825	0.180	0.170	0.0524
2	825	0.178	0.167	0.05
2	825	0.176	0.164	0.0474
2	825	0.173	0.161	0.047
2	825	0.167	0.153	0.0445
2	825	0.168	0.155	0.0445
2	825	0.165	0.151	0.042
2	825	0.155	0.141	0.0392
2	825	0.156	0.141	0.0392
2	825	0.156	0.141	0.0378
2	825	0.151	0.136	0.0327
2	825	0.141	0.126	0.0296
2	825	0.136	0.121	0.0249
2	825	0.135	0.120	0.0248
2	800	0.186	0.179	0.0662
2	800	0.187	0.181	0.0656
2	800	0.189	0.183	0.0529
2	800	0.176	0.166	0.0487
2	800	0.174	0.164	0.045
2	800	0.173	0.163	0.045
2	800	0.169	0.157	0.0331
2	800	0.165	0.153	0.0331
2	800	0.167	0.155	0.0305
2	800	0.159	0.146	0.0223
2	800	0.158	0.144	0.0182
4	800	0.088	0.189	0.0294
4	800	0.086	0.182	0.0212
4	800	0.084	0.178	0.0206
4	800	0.084	0.179	0.0191
4	800	0.082	0.174	0.0167
4	800	0.079	0.167	0.0138
4	800	0.079	0.167	0.0138
4	800	0.078	0.165	0.0112
4	800	0.075	0.156	0.0082
5	800	0.209	0.307	0.0423
5	800	0.206	0.301	0.0491
5	800	0.202	0.294	0.0408
5	800	0.196	0.282	0.0399
5	800	0.185	0.263	0.0325
5	800	0.182	0.256	0.0313
5	800	0.174	0.244	0.0383
5	800	0.171	0.238	0.0326
5	800	0.165	0.230	0.0434
5	800	0.156	0.216	0.0352

5	800	0.148	0.203	0.0267
5	800	0.149	0.205	0.0267
5	800	0.142	0.194	0.0298

(*) See table below for the detail of feed gas composition

Case	P_{CO} [bar]	P_{CH4} [bar]	P_{CO2} [bar]
1	0.15	0.21	0.64
2	0.2	0.2	0.6
3	0.25	0.19	0.56
4	0.1	0.22	0.66
5	0.22	0.33	0.99

Reference:

1. Zhang, J., Ju, X., Wu, Z.Y., Liu, T., Hu, T.D., Xie, Y.N., Zhang, Z.L., Chem. Matter. 13 (2001) 4192.
2. Zhang, F., Wang, P., Koberstein, J., Khalid, S., Chan, S.-W., Surface Sci. 563 (2004) 74.
3. Feng, L., Li, X., Dadyburjor, D.B., Kugler, E.L., J. Catal., 190 (2000) 1.
4. Barath, F., Turki, M., Keller, V., Maire, G., J. Catal. 185 (1999) 1.
5. Jiang, M., Bian, G-Z., Fu, Y-L., J. Catal. 146 (1994) 144.